Studies in Quantum Chaos: From an almost exactly solvable model to Hypersensitive operators

A THESIS

submitted by

N. MEENAKSHISUNDARAM

for the award of the degree

of

DOCTOR OF PHILOSOPHY

DEPARTMENT OF PHYSICS
INDIAN INSTITUTE OF TECHNOLOGY MADRAS.

February 2010

THESIS CERTIFICATE

This is to certify that the thesis titled **Studies in Quantum Chaos: From an almost exactly solvable model to Hypersensitive operators**, submitted by **N. Meenakshisundaram** to the Indian Institute of Technology Madras for the award of the degree of **Doctor of Philosophy**, is a bona fide record of the research work done by him under my supervision. The contents of this thesis, in full or in part, have not been submitted to any other Institute or University for the award of any degree or diploma.

Arul Lakshminarayan
Research Guide
Associate Professor
Dept. of Physics
IIT Madras

Place: Chennai 600 036, India
Date: February 6, 2010

ABSTRACT

Keywords: Quantum chaos; Eigenfunctions; Quanutm baker's map; Hadamard transform; Fourier transform; Thue-Morse sequence; Multifractals; Modular exponentiation; Hypersensitivity

The classical baker's map is a simple and paradigmatic model of a fully chaotic system. Its quantization has been studied for many years now as a simple model of quantum chaos. The quantum baker's map is reviewed and various quantization schemes are discussed. The quantization scheme of Shack and Caves is also given a novel classical interpretation. Some statistical features of the eigenfunctions of the quantum baker's map is displayed, and the special nature of powers of 2 Hilbert spaces is noted in both eigenvalue and eigenfunction statistics.

The heart of this thesis studies eigenfunctions of the usual quantum baker's map for Hilbert space dimensions that are powers of 2. The Walsh-Hadamard (WH) transform, widely used in digital signal processing and quantum computing, is used for analyzing the eigenstates of the quantum baker's map. We find the emergence of the ubiquitous Thue-Morse sequence, a simple sequence which is at the border between quasiperiodicity and random, hence a good paradigm for quantum chaotic states. This happens most prominently in a state we call the "Thue-Morse" state and can be largely constructed from the Thue-Morse sequence and its Fourier transform. It is shown analytically that indeed the Thue-Morse sequence is an approximate eigenstate of the quantum baker's map. In addition we find other families of states that are simply related to the Thue-Morse sequence and its Fourier transform. In general such states are strongly scarred by short periodic orbits of periods that are powers of 2, and their homoclinic excursions. Approximate analytical expressions for these and other families states are given and evidence is exhibited that they are multifractal.

We introduce a class of functions that limit to multifractal measures and which arise when one takes the Fourier transform of the Hadamard transform. This introduces generalizations of the Fourier transform of the well-studied and ubiquitous Thue-Morse sequence, and introduces also generalizations to other intriguing se-

quences. We show their relevance to the quantum baker's map a few of whose eigenfunctions are approximated well by such measures,.

Subsequently we rationalize the efficacy of the WH transform in simplifying the eigenstates of the quantum baker's map. This is done by constructing closely related, but *new*, unitary transforms that do signicantly better, thus nearly solving many states of the quantum bakers map. These transforms, which combine the standard Fourier and Hadamard transforms in an interesting manner, are constructed from eigenvectors of the shift permutation operator that are also simultaneous eigenvectors of bit-flip (parity) and possess bit-reversal (time- reversal) symmetry.

To check the efficacy of the WH transform and the new transform on maps other than the usual baker' s map, it is used to study a closed tetradic map and a lazy baker' s map. Also these transforms are applied to resonances of an open tetradic quantum baker's map. Significant simplifications of the eigenstates on using WH transform and the new transform are found, and studied using the participation ratios. Some of the eigenstates and resonances are further displayed and underlying sequences are uncovered.

Finally we study hypersensitivity to perturbation of the transforms and operators related both to the quantum baker's map and Shor's factoring algorithm namely the Fourier transform, WH transform and the shift permutation operator. The Fourier transform is not sensitive to perturbations, while both the Hadamard and shift operator show intermediate sensitivities.

TABLE OF CONTENTS

ABSTRACT **i**

ABBREVIATIONS **v**

1 Introduction **1**

1.1 Classical Hamiltonian chaos 4

1.1.1 Chaos 7

1.1.2 Measuring the chaos: Lyapunov exponent 8

1.1.3 The classical baker's map 10

1.2 Quantum chaos 12

1.2.1 Quantum Maps 13

1.2.2 Eigenfunctions 16

1.2.3 Semiclassics of Eigenvalues 17

1.2.4 Random matrix theory 18

2 Quantum baker's map and Statistics of its Eigenfunctions **21**

2.1 Overview 21

2.2 The quantization 23

2.2.1 Quantum kinematics on the torus 23

2.2.2 The Balazs-Voros-Saraceno construct 25

2.2.3 Symmetries and other properties 27

2.2.4 Schack-Caves quantization 28

2.2.5 Classical interpretation of the Schack-Caves quantizations 32

2.2.6 The shift operator and the baker's map 34

2.3 Statistical properties of eigenfunctions of the quantum bakers map 38

2.3.1 Intensity Distributions 38

3 The Thue-Morse sequence and eigenfunctions of the quantum

baker's map **43**

3.1 Compression using the Walsh-Hadamard basis 44

3.2 The Thue-Morse state and an ansatz 51

3.3 Other families of states 60

3.4 The Fourier transform of the Hadamard transform 66

3.5 The participation ratio or the correlation dimension 67

3.6 Connections to quantum baker's map 70

4 A new transform nearly solving the Quantum baker's map **73**

4.1 Introduction 73

4.2 Eigenfunctions of the Shift operator 74

4.2.1 Simultaneous eigenstates of parity and the shift operator 76

4.2.2 Time-reversal adapted states of the shift operator 77

4.3 The eigenstates of the quantum baker's map in the new basis . . 79

5 Application of the transforms to other quantum baker's maps **88**

5.1 A closed tetradic baker 88

5.2 A lazy baker 93

5.3 An open tetradic baker 96

6 Hypersensitivity to perturbation **104**

6.1 Description of the algorithm 105

6.2 Hypersensitivity study for the operators G_N, H_N and $G_N H_N$ . . 106

6.3 Hypersensitivity of the shift operator 110

7 Conclusions **116**

Bibliography 121

ABBREVIATIONS

RMT	Random Matrix Theory
BGS	Bohigas-Giannoni-Schmit
TM	Thue-Morse
KAM	Kolmogorov-Arnold-Moser
TR	Time-reversal
NNS	Nearest Neighbour Spacing
BVS	Balazs-Voros-Saraceno
CUE	Circular Unitary Ensemble
GUE	Gaussian Unitary Ensemble
WH	Walsh-Hadamard
GOE	Gaussian Orthogonal Ensemble
FFT	Fast Fourier transform
IPR	Inverse Participation Ratio
DFT	Discrete Fourier transform
PR	Participation Ratio

CHAPTER 1

Introduction

It is recognized for sometime now that most Hamiltonian systems are chaotic, to be more precise their phase space has a nonzero measure of chaotic orbits [1]. This is due to the ubiquity of nonlinearity and the fact that most systems have more than one effective degree of freedom. One can say that the clockwork universe epitomized by the simple pendulum has given way to the intrinsic chaos of the double pendulum. Since the late 1970's there has been interest in what happens on quantization of classically chaotic systems, a subject that has now come to be called "quantum chaos". Early applications were mostly motivated from atomic physics, for instance microwave ionization of hydrogen atoms [2] or the hydrogen atom in a strong magnetic field [3]. Thus even the simplest of atoms, hydrogen, one of the driving forces in the very formulation of quantum mechanics could in the presence of external fields be examples of quantum chaos. Later applications encompass a wide range of physical phenomena including mesoscopic physics, optical and nuclear physics for instance. There are suggestive links between quantum chaos and the open problem of Riemann's conjecture in Number Theory [4]. Furthermore it is now recognized that the states of quantum chaos possess a significant amount of entanglement, especially of the multipartite kind. Entanglement being a resource for quantum information processing [5] has been intensively studied in the recent past, and systems with quantum chaos have been especially studied from this point of view [6, 7].

The principal analytical handle over quantized chaotic system has been semiclassical theories. Gutzwiller in the late 1960's, M. V. Berry and others later on developed what is today called "periodic orbit theory" as the principal classical structures that appear in such theories are classical periodic orbits. Being chaotic systems, these periodic orbits are unstable and furthermore *dense* in phase space and exponentially increasing in number with period. Yet, these conspire to add with phases determined by the actions of these orbits and amplitudes by their stability to produce approximate quantum quantities, such as importantly discrete energies. It is obviously a challenge finding classical periodic orbits of chaotic systems and this limits the usefulness of these theories. However, the ergodic nature of chaotic systems then make their mark, and an important classical sum rule due to Hannay and Ozorio de Almeida, called the "principle of uniformity" [8] is used

to deal with long periodic orbits. In fact this sum rule also provided the first idea of why random matrix theory (RMT), developed in the 50's, and 60's by Wigner, Dyson and Mehta provides a statistical framework from quantum chaos [9]. RMT which had hitherto been applied to nuclear resonance spectra, was applied to very simple, but chaotic, systems in 1984 by Bohigas, Giannoni and Schmit [10]. They found that while spectra of quantized chaotic systems such as the Bunimovitch stadium had fluctuations that were identical to those from RMT, integrable systems did not. This gave rise to the BGS conjecture that RMT is applicable for all fluctuations in the spectra of quantum chaotic systems. A thorough review of the use of RMT in quantum chaos is found in the monograph by F. Haake [11].

The understanding of classical chaos has been facilitated by the study of very simple models, many of them being exactly solvable. For example the cat map of V. I. Arnold or the baker's map [12, 13, 14]. In fact the baker's map is more than a model: it is an abstraction of the genesis of Hamiltonian chaos, namely the behaviour on a homoclinic tangle which is the structure created by intersecting stable and unstable manifolds and is the heart of chaos. This gives rise to the "left-shift" of symbolic dynamics, which lays bare the alarming tendency of chaos to eat up the number of significant figures in any initial data [12, 13]. Given this, it was only natural that those who started the study of quantum chaos should look to quantize these simple models first. It turned out that the exactly solvable quantum cat map, first studied by J. Hannay and M. V. Berry [15] and subsequently by J. Keating [16], B. Eckardt [17], and others was very nongeneric, giving rise to unusual spectra and exact recurrences. Nevertheless, this is a very interesting model and its study has been an useful one. For instance it was shown for this system that there are states that in the semiclassical limit are supported upto 50% by periodic orbits and the rest is the Lebesgue measure [18] . The quantum baker's map, first studied by N. L. Balazs, A. Voros [19], and subsequently by M. Saraceno [20] and others, had a much more generic behaviour, including spectral fluctuations that more closely agree with those of RMT. However it has remained analytically unsolvable, despite a deceptively simple structure involving only Fourier transforms. It has been a very important and "paradigmatic" model due to the fact that its classical mechanics is completely solvable, for instance all the periodic orbits, homoclinic orbits etc. are known explicitly. This then helps with the study of semiclassical theories.

Eigenfunctions of quantum chaotic systems are less understood, although important phenomena such as "scarring" [21] have been known since 1984. Practically no analytic expressions exist for eigenfunctions of any quantum chaotic

system (such as the hydrogen atom in a strong magnetic field). An exception is the exceptional quantum cat map for which there exist analytical formulae [17]. Another interesting example is a chain of four nonlinear oscillators on a circle studied by Jain, Grémaud, and Khare [22] for which they were able to display some analytically exact eigenfunctions, but whose classical limit shows chaos. Interestingly these functions seemed to show scaling properties. However, it is fair to say that most generic quantum chaotic systems seem to defy the mathematics which is at our disposal. Statistical treatment of eigenstates and eigenvalue fluctuations are important and RMT is successful by and large in this [11]. However it is not clear how simple models such as the baker's map can give rise such a statistical phenomena, which is also strongly influenced by deterministic features such as short periodic orbits.

One of the major components of this thesis is the uncovering of many analytical features of the quantum bakers map, in especially its eigenfunctions when the dimension of the Hilbert space is a power of 2. This thesis suggests various novel ansatz for classes of eigenstates, based on automatic sequences such as the Thue-Morse (TM) sequence [23, 24] and its generalizations. Chaotic eigenstates cannot be assigned quantum numbers, as good quantum numbers are associated with constants of the motion. Thus classification of states apart from their energy is largely unknown. This thesis shows how this can be done, to some extent, with the quantum bakers map. We show that the eigenfunctions of the quantum bakers map are multifractal. Schnirelmann's theorem [25] requires that most of the states be equidistributed if the classical limit is ergodic. Thus our examples fall in the category of exceptional states. Following this we turn to a discussion of *why* such a simplification occurs in the case of the quantum bakers map, developing in the process a completely new unitary transform that has elements of Hadamard and the Fourier Transform, both widely used. This transform almost diagonalizes the quantum baker's map. We will also discuss about applications of this transform to generalized quantum baker's maps both open and closed. The initial work based on this thesis has also been extended by other studies, notably that of Ermann and Saraceno [26]. They constructed an "essential" baker's map whose spectral properties are close to that of the quantum baker's map. There are also interesting connections between results of this thesis and those of Nonnenmacher and co-workers on fractal Weyl laws in open systems [27].

In the final part we deal with the hypersensitivity of operators that are closely related both to the baker's map as well as to Shor's factoring algorithm and to quantum computation in general. We find, along with earlier workers [28], that

the quantum Fourier transform is not hypersensitive, while for the first time we show that the Hadamard transform is sensitive. We have also studied the case of the shift operator. This may have implications for experimental implementations of various quantum algorithms for which the Hadamard is a main ingredient.

1.1 Classical Hamiltonian chaos

Classical mechanics had the aura of complete ability to predict around it, a fact that is exemplified by Laplace's demon. This demon could, given enough initial conditions, be able to predict the future of the universe and its constituents, presumably including the fate of living beings. This hold of a deterministic, clockwork universe was dealt two blows, one by the intrinsic uncertainty of quantum mechanics, and other a much more internal consequence of classical mechanics, namely chaos. However the "deterministic" nature of classical mechanics renders this randomness "deterministic chaos", that is there are no external sources of stochasticity that are assumed. The first to realize the possible complex orbits of deterministic classical mechanics was Poincaré in his famous study of the three-body problem. After a lull, broken by important investigations by mathematicians such as Birkhoff, Julia and others came the seminal works of Kolmogorov, Arnold and Moser in the 50's and 60's which explained under what conditions stable motions are retained under perturbations (the famous KAM theorem). The word "chaos" came to be a household name for physicists after the advent of the personal computer and the works of Li, Yorke (who brought the word "chaos" into scientific usage in 1976), Ruelle, Lorenz, and others. We will briefly review the elements of classical chaos that are of importance to the work in this thesis.

Consider a Hamiltonian system with d degrees of freedom with the phase space variables (q_i, p_i), $i = 1, \ldots, d$ and the Hamiltonian H. Hamilton's equations of motion are

$$\dot{q}_i = \frac{\partial H}{\partial p_i}, \quad \dot{p}_i = -\frac{\partial H}{\partial q_i}. \tag{1.1}$$

These specify an incompressible flow in a space of dimension $2d$. However the flow also preserves several other integral invariants, actually d of them and these are the Poincaré-Cartan integral invariants. This symplectic flow has certain important consequences.

Before we come to that we state briefly that if there are d independent constants of motion say F_i that are in involution, that is $\{F_i, F_j\} = 0$, where the brackets are the usual Poisson brackets, then the system is *integrable*. In this case the motion

in phase space takes place in a periodic or quasi-periodic manner on d dimensional tori. In this case the dynamics admits a good action-angle set of coordinates such that the Hamiltonian is a function of only the actions. If this is the case the system is said to be integrable in the sense of Liouville and Arnold. Most systems do not have d such constants. The symmetries of the system are such that less than this number of conserved quantities exist. In such cases non-integrability invariably leads to chaos, or exponential sensitivity.

An important simplification was introduced by Poincaré when he suggested to study instead of the full flow, its intersections with a co-dimension 1 surface. Thus for a two-degree of freedom Hamiltonian system, this meant that on a surface of constant energy the section was two-dimensional. Due to the invariance of the sums the areas projected on conjugate planes (one of the Poincaré-Cartan invariants), the dynamics restricted to such a two dimensional section is *area-preserving*. Thus two-dimensional area-preserving maps have been intensively studied in the recent past as the simplest possible models of Hamiltonian chaos. As we are mostly concerned with two-dimensional maps in this thesis, we will therefore talk in terms of such maps although the concepts are of wider applicability.

Let $(q', p') = T(q, p)$ be a two dimensional area-preserving map. Let $X_t = \{q_t, p_t\}$ denote a phase space point at discrete time t. The discreteness could from the discrete set of intersections in the Poincaré surface of section, or could be the period of forcing in a stroboscopic map, or could be just from the definition of an abstract map. An orbit is the bi-infinite set $\{\ldots X_{-2}, X_{-1}, X_0, X_1, X_2, \ldots\}$. There are some very special types of orbits that are of interest:

1. **Periodic Orbits:** If X_0 is such that $X_T = X_0$ then the orbit will repeat itself and is a periodic orbit of period T. if T is the *smallest* such number then it is a prime periodic orbit of period T. When T is equal to 1 it is called as the fixed point of the given map.

2. **Stable/Unstable manifold:** The collection of orbits that in the far future/distant past will come arbitrarily close to an orbit X constitutes the stable/unstable manifold of this orbit.

3. **Homoclinic Orbit:** If Y_i is an orbit such that as $i \to \pm\infty$ Y_i tends to the periodic orbit X then it is homoclinic to this periodic orbit. That is, in the distant past and the far future the Y orbit will be arbitrarily close to the periodic orbit X.

4. **Heteroclinic Orbit:** Let X and X' be two periodic orbits, not necessarily of the same period. Then an orbit Y_i is an heteroclinic orbit if in the distant past it comes arbitrarily close to one of the periodic orbits, say X and in the far future comes arbitrarily close to the other.

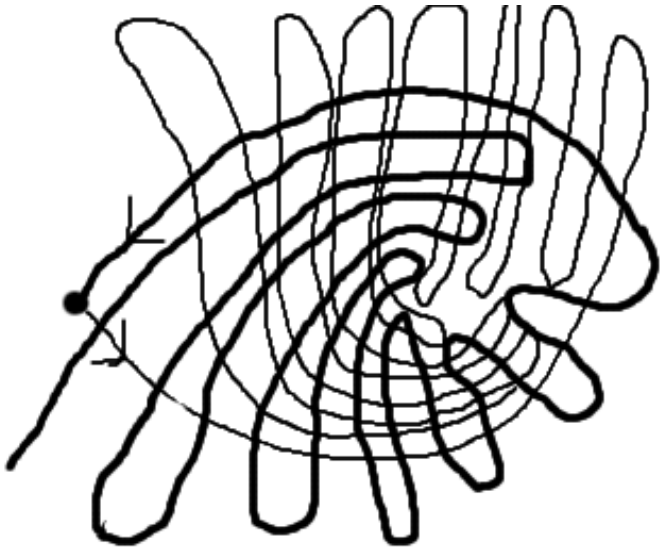

Figure 1.1: Cartoon of a homoclinic tangle. The dark line is the stable manifold and the light line is the unstable manifold. Their intersection forms loops in such a way that they do not self intersect.

While in general two orbits cannot intersect, the stable and unstable manifolds can and do intersect and these constitute the homoclinic and heteroclinic orbits. These intersection of stable and unstable manifolds are generically transversal. Tangential intersections are nongeneric and they can only arise in integrable systems (e.g., one-dimensional simple pendulum). Stable/unstable manifolds cannot self intersect due to continuity and invertibility of the map. However stable and unstable manifolds forms structures as shown in the cartoon in Fig. (1.1) such that they do not self intersect. Since the map is area preserving the areas formed by successive loops should be same and this makes the loops thinner and longer on successive iterations of the map. These form a complex network termed as the *homoclinic tangle*. Although the dynamics is deterministic the phase space points in this complex network behave in a apparently random manner. This was appreciated by Poincaré, who wrote about it in his seminal treatise *Les Methodes Nouvells de la Mechanique Celeste* in 1892 as follows:

"The intersections form a kind of lattice, web or network with infinitely tight loops; neither of the two curves must ever intersect itself but it must bend in such a complex fashion that it intersects all the loops of the network infinitely many times. One is struck by the complexity of this figure which I am not even attempting to draw. Nothing can give us a better idea of the complexity of the three body problem and of all the problems in dynamics where there is no holomorphic integral and Bohlin's series diverge." [29]

Now, thanks to computers, it is quite easy to draw and visualize such tangled webs, at least in two-dimensions. In Fig. (1.2) we see such a finite portion of the stable and unstable manifolds for the unstable fixed point of the area-preserving two-dimensional standard map. The value of the parameter k is such that at $k = 0.97\ldots$, the last "golden mean" rotational KAM torus breaks. The standard map is discussed in many textbooks [29, 14, 30] and we also briefly define it further below.

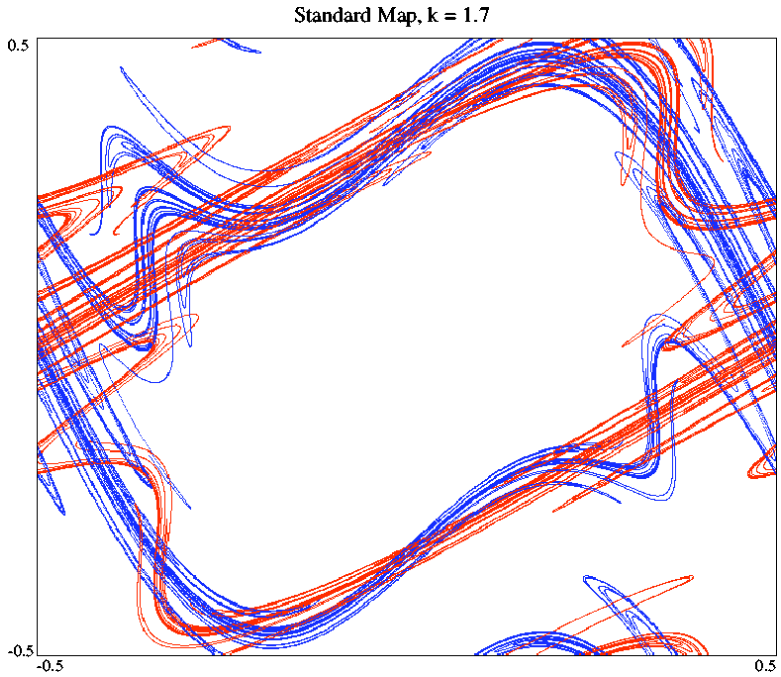

Figure 1.2: The tangle showing the stable and unstable manifolds of the hyperbolic fixed point of the standard map at $k = 1.7$.

1.1.1 Chaos

The term chaos is defined in different ways in the literature. A brief and concise presentation of them is found in this [31]. We adopt here one of the mathematical definition of chaos due to Devaney[12]. Definition: Let V be a set and $f : V \to V$ a map on this set. We say that f is chaotic on V if

1. f has sensitive dependence on initial conditions. $f : V \to V$ has sensitive dependence on initial conditions if there exists $\delta > 0$ such that, for any $x \in V$ and any neighborhood Δ of x, there exist $y \in \Delta$ and $n \geq 0$, such that $|f^n(x) - f^n(y)| > \delta$, where f^n denotes n successive applications of f. Practically this definition implies that there exist points arbitrarily close to x which eventually separate from x by at least δ under iterations of f . We point out that not all points near x need eventually move away from x under

iteration (periodic points for example), but there must be at least one such point in every neighborhood of x.

2. f is topologically transitive. $f : V \to V$ is said to be topologically transitive if for any pair of open sets $U, W \subset V$ there exists $n > 0$ such that $f^n(U) \cap W \neq \emptyset$. This definitions implies the existence of points which eventually move under iteration from one arbitrarily small neighborhood to any other. Consequently, the dynamical system cannot be decomposed into two disjoint invariant open sets, what constitute ergodicity.

3. periodic points are dense in V. This is a very important condition which implies that arbitrarily close to any point there exists a periodic orbit in a chaotic system. This is the hidden order in deterministic chaos. This also forms the backbone of many classical and semiclassical theories that constitute periodic orbit theories. The fact that they are dense, means that a subset of them may be used to approximate any orbit. Of course in a chaotic system all such periodic orbits are *unstable* and it is altogether a different and difficult task to *find* them.

From the definition we see that a chaotic system possesses three ingredients: a) unpredictability because of the sensitive dependence on initial conditions, b) indecomposability, because it cannot be decomposed into noninteracting subsystems due to topological transitivity, and c) an element of regularity because it has a dense set of periodic points or orbits. Banks et al.,[32] pointed out that topological transitivity and dense set of periodic points *implies* sensitive dependence on initial conditions. Thus conditions 2 and 3 are sufficient for a system to be chaotic.

1.1.2 Measuring the chaos: Lyapunov exponent

From a physicist's perspective, there is chaos if the phase-space of the system is bounded and there is a nonzero measure of orbits that are exponentially unstable. Now we turn our discussion to this important characterizer, the Lyapunov exponents which gives details about linearized stability of any trajectory in the phase space. Roughly speaking, for a given trajectory, the Lyapunov exponents characterize the mean exponential rate of divergence of trajectories surrounding it. The stability of any trajectory can be stated in terms of Jacobian matrix. For a $2D$ area preserving map of the form

$$\begin{aligned} x_{n+1} &= f(x_n, y_n) \\ y_{n+1} &= g(x_n, y_n) \end{aligned} \tag{1.2}$$

As a well-known class of examples [30, 14] consider the stroboscopic map with $V(x)$ a periodic function periodic on $x \in [0, 1)$:

$$\begin{aligned} y_{n+1} &= y_n - V'(x_n) \bmod 1 \\ x_{n+1} &= x_n + y_{n+1} \bmod 1. \end{aligned} \tag{1.3}$$

where we have made the choice to apply the potential kick before the free motion. The notation V' indicates the derivative of V with respect to x. The standard map corresponds to

$$V(x) = -\frac{k}{4\pi^2} \cos(2\pi x). \tag{1.4}$$

At $k = 0$ the map is integrable and is a stroboscopic map of a freely rotating particle. At this value of k there are both rational and irrational tori, depending on if the momentum is rational or irrational, and constitute "unperturbed tori". For nonzero, but small, k the incommensurate or irrational tori survive in accordance with the KAM theorem, while the commensurate or rational ones break up into a pair of stable and unstable orbits in accordance with the Poincare -Birkhoff theorem. The phase space starts getting mixed with stable and chaotic orbits for increasing k. At around $k \approx 0.97$ the last rotational irrational KAM tori, with a winding number of the golden mean, breaks and leads to global diffusion. For $k > 5$ the standard map is considered to be largely chaotic, although it is also not *proven* to be so for any value of k, however large. This map is a typical scenario for a two-degree of freedom Hamiltonian system. The chaos comes mixed with regularity. In this thesis we study models in which the chaos is complete and distilled, with no trace of regularity.

The Jacobian or stability matrix of the general 2D map in Eq. (1.2) evaluated at the phase-space point (x_n, y_n) is

$$J(x_n, y_n) = \begin{pmatrix} \partial f/\partial x_n & \partial f/\partial y_n \\ \partial g/\partial x_n & \partial g/\partial y_n \end{pmatrix}. \tag{1.5}$$

Area-preservation implies that $\mathrm{Det}(J) = 1$. the stability matrix of an forward orbit segment of length n with an initial point (x_1, y_1) is given by

$$M_n(x_1, y_1) = \prod_{i=1}^{n} J(x_i, y_i) \tag{1.6}$$

The finite time Lyapunov exponents are strictly speaking defined via the singular values of M_n, which are the eigenvalues of $M_n^T M_n$. If the eigenvalues of these are

$\kappa_i(n)$, $i = 1, 2$ then the Lyapunov exponents are

$$\lambda_i = \lim_{n\to\infty} \frac{1}{2n} \log(\kappa_i(n)). \tag{1.7}$$

Note that this is in principle dependent on the initial point (x_1, y_1), but thanks to ergodicity this dependency gets obliterated and we can talk of *a* Lyapunov exponent valid for almost all trajectories. Short time periodic orbits could have significantly different Lyapunov exponents however. The entire set of periodic orbits, although dense, are of measure zero. While the eigenvalues defined above are guaranteed to be positive, it is very common in the literature to define the Lyapunov exponents directly from the exponential growth rate of the magnitudes of the, in general complex, eigenvalues of the stability matrix M_n, asymptotically in time n. For most systems these two procedures yield the same "Lyapunov" exponents. We note that a recent detailed study of finite-time Lyapunov exponents and stability exponents defined as the growth rate from the Jacobian, especially for the standard map is in [33].

We now recall the definitions and properties of an abstract model of chaos, the baker's map. The properties of the quantization of this model will be one of the main topics of this thesis and hence we will expand on the classical baker's map first.

1.1.3 The classical baker's map

This map imitates the action of the bakery baker who is kneading dough. The action which leads to a homogenization of the ingredients called for in the cake's recipe is distilled as the action which leads to Hamiltonian chaos and the tangle. The classical baker's map [14], T, is the area preserving transformation of the unit square $[0, 1) \times [0, 1)$ onto itself, which takes a phase space point (q_n, p_n) to (q_{n+1}, p_{n+1}) given by

$$\left.\begin{array}{ll} q_{n+1} & = 2\,q_n \\ p_{n+1} & = p_n/2 \end{array}\right\} \; 0 \le q_n < 1/2; \quad \left.\begin{array}{ll} q_{n+1} & = 2\,q_n - 1 \\ p_{n+1} & = (p_n + 1)/2 \end{array}\right\} \; 1/2 \le q_n < 1. \tag{1.8}$$

where the stretching along the horizontal q direction by a factor of two is compensated exactly by a compression in the vertical p direction. Pictorial representation of the map is given in Fig. (1.3). Its Jacobian is simply $\mathrm{diag}(2, 1/2)$ everywhere, the eigenvalues are 2 and 1/2. The Lyapunov exponents are $\log(2)$ corresponding to horizontal q direction and $-\log(2)$ corresponding to vertical p direction

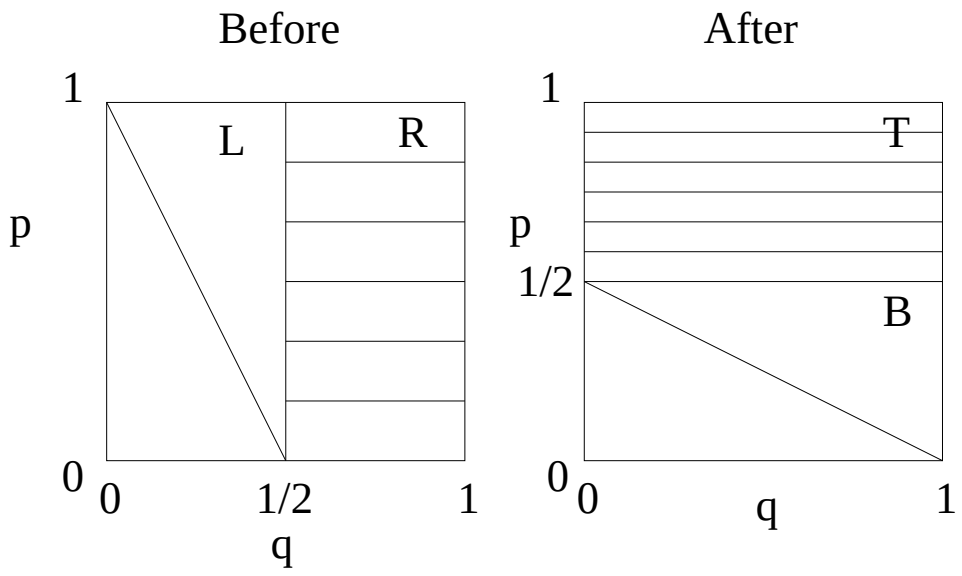

Figure 1.3: The classical baker's map. The two disjoint parts Left(**L**) and Right(**R**) is mapped to Top(**T**) and Bottom(**B**) after one iteration with stretching along the horizontal q direction and compression along the vertical p direction by a factor of 2.

and their sum equals to zero. Thus with a positive nonzero Lyapunov exponent the map is a candidate for chaos. It will become clear if we write any initial phase point(namely (q_0, p_0)) in terms of binary representation of numbers say as $q_0 = 0.a_0a_1a_2\ldots$ and $p_0 = 0.a_{-1}a_{-2}a_3\ldots$, where $a_i = 0, 1$. Note that $a_0 = 0$ if q_0 lies in left half L and it is 1 otherwise. Thus $q_1 = 2\,q_0 - a_0$ whether $a_0 = 0\,\text{or}\,1$. Similarly $p_1 = (p_0 + a_0)/2$ in either case.

If we write (q_0, p_0) as a *bi-infinite* sequence of the following form

$$(p_0|q_0) \;=\; \ldots a_{-3}a_{-2}a_{-1} \circ a_0a_1a_2\ldots \tag{1.9}$$

then

$$(p_1|q_1) \;=\; \ldots a_{-2}a_{-1}a_0 \circ a_1a_2a_3\ldots \tag{1.10}$$

The notation $(p|q)$ is to indicate a phase space point, the right side is to be thought of symbolically, with the small circle separating the p in the left from the q on the right and the circle denotes the present moment. The classical baker's map action is to shift the entire sequence of a_i to the left by one place. This dynamics is known as a *left shift*.

We can easily obtain periodic points, stable/unstable manifolds and homoclinic/heteroclinic points interms of binary representation of phase space points.

Consider the phase space points such as

$$(p_0|q_0) \;=\; \ldots u_k\, u_k \;\circ u_k\, u_k \ldots \tag{1.11}$$

where u_k is any binary string of length k. It is then clear from the left shift dynamics that $(p_k|q_k) = (p_0|q_0)$, that is this initial point comes back to itself after k steps. It also immediately follows that after any multiple of k the point recurs, in short we have a *periodic point* of period k. As there are 2^k possible u_k strings for any k, there are exactly 2^k possible periodic points for the baker map of period k. The repeating string is often denoted by an overbar, thus $(p_0|q_0) = \overline{u_k} \circ \overline{u_k}$. The decimal representation of $(p_0|q_0) \;=\; \overline{u_k} \circ \overline{u_k}$, is

$$q_0 = d(u_k)/(2^k - 1),\; p_0 = Rd(u_k)/(2^k - 1). \tag{1.12}$$

If the string $u_k = a_0 a_1 \ldots a_{k-1}$ then $d(u_k) = 2^{k-1}a_0 + 2^{k-2}a_1 + 2^{k-2}a_2 + \ldots + a_{k-1}$ is the value of the binary string u_k, and $Rd(u_k) = 2^{k-1}a_{k-1} + 2^{k-2}a_{k-2} + \ldots a_0$ is the value of the string that is obtained by *reversing* the string u_k, with the least significant bit becoming the most significant bit etc. For example the point $\overline{01} \circ \overline{01}$ is a periodic point of period 2, and in usual decimal representation it is $(q_0 \;=\; 1/3\,, p_0 \;=\; 2/3)$. For any point or orbit in the baker's map the stable and unstable manifolds are easily found using the left shift. For instance for the fixed point at the origin any point whose position (in binary) ends in an infinite string of zeros is in the stable manifold. In general for a periodic orbit of period k characterized by the string u_k the following is easily seen:

1. Stable Manifold: $something \circ somethingelse\, \overline{u_k}$.
2. Unstable Manifold: $\overline{u_k}\, something \circ somethingelse$.
3. Homoclinic points: $\overline{u_k}\, something \circ somethingelse\, \overline{u_k}$.
4. Heteroclinic points: $\overline{u'_l}\, something \circ somethingelse\, \overline{u_k}$.

For example $\overline{01} \circ 10\overline{01}$ is a point that is homoclinic to the period 2 point $(2/3|1/3) = \overline{01} \circ \overline{01}$, while $\overline{101} \circ 00101\overline{10}$ is an heteroclinic *connection* between the period 2 orbit $\overline{10} \circ \overline{10} = (1/3|2/3)$, to which it comes arbitrarily close in the future and the period 3 orbit $\overline{101} \circ \overline{101} = (5/7|5/7)$, from which it deviated arbitrarily closely the sufficiently distant past.

The transformation Eq. (1.8) has two basic symmetries. The first is parity symmetry obtained by $p \to 1-p$ and $q \to 1-q$ which corresponds to reflection of a trajectory with respect to the center of the square. The second is an anticanonical

time reversal symmetry related to the interchange of p and q and the reversal $t \to -t$. The repeated action of T on the square leaves the phase space mixed, this is well known to be a fully chaotic system that in a mathematically precise sense is as random as a coin toss. The area-preserving property makes this map a model of chaotic two-degree of freedom Hamiltonian systems.

1.2 Quantum chaos

"Quantum chaos" is really a short form for saying that it is the study of the quantization of classically chaotic systems. Michael Berry has recommended the term quantum chaology, but the short form seems to be in wide usage, and we will use it in this thesis. A mentioned earlier, the motivations for this study stem from even the simplest of systems, such as hydrogen atom in external electromagnetic fields or the helium atom excitation spectra. The effects of quantum chaos on transport has been studied through measurements of magneto-resistance in quantum dots [34]. The classical motion of the electrons inside these is like the motion of a ball on billiard tables, and this class of billiard problems have been at the center of many classical as well as quantum studies. Experimental work on such systems has been on for more than a decade now. Recent explorations of the possibility of a quantum computer, has also brought to the forefront issues of the effect of chaos on the functioning of many-body quantum computers [35, 36]. In particular the "entangling" power of quantum chaos is a current research topic [6]. Entanglement which measure how nonseparable quantum systems are in a genuinely quantum way, is influenced by chaos in an apparently very nontrivial manner. The fundamental nature of quantized chaotic systems could also lie at the foundations of quantum statistical mechanics [37]. Studies also suggest that decoherence, which is the entanglement of a system with its environment, is strongly influenced by chaos in the system and/or environment [38].

The field of quantum chaos had its origins with the independent and almost simultaneous publication of two papers, one on the quantized standard map [39] which lead to the discovery of the phenomenon of dynamical localization, while the other was on general planar area-preserving maps [40] in 1979. This was immediately followed by a work that quantized the classical cat map, which is like the baker's map a fully chaotic linear map of the 2-torus onto itself. Thus the earliest quantized chaotic systems where quantizations of stroboscopic maps, and area preserving abstract maps. In addition to these "quantum maps" there was also an extensive numerical study of the eigenfunctions of the stadium billiard

[41] who looked at nodal pattern of these functions and concluded that they were random and had no apparent order. The study of quantum billiards (again two-dimensional) forms a very important and rich class of models with immediate applications to quantum dots. As this thesis is concerned with a quantum map, we provide an introduction to these here.

1.2.1 Quantum Maps

Broadly speaking quantum maps come in two flavors: (1) quantizations of non-autonomous systems with periodic time dependence mostly of the "kicked" variety, and (2) quantization of abstract dynamical systems, such as the baker's map, and the cat map. Although in some cases (like the cat map) there have been mappings on to kicked systems [42]. Most of the studies so far on this have been restricted to 2D area preserving mappings. Experimentally kicked Hamiltonians have been realized using pulsed fields that provide a very good approximations to delta function impulses. One important phenomenon studied here is the dynamical localization of wave packets [43]. Experimental realizations of the quantum baker's map have been proposed using simple quantum gates [44].

Quantum maps are quantizations of classical maps. Classical two-dimensional area preserving maps are special cases of symplectic or canonical transformations. Thus quantum maps may be thought of as the quantum equivalents of canonical transformations. The quantum equivalent is an unitary operator, and it is not immediately clear how this association is to be done. For the class of maps derived from kicked Hamiltonians we can derive the quantum map quite easily. We will first deal with the broad class of canonical transformations that comes from kicked systems. Consider the Hamiltonian:

$$H \;=\; H_0 \;+\; V \sum_{n=-\infty}^{\infty} \delta(t/T - n), \tag{1.13}$$

where H_0 and V are time independent operators. The Schrödinger equation we want to solve is

$$i\hbar \frac{\partial}{\partial t}|\psi\rangle \;=\; H_0|\psi\rangle \;+\; V\delta_T(t)|\psi\rangle; \tag{1.14}$$

given an initial state $|\psi(0)\rangle$, we wish to solve for the state at a later time, $|\psi(t)\rangle$. Let $\delta_T(t)$ be an abbreviation for the train of delta impulses. Say that the classical map relates phase space variables just after consecutive kicks. Similarly then we may consider the quantum map to be that unitary operator, say U, that connects states just after consecutive kicks. Thus if we write the state just after kick n as

$|\psi(n^+)\rangle$ we are seeking that U such that

$$U\,|\psi(n^+)\rangle \;=\; |\psi(n+1^+)\rangle. \tag{1.15}$$

From just after kick n to just before kick $n+1$, the delta function term is effectively absent in Eq. (1.14). Thus we have:

$$|\psi(n+1^-)\rangle \;=\; \exp(-iH_0T/\hbar)\,|\psi(n^+)\rangle. \tag{1.16}$$

Now we have to deal with integration over a kick, during which time the wave function changes abruptly. Integrating the schrödinger equation over the infinitesimal time about the kick, eliminates the H_0 part of the Hamiltonian, or alternatively we could say that the kick dominates the Hamiltonian during this time. Therefore we get that

$$|\psi(n+1^+)\rangle \;=\; \exp(-iVT/\hbar)\,|\psi(n+1^-)\rangle. \tag{1.17}$$

Combining this with Eq. (1.16) we get:

$$|\psi(n+1)\rangle \;=\; \exp(-iVT/\hbar)\,\exp(-iH_0T/\hbar)\,|\psi(n)\rangle, \tag{1.18}$$

where we have dropped all the + superscripts, all the states are understood to be immediately after the stated times. Thus the quantum map is the unitary operator:

$$U \;=\; \exp(-iVT/\hbar)\,\exp(-iH_0T/\hbar) \tag{1.19}$$

Since the Hamiltonian is explicitly time dependent the usual description in terms of eigenstates and energy eigenvalues does not exist. However the quantum map, is "stationary" in the sense that it does not depend on the kick number, and is a special case of the Floquet operator for general periodic time dependence. Iterating the classical map produces time evolution while in quantum maps repeated multiplication by the operator U is required:

$$|\psi(n)\rangle \;=\; U^n\,|\psi(0)\rangle. \tag{1.20}$$

The powers of an operator is determined by its eigenvalues and vectors and hence the problem of time evolution is in this case also solved by an eigenvalue problem. The eigen angles of U take the role of the energies and the eigen vectors of U are the "stationary" states. Since U is an unitary operator its eigenvalues lie on the

unit circle, the eigenvalue equation may be written as:

$$U|\phi_k\rangle = \exp(i\phi_k)|\phi_k\rangle. \tag{1.21}$$

where $0 \leq \phi_k < 2\pi$ are real numbers, the eigen angles, and also referred to as the "quasi-energies". The index k may be discrete, or continuous, as the eigen angles are discrete or continuous.

One of the most extensively studied quantum maps corresponds to the quantum standard map with $H_0 = p^2/2$, and $V = k\cos(2\pi q)$ [45]. This has been studied with a phase space topology of a cylinder as well as a torus. The Harper map with $H_0 = g\cos(2\pi p)$ and $V_0 = g\cos(2\pi q)$ has also been quite extensively studied [46, 47]. While the above quantization works for kicked systems with a Hamiltonian generating the map, there are abstract maps for which this is not a given. We will deal in the next chapter with the quantization of the baker's map which is a prime example of this kind.

1.2.2 Eigenfunctions

We very briefly describe here some of the phenomenology associated with eigenfunctions of quantum chaos.

Scarring.

Eigenfunctions are semiclassically associated with classically invariant sets. For classically completely chaotic systems, the only such set which is not of measure zero is the energy shell. The smaller invariant sets, for instance associated with periodic orbits whose measure is zero was not expected to influence the eigenfunctions. This gave rise to the Berry-Voros hypothesis which said that the Wigner representation of typical eigenstates will be uniformly spread on the energy shell [48, 49]. A mathematical formulation known as Schnirelmann's theorem is a statement of eigenfunction ergodicity.

However numerical investigation of the eigenfunctions of the chaotic stadium billiard by Heller showed that most of the eigenfunctions had strong enhancements that could be unambiguously identified with classically unstable and isolated periodic orbits. Heller called these "scars" of periodic orbits in quantum wave functions [21]. Since these investigations many examples have been found. Heller has put forward certain explanations for this phenomena based on wave packet dy-

namics, while Bogomolny [50] and Berry [51] have advanced semiclassical theories based on Gutzwiller's periodic orbit theory. Today we know that apart from periodic orbits there are also scars of homoclinic and heteroclinic orbits. However our understanding is far from complete, in the sense that we cannot say which eigenfunction will be influenced by which classical orbits. Heller gave a criteria that restricts those periodic orbits that could scar the wave functions, which effectively cuts off long periodic orbits. Almost all scarring studies have been done with two-degree of freedom systems or quantum maps. Experimental evidence exists from resonant tunneling experiments [34] and in analogy experiments such as in microwave cavity billiards [52].

When the baker map was first quantized, the bakers Balazs and Voros concluded that the eigenfunctions in the position representation were mostly erratic, or random looking. However when subsequently Saraceno made use of coherent states to study the functions a bewildering variety of patterns became visible, most of which could be identified with some classical feature, such as periodic orbits, or homoclinic orbits, or stable and unstable manifolds, but the way they were appearing held no particular rule. We will have opportunity in later chapters, and especially in chapter 3 to display these eigenfunctions and uncover some mathematical structure in them.

Eigenfunctions in a mixed phase space, containing a measure of both chaotic and regular orbits is even more complicated. This is primarily because the border between order and chaos is not clean and is in general a fractal one. However a rough rule seems to be either that the eigenfunctions are supported in the regular regions, or in the chaotic one, but not by both simultaneously. This was conjectured to be the case by Percival [53] in the early 1970's, and while it is seen to hold for many two-degrees of freedom systems, it is not clear if this is valid in higher dimensions. Violations of these have come to light in certain periodic systems, and states that are localized in both chaotic and regular regions have been called "amphibious" [54].

1.2.3 Semiclassics of Eigenvalues

Although this thesis is not directly concerned with eigenvalues, they have formed the principal object of investigation due to the existence of semiclassical periodic orbit theory or the trace formula. The Gutzwiller trace formula connects the trace of the energy Green's function to a weighted sum over the periodic orbits on energy shells [55]. The trace formula is more simply studied using quantum maps. One

central object is the trace of the propagator after time t:

$$\mathrm{Tr}(U^t) = \sum_{i=0}^{N-1} \exp(it\phi_i) \tag{1.22}$$

where U is some unitary map, the ϕ_i are the eigen angles. This implies that if we know the traces of the powers of U we can know the eigen angles. This is seen by Fourier transforming both sides:

$$\sum_{t=-\infty}^{\infty} e^{-i\omega t}\mathrm{Tr}(U^t) = \sum_{m=-\infty}^{\infty} \sum_{i=0}^{N-1} \delta(\phi_i - \omega - 2\pi m) \tag{1.23}$$

where we have made use of the Poisson summation formula.

$$\sum_{n=-\infty}^{\infty} \int_{n=-\infty}^{\infty} f(x) e^{2\pi i n x}\, dx = \sum_{m=-\infty}^{\infty} f(x). \tag{1.24}$$

Thus Fourier transforming the traces of the powers of the propagator will give us delta functions at the eigenangles.

Semiclassical theory then attempts to find $\mathrm{Tr}(U^t)$ from purely classical quantities. The general structure of this trace formula is

$$\mathrm{Tr}(U^t) \sim \sum_{\gamma(t)} A_\gamma \, \exp(2\pi i S_\gamma/\hbar) \tag{1.25}$$

where γ enumerates classical *periodic orbits* of period t, S_γ is the action of the periodic orbit, and A_γ is a weight that typically exponentially falls with the period t. This last statement may give rise to the expectation that the long orbits can be neglected, but in chaotic systems there is an exponential proliferation of periodic orbits with period. Therefore this is a delicate problem that needs care and in fact while the trace of quantum maps on finite dimensional Hilbert spaces hardly poses a problem, whole of semiclassics is beset with convergence issues. There is also the question of *how long* the above approximation holds good, while a fair amount of work has gone into this it is again not very clear what exactly this time is and how it depends on the scaled Planck constant and the parameters of chaos.

A semiclassical theory of the quantum baker's map also exists [56, 57] and has the generic form of the trace formula above. For instance one surprising result that has emerged from the study of simple systems such as the quantum baker's map is that semiclassics can be valid over much longer time scales than the Ehrenfest time, which signals the end of quantum-classical correspondence. The use of the

quantum baker's map is crucial as it permits calculating very long periodic orbits with ease.

1.2.4 Random matrix theory

As has been said earlier, the statistical aspect of quantum chaos is well described by random matrix theory (RMT), and is widely used in many areas from nuclear to mesoscopic physics [58]. Wigner in the 1950's suggested that since complex many body Hamiltonians such as for nuclei were unknown or were difficult to solve, especially for higher excitation spectra, we may assume that the Hamiltonian matrix is a random matrix, that is a matrix whose elements are drawn from a distribution at random. The model that is most often used is when the distribution is a Gaussian and the matrix elements are independently drawn. This leads to the Gaussian ensembles. There are some fundamental symmetries that systems may obey despite all the complexity and chaos. For instance time-reversal (TR) symmetry is quite fundamental and implies that given any arbitrary basis, we can find a related basis, the time-adapted one, in which the Hamiltonian is real. Therefore TR symmetric Hamiltonians are generically real, while TR nonsymmetric Hamiltonians are in general complex. We have till now talked of unitary matrices, maps rather than Hamiltonians. Therefore the appropriate ensembles are called circular, as the matrices are unitary and were first studied by Dyson [59]. For the results we will recall, the most simplest, it does not make a difference in the leading order if the ensembles were Gaussian or circular. One such very popular result is immediately described below.

The nearest neighbor spacing distribution. (NNS)

This is one of the most widely used RMT measures in quantum chaos, and is about how the nearest neighbor energy differences are distributed distributed. First a procedure called unfolding is done which makes all spectra have average unit mean spacing. This allows us to consider spectra from very different physical origins. It is also important that this analysis included only states that belong to the same symmetry class.

If the system were integrable the NNS is Poisson distributed, which will happen if the energy levels do not have any correlation between them. If the system is chaotic (in the classical limit) the distribution will be one of two types depending of if there is TR symmetry or no TR symmetry. These are universal distributions,

independent of the system. The only requirement is that the classical limit be fully chaotic. In the case of the unitary operators such as quantum maps, the mean spacing is simply $2\pi/N$ as the eigenangles are uniformly distributed over $[0, 2\pi)$. Therefore define

$$s_i = \frac{N}{2\pi}(\theta_i - \theta_{i-1}), \tag{1.26}$$

and consider the set of normalized spacings $\{s_i, i = 1, \ldots, N-1\}$. If these are distributed according to the function $P(s)$, RMT says that for the Gaussian or Circular ensembles:

$$P(s) = \begin{cases} \exp(-s) \text{ Integrable.} \\ \\ \dfrac{\pi}{2} s \exp(-\pi s^2/4) \text{ Chaotic. TR symmetric.} \\ \\ \dfrac{32}{\pi^2} s^2 \exp(-4s^2/\pi) \text{ Chaotic. No TR symmetry.} \end{cases} \tag{1.27}$$

These are understood to be asymptotic results valid for large matrix sizes. However one remarkable fact is that even small matrices have NNS that are very good approximations to these. Indeed Wigner first studied 2×2 matrices to derive the Wigner law valid for chaotic TR symmetric systems, the second of the equations above. This law was found to hold good for a simple but chaotic system by Bohigas and others when they found the NNS from several hundred numerically levels of the stadium and the Sinai billiard [10]. For mixed systems, distributions are found that are intermediate between the Poisson and the Wigner. In the next chapter we will talk about what RMT has to say about eigenfunctions.

CHAPTER 2

Quantum baker's map and Statistics of its Eigenfunctions

2.1 Overview

The baker's map was quantized by Balazs and Voros [19] in 1989. Being a map that does not have a Hamiltonian generating it (at least a "natural one"), it required a certain amount of classical-quantum reasoning to quantize the map. As it later turned out the quantization was consistent with those suggested by quantizations based on generating functions. A mixed $(q-P)$ generating function is natural for the baker's map and this results in the quantum baker being simple in the mixed representation. This was first realized in the works of Balazs and Voros. However as is well recognized quantization is not a unique process, and today there is a whole community of quantum bakers who share the common classical limit. As an aside, the population of this community is more than the smallest accounted towns in the United States of America (for instance, Maza, North Dakota, population: 5).

Then there are "semi-quantum" bakers, appreciated early on by Balazs and Voros but more thoroughly studied by Saraceno and Voros [57]. These are quantizations after some classical time has elapsed. That is, quantization is done after compounding the map with itself a certain number of times. Later there was a very interesting series of quantum bakers published by Schack and Caves [60], one of which was identical to the Balazs-Voros quantum baker. We will subsequently present these quantizations as it has an impact on this thesis. We will also present an interpretation of this quantization from a classical point of view, which we believe is either new or at least unpublished. It must be mentioned that before all these quantizations of the baker's map was done, Penrose in his remarkable book on Statistical Mechanics [61], gave the quantization as an exercise and presented a solution himself. This solution which is a simple shift operator does not have the correct classical limit. The last of the Schack-Caves series of quantum bakers is in fact very closely allied to the shift operator. Lakshminarayan recently made use of the shift operator and projectors to construct a quantum baker map that has

the correct classical limit, but does not preserve time reversal symmetry exactly in the quantum mechanical case. This allowed the reverse process of using the quantum bakers to be used to construct the shift operator. The significance of this is that the shift operator is an example of the so-called modular exponentiation part of Shor's celebrated quantum algorithm for factoring. Thus this work displayed an intimate connection between this algorithm and quantum chaos, opening up questions about the algorithm's sensitivity to perturbations [62, 63].

In this chapter we will recount some of these varied quantizations and introduce the main players, or operators, in this thesis. We will also present a first look at the eigenfunctions of the quantum baker's map, via their statistical distributions. The components of quantum chaotic states are known to be normally distributed in the small $\hbar$ limit. Earlier studies of the statistics of the eigenfunctions of the quantum baker's map were by O' Connor and Tomsovic [64]. They point out that the quantum baker's map shows deviations especially for the case when N, which is the dimensionality of the Hilbert space and also the inverse scaled Planck constant is a power of 2. We also observed this, and in addition observe that the distributions for this case are *heavy tailed* and have power law scaling of the tails. Such distributions are of very general interest and are sometimes called Pareto distributions. These occur in a wide variety of statistical data, ranging from sand piles to citation indices [65]. It is interesting that the quantum baker's map shows such distributions. We will see in later chapters that these eigenfunctions are also multifractal. We will evaluate the power laws that occur in the quantum baker's map and provide evidence that there are very strong correlations present. Thus models of power law processes that rely on i.i.d. are of little relevance in this case.

Recently there has been studies of the largest and smallest intensities of chaotic or random states. These extreme value statistics studies of eigenfunctions showed that due to the weak correlations present in the states, only due to overall normalization, the largest intensity distribution tends towards the universal Gumbel distribution, while the smallest intensity is exponentially distributed[66]. We have found that in the case of the quantum baker's map there is a clear deviation from the Gumbel distribution, however we do not present these results in this thesis as they are of a preliminary nature. The study of extremes in the case when the events are power-law distributed and strongly correlated needs to be further addressed. That this is of relevance to quantum systems with fractal eigenfunctions is rather evident. The study of extremes in these case is bound to be of even more interest that in the normal case as extreme events can occur with larger probability. However in the absence of a knowledge of how exactly the correlations occur,

this is a difficult task.

2.2 The quantization

We now briefly discuss the Balazs-Voros quantisation of the baker's map. The procedure consists of two steps. First one specifies the kinematics [67] *i.e.*, the states and operators associated with the description of the system and then dynamics, that is the time evolution of these objects. Saraceno [20] imposed anti-periodic boundary conditions when studying the quantum baker's map and this was a very important step as it restored the broken parity symmetry of the quantum map.

The baker's map is defined on a unit square. It is convenient to impose periodic boundary conditions on the square and make it a torus. Quantum mechanically this gives us a freedom to choose two phases as will become evident below. In hindsight torus boundary conditions are not natural for the baker's map as on a closed square there are two fixed points at the corners $(0, 0)$ and $(1, 1)$ while the other corners are not fixed. This leads to unusual semiclassical contributions that are of the order of $\log(1/\hbar)$ [57]. Lakshminarayan [68] for instance showed that imposing reflective boundary conditions removed these anomalous effects. However this was at the cost of studying four classically noninteracting bakers (the four-baker's map) with interesting quantum tunneling properties. For most purposes, the simpler single baker with torus boundary conditions is desirable and sufficient. Therefore this has continued to be studied as such. Hence our first stop is to indicate the kinematics of quantum states when the phase space is a torus.

2.2.1 Quantum kinematics on the torus

Let the torus (square with opposite edges identified) $[0, 1) \times [0, 1)$ be the classical $(q - p)$ phase space. As is well known in the case of angular momenta, imposing periodic boundary conditions for the angle variable leads to the quantization of momenta. Imposing periodic boundary conditions on *both* position and momentum, results in a discrete set of states in both these variable, and more importantly then to a state space, or Hilbert space, of finite dimensions. Thus the quantum mechanics on the torus is finite dimensional quantum mechanics and has applications to many diverse areas of physics. The first systematic treatment of this was by Schwinger [67].

Let $|q_n\rangle$ and $|p_n\rangle$ be the position and momentum eigenstates with $n = 0, 1, \ldots, N-$

1, where N is the dimensionality of the Hilbert space. As is well-known in usual continuum quantum mechanics $\exp(-ipa/\hbar)$ is the position translation operator in the sense that $\exp(-ipa/\hbar)|q\rangle = |q+a\rangle$,, while $\exp(iqb/\hbar)$ is the momentum translation (or boost) operator [69], where a and b are arbitrary real numbers. In finite dimensional spaces, infinitesimal generators such as position and momentum are not well defined, but their unitary extensions, the translation operators are. Hence rather than deal with position and momentum operators we deal with position and momentum *translation* operators.

The position translation operator is denoted by U, and is such that

$$\langle q_n|U = \langle q_{n+1}|, \text{ and } \langle q_n|U^N = \langle q_{n+N}| = \exp(2\pi i\beta)\langle q_n|. \tag{2.1}$$

Here $0 \leq \beta < 1$, is the phase accumulated as one goes along the q direction. For periodic boundary conditions $\beta = 0$, while for anti-periodic, it is $\beta = 1/2$. Phases such as these are very useful in controlling quantum symmetries. The physical interpretation of this phase is possible as a magnetic flux line threading the particle's circular configuration space. The phase then appears as the Aharanov-Bohm phase and is useful in controlling time-reversal symmetry. The translation operator in momentum, V, is similarly defined.

$$V|p_n\rangle = |p_{n+1}\rangle, \text{ and } V^N|p_n\rangle = |p_{n+N}\rangle = \exp(2\pi i\alpha)|p_n\rangle. \tag{2.2}$$

Here the phase α $(0 \leq \alpha < 1)$, often controls parity symmetry. We find the relationship between the two bases, the position and momentum, by requiring that the momentum states be eigenstates of the position translation operator and vice-versa; just as in continuum mechanics.

It is then easy to show by direct verification that

$$|p_m\rangle \equiv \frac{1}{\sqrt{N}} \sum_{n=0}^{N-1} \exp\left(2\pi i(n+\alpha)(m+\beta)/N\right)|q_n\rangle \tag{2.3}$$

is an eigen vector of U, that is

$$U|p_m\rangle = \exp\left(2\pi i(m+\beta)/N\right)|p_m\rangle. \tag{2.4}$$

Similarly

$$V|q_n\rangle = \exp\left(2\pi i(n+\alpha)/N\right)|q_n\rangle. \tag{2.5}$$

Hence we get the transformation between position and momentum states to

be a *generalized discrete Fourier transform*:

$$\langle p_m|q_n\rangle = \frac{1}{\sqrt{N}} \exp\left(-2\pi i(n+\alpha)(m+\beta)/N\right) \equiv (G_N)_{nm}\,. \tag{2.6}$$

We have defined the matrix G_N via this means. We will mainly use either $\alpha = \beta = 0$ or $\alpha = \beta = 1/2$. We may also identify "position" and "momentum" eigenvalues from the eigenvalues of the translation operators as $q_n = (n+\alpha)/N$ and $p_m = (m+\beta)/N$). As stated earlier we have a 2 parameter family of quantizations and this freedom with boundary conditions is absent in ordinary quantum mechanics on the plane. The operator U is diagonal in the momentum representation and the operator V is diagonal in the position representation. They satisfy the commutation relation given by

$$UV = VUe^{-2\pi i/N}, \tag{2.7}$$

which is the equivalent of the more usual commutation relation $[q,p] = i\hbar$. From comparing the transformation function with the continuum formula for $\langle q|p\rangle$ we may infer that $N = 1/h$. This also follows from semiclassical arguments: as there are N states on the unit phase space, and there is one state per h, it follows that

$$h = \text{Total area of phase space/Total number of states} = 1/N. \tag{2.8}$$

as the area of the phase space is unity. Thus $1/N$ is the effective *scaled* Planck constant, the Planck constant divided by the phase-space area. The classical limit is then the large N limit, $N \to \infty$.

2.2.2 The Balazs-Voros-Saraceno construct

Quantization of the classical baker's map is an unitary transformation which ideally has the symmetry properties of the classical system and must reproduce the area preserving transformation in the classical limit. Recall that the classical baker's map begins by decomposing the phase space into two disjoint and equal vertical halves L (Left) and R (Right), refer to the Fig. (1.3). Then each part is separately mapped into two disjoint and equal horizontal halves B (Bottom) and T (Top) where $(L \to B, R \to T)$. Each map separately compresses p and dilates q by a factor of two.

The quantization of Balazs and Voros proceeds in an analogous way. The vector space of states $\mathcal{H}_N$ is divided into two orthogonal subspaces, $\mathcal{R}$, $\mathcal{L}$ with

vectors $|\psi_R\rangle$, $|\psi_L\rangle$ respectively . We require that in the position representation:

$$\langle q_n|\psi_L\rangle = 0, \quad \text{for } n \geq N/2, \tag{2.9}$$

and similarly

$$\langle q_n|\psi_R\rangle = 0, \quad \text{for } n \leq N/2. \tag{2.10}$$

Thus $\mathcal{H}_N = \mathcal{R} \bigoplus \mathcal{L}$.

To maintain complete symmetry between $\mathcal{L}$ and $\mathcal{R}$, N is restricted to *even* integers. One iteration must transfer the vectors $|\psi_L\rangle$ and $|\psi_R\rangle$ into $\mathcal{B}$ and $\mathcal{T}$ which belong to spaces $\mathcal{B}$ and $\mathcal{T}$. These spaces $\mathcal{B}$ and $\mathcal{T}$ are mutually orthogonal and complete: $\mathcal{H}_N = \mathcal{B} \bigoplus \mathcal{T}$. They are now distinguished by vanishing components in the momentum representation:

$$\langle p_m|\phi_B\rangle = 0, \quad \text{for } m \geq N/2, \tag{2.11}$$

and

$$\langle p_m|\phi_T\rangle = 0, \quad \text{for } m \leq N/2. \tag{2.12}$$

The quantum counterpart of the classical $L \to B$ transform is denoted B_{LB} and is such that $B_{LB}|\psi_L\rangle$ belongs to $\mathcal{B}$. Further Balazs and Voros required that it satisfy the following conditions, which have clear classical motivations:

$$\langle 2q_n|B_{LB}|\psi_L\rangle = \frac{1}{\sqrt{2}}\langle q_n|\psi_L\rangle, \quad \text{for } 0 \leq n \leq N/2 - 1. \tag{2.13}$$

and

$$\langle p_m|B_{LB}|\psi_L\rangle = \sqrt{2}\langle 2p_m|\psi_L\rangle, \quad \text{for } 0 \leq m \leq N/2 - 1. \tag{2.14}$$

Using the last of these, completeness, and the fact that $|\psi_L\rangle$ belongs to $\mathcal{L}$ we have that

$$\langle p_m|B_{LB}|\psi_L\rangle = \sqrt{2}\sum_{n=0}^{N/2-1} \langle 2p_m|q_n\rangle\langle q_n\psi_L\rangle. \tag{2.15}$$

We have used only one half of the conditions, but this turns out to be sufficient and consistent with the other. Since $|\psi_L\rangle$ is an arbitrary vector from $\mathcal{L}$ we can write the operator B_{LB} in the mixed, momentum-position basis as the matrix:

$$B_{LB} = \begin{pmatrix} G_{N/2} & 0 \\ 0 & 0 \end{pmatrix} \tag{2.16}$$

Likewise, the mapping from $\mathcal{R}$ to $\mathcal{T}$ is done and the matrices are added to give

the *mixed* representation:

$$\begin{pmatrix} G_{N/2} & 0 \\ 0 & G_{N/2} \end{pmatrix}. \tag{2.17}$$

Finally we obtain the $N \times N$ unitary matrix B matrix in the position representation as

$$B = G_N^{-1} \begin{pmatrix} G_{N/2} & 0 \\ 0 & G_{N/2} \end{pmatrix} \tag{2.18}$$

This is our main protagonist and object of interest. Balazs and Voros had assumed periodic boundary conditions on the states and had taken $\alpha = \beta = 0$, while Saraceno made the important observation that $\alpha = \beta = 1/2$ is more natural and fully preserves classical symmetries. But right here it maybe noted that there are an infinity of quantum baker's maps corresponding to the two-fold infinity of these phases.

2.2.3 Symmetries and other properties

The quantum baker's map B is a product of two noncommuting unitary matrices. Although the matrices that make up B are only discrete Fourier transforms, this leads to nontrivial spectral properties for the product as a whole. Surprisingly this can have a behaviour that is very close to those of random matrices. The unitarity of B leads to the following eigenvalue problem:

$$B|\psi_j\rangle = e^{-i\phi_j}|\psi_j\rangle \quad \text{with} \;\; \phi_j \in [0, 2\pi), \quad j = 0, 1, 2, \cdots N \tag{2.19}$$

Where $|\psi_j\rangle$ is $j-$th eigenstate of the quantum baker's map with eigenvalue equal to $e^{-i\phi_i}$, (with modulus equal to 1). The eigen angles ϕ_i lie in the interval $[0, 2\pi)$ and for the quantum baker's map they in general take irrational values. It maybe noted that for the quantum cat maps the eigen angles are in general rational multiples of 2π due to the periodicity of the map. This non-generic feature is absent in the quantum baker's map.

The two important symmetries of the classical baker's map which has been already discussed are parity and time-reversal. We now discuss their quantum counterparts.

1. **Parity:** The classical parity operator R_{cl} is such that $R_{cl}(q, p) = (1-q, 1-p)$. If B_{cl} denotes the classical baker's map, then $B_{cl} \circ R_{cl} = R_{cl} \circ B_{cl}$. The action of the quantum parity operator R_N on the position eigen vectors is given by

$$R_N|n\rangle = |N - n - 1\rangle \tag{2.20}$$

In terms of matrix elements it is given by

$$\langle q_{n'}|R_N|q_n\rangle \;=\; \delta(n'+n+1,N) \tag{2.21}$$

which is zero except for the secondary diagonal which has ones. As with any parity operator this is idempotent, that is $R_N^2 = I_N$, where I_N is the identity and the eigenvalues of this are ± 1. For the choice of anti-periodic boundary conditions, that is when $\alpha = \beta = 1/2$

$$[B, R_N] = 0 \tag{2.22}$$

and the eigenstates can be classified as having even or odd parity. For this choice of phases there is an important identity:

$$G_N^2 = -R_N. \tag{2.23}$$

The original quantization of Balazs and Voros did not respect this particular parity symmetry. As mentioned earlier this was done by Saraceno shortly thereafter.

2. **Time reversal:** The classical baker has another symmetry, that of time reversal. Corresponding to every orbit, there is one that is reflected across the secondary diagonal or the line $q = p$ and time reversed. This is most easily seen using the binary left shift. Let

$$X = \cdots a_{-3}a_{-2}a_{-1}.a_0a_1a_2\cdots$$

be a point in phase space. Then interchanging q and p leads to

$$X' = \cdots a_2a_1a_0.a_{-1}a_{-2}a_{-3}\cdots,$$

and further

$$B_{cl}^{-1}X' = \cdots a_3a_2a_1.a_0a_{-1}a_{-2}\cdots.$$

But this is the forward iterate $B_{cl}X$ followed by interchanging q and p. This overall symmetry is denoted T.

This is classically an anti-canonical symmetry and quantum mechanically the symmetry is anti-unitary. Quantum mechanically the T symmetric partner of a state ψ in position representation is the momentum representation of its complex conjugate. Thus the T symmetry operator is $G_N^{-1}K$ where K is the complex conjugation operator. If the operator B has time-reversal symmetry then it must be true that

$$BG_N^{-1}K = G_N^{-1}KB, \tag{2.24}$$

which implies that

$$B = G_N^{-1}\left(B^{-1}\right)^* G_N \tag{2.25}$$

which is easily verified to be true from the definition of B. Note that this is independent of the phases α and β. This symmetry has the important implication a global phase can be fixed such that the position and momentum

representations are complex conjugates of each other.

2.2.4 Schack-Caves quantization

Schack and Caves [60] introduced a class of quantum baker maps that are closely connected to the left shift and is usually formulated for the case when the dimension of the Hilbert space is a power of 2, that is $N = 2^K$ for some integer K. This case is of major interest in this thesis. When $N = 2^K$ we can consider the Hilbert space as being isomorphic to that of K qubits. Roughly speaking we make an "expansion" of the state in this qubit space:

$$|q_n\rangle = \prod_{i=1}^{K} \otimes |x_i\rangle \tag{2.26}$$

where x_i are 0 or 1 and $n = x_1 x_2 \cdots x_K = \sum_{j=1}^{K} x_j 2^{K-j}$ is the binary expansion of n. Note that the position is related to this as $q_n = (n + 1/2)/N = 0.x_1 x_2 \ldots x_K 1$. Define

$$|.x_1 x_2 \cdots x_K\rangle = e^{i\pi/2} |q_n\rangle. \tag{2.27}$$

The position of the dot will have an important meaning in the following and up to a phase (which is anticipated here due to anti-periodic boundary conditions) these state are position states only if all the bits are to the *right* of the dot.

Now we define the momentum states through the Fourier transform: $|p_n\rangle = G_N^{-1} |q_n\rangle$. Thus

$$|p_n\rangle = \frac{1}{\sqrt{N}} \sum_{j=0}^{N-1} |q_j\rangle \exp\left(i p_n q_j/\hbar\right) = \frac{1}{\sqrt{2^K}} \sum_{x_1,\ldots x_K} |x_1\rangle \otimes \cdots \otimes |x_K\rangle \exp\left(2\pi i a x/2^K\right). \tag{2.28}$$

where $a = n + (1/2) = a_1 \ldots a_K.1 = 2^K p_n$ and similarly $x = j + (1/2) = x_1 \ldots x_K.1$. Note that henceforth in this chapter the phase will be $\alpha = \beta = 1/2$, the case of maximal symmetries. These momentum states are then associated with a notation similar to the "binary expansion" of position states:

$$|p_n\rangle = |a_K \ldots a_1.\rangle. \tag{2.29}$$

Note that momentum states are such that all the bits are to the *left* of the dot. Also note that while the position states are taken to be unentangled qubits, that is a tensor product form of these is assumed, the momentum states are in general entangled and are not in the form of complete tensor products.

The central observation of Schack and Caves in 1998 was that it is useful to define a *partial* Fourier transform, F_k^{-1}. We must point out that there are some notational differences as well as some convention divergence in the literature. For one, the Fourier transform as used by Balazs and Voros is the inverse of that used by Schack and Caves. We have been and continue to use the Balazs-Voros convention. We have also been using G_N with the subscript to denote dimension of the space, while Schack and Caves use the subscript to denote the number of qubits on which the partial transform acts (as will be explained below). Also often in the literature F is used to denote the Fourier transform with the phases set to zero. In the following part of this chapter we adopt the convention that F denotes a *partial* Fourier transform and its subscript tells how partial it is.

Schack and Caves defined the partial Fourier transform, F_k^{-1}, acting on the last $K-k$ bits of a state as follows:

$$\begin{aligned} & F_k^{-1}|x_1\rangle \otimes \ldots \otimes |x_k\rangle \otimes |a_1\rangle \otimes \ldots \otimes |a_{K-k}\rangle \\ & = |x_1\rangle \otimes \ldots \otimes |x_k\rangle \otimes \frac{1}{\sqrt{2^{K-k}}} \sum_{x_{k+1},\ldots x_K} |x_{k+1}\rangle \otimes \cdots \otimes |x_K\rangle \exp\left(2\pi i a x/2^{K-k}\right) \\ & \equiv |a_{K-k}\ldots a_1.x_1\ldots x_k\rangle \end{aligned} \quad (2.30)$$

where $a = a_1 \ldots a_{K-k}.1$ and $x = x_1 \ldots x_{K-k}.1$. The final line of the above equation defines new states that are exactly localized along the position in region of width $1/2^k$ and are fuzzy along the momentum, but with a fuzzy width of $1/2^{K-k}$ It is roughly a state localized at phase space point $a_{K-k}\ldots a_1.x_1\ldots x_k$. The partial Fourier transform is unitary and these set of states are therefore orthonormal. Note that for $k=0$ *all* the bits are transformed and hence $F_0 = G_N$. When $k=K$ none are transformed, but $G_N = i\, I_N$ and hence the state becomes $e^{i\pi/2}|x_1\rangle\otimes\ldots\otimes|x_K\rangle = |.x_1\ldots x_K\rangle$. This is the reason for the phase in the definition of $|.x_1\ldots x_K\rangle$, and the origin is the anti-periodic boundary conditions.

We are now ready to construct the quantum baker maps. If B is an operator such that

$$B|a_{K-1}\ldots a_1.x_1\rangle = |a_{K-1}\ldots a_1 x_1.\rangle \quad (2.31)$$

it qualifies as a quantum equivalent of the left shift operator. We note that

$$F_1^{-1}|x_1\rangle \otimes |a_1\rangle \otimes \ldots \otimes |a_{K-1}\rangle = |a_{K-1}\ldots a_1.x_1\rangle \quad (2.32)$$

while

$$F_0^{-1}|x_1\rangle \otimes |a_1\rangle \otimes \ldots \otimes |a_{K-1}\rangle = |a_{K-1}\ldots a_1 x_1.\rangle \quad (2.33)$$

Thus it is follows that

$$B = F_0^{-1} F_1 \tag{2.34}$$

We will see below that this is *identical* to the Balazs-Voros-Saraceno quantum baker's map. Thus we have not really achieved any new yet. The other operators arise because there are many ways to define the initial states for the shift. That is the generalizations are operators $B_{K,k}$ which are such that

$$B_{K,k}|a_{K-k}\ldots a_1.x_1\ldots x_k\rangle = |a_{K-k}\ldots a_1 x_1.x_2\ldots x_k\rangle \tag{2.35}$$

This operator is not to be confused with the BVS quantum baker of dimension K. The BVS baker of dimension N is written either simply as B_N or is the same as $B_{K,1}$. There are K such generalized quantum bakers maps and are the quantizations introduced by Schack and Caves. While $B_{K,1}$ is spectrally complex, being just the usual BVS quantum baker map, $B_{K,K}$ is spectrally simple, and is in fact exactly periodic and has rational eigenvalues. It is very closely allied to the shift operator. A *partial* shift operator S_k is defined as a shift on the *first* k bits:

$$S_k|x_1\rangle\otimes\ldots\otimes|x_k\rangle\otimes|x_{k+1}\rangle\otimes\ldots\otimes|x_K\rangle = |x_2\rangle\otimes\ldots\otimes|x_k\rangle\otimes|x_1\rangle\otimes|x_{k+1}\rangle\otimes\ldots\otimes|x_K\rangle \tag{2.36}$$

We will now write the generalized baker operator in terms of partial Fourier transforms and partial shifts. Consider the following actions:

$$F_k|a_{K-k}\ldots a_1.x_1\ldots x_k\rangle = |x_1\rangle\otimes\cdots\otimes|x_k\rangle\otimes|a_1\rangle\cdots\otimes|a_{K-k}\rangle. \tag{2.37}$$

Therefore

$$S_k\, F_k|a_{K-k}\ldots a_1.x_1\ldots x_k\rangle = |x_2\rangle\otimes\cdots\otimes|x_1\rangle\otimes|a_1\rangle\cdots\otimes|a_{K-k}\rangle. \tag{2.38}$$

Finally we do a partial Fourier transform, but now on the last $K-(k-1) = K-k+1$ bit:

$$F_{k-1}^{-1} S_k\, F_k|a_{K-k}\ldots a_1.x_1\ldots x_k\rangle = |a_{K-k}\ldots a_1 x_1.x_2\cdots x_k\rangle \tag{2.39}$$

Thus we have that the generalized baker map can be written as

$$B_{K,k} = F_{k-1}^{-1}\, S_k\, F_k = F_{k-1}^{-1}\, F_k\, S_k, \tag{2.40}$$

the last equality follows from the commutativity of S_k and F_k, they acting on completely exclusive sets of bit. To our knowledge the first explicit form of this

appeared in a work of Scott and Caves [70]. The complete shift operator, which we use later in this thesis is S_K acting on all the K bits. We have by now introduced almost all of the principal players in this thesis. In addition the Hadamard transform will play a central role, but we postpone this for later. For now, we stand back and look at the quantizations $B_{K,k}$. Their classical limits were analyzed by Tracy and Scott [71, 72]. Sokalakov and Schack studied the classical limit of the usual bakers map (or $B_{K,1}$) in terms of symbolic dynamics [73]. We will however take a different approach and give a classical meaning or interpretation for the series $B_{K,k}$. Why do there exist so many quantizations? Is this something special for the baker's map, or can we expect such prolificacy from other dynamical systems? In the process the requirements for the classical limit will become clearer.

2.2.5 Classical interpretation of the Schack-Caves quantizations

We will now write the generalized baker's maps $B_{K,k}$ in different forms that will make the classical interpretation possible. First we note that

$$F_k^{-1} = \mathbb{1}_{2^k} \otimes G_{2^{K-k}}^{-1}, \tag{2.41}$$

which follows from the definition of the partial Fourier transform. Thus we can write

$$B_{K,k} = \left(\mathbb{1}_{2^{k-1}} \otimes G_{2^{K-k+1}}^{-1}\right)\left(\mathbb{1}_{2^k} \otimes G_{2^{K-k}}\right) \times S_k = \left(\mathbb{1}_{2^{k-1}} \otimes B_{2^{K-k+1}}\right) \times S_k. \tag{2.42}$$

This form was published in [70], and the authors note that this implies that first a shift is performed on the first k qubits, subsequent to which the last $K-k+1$ qubits are subject to the usual BVS quantum baker map (or $B_{K-k+1,1}$). The next iteration will see that the most significant qubit that was not "baked" is baked, while the most significant qubit that was baked will be shifted out of the region of baking.

This characterization of the generalized quantum baker's map is readily susceptible to a classical interpretation. This part of the work is based on that jointly done with a M.Sc. student as part of his project [74]. For clarity first consider the simplest case which is not the usual BVS quantum map, namely $B_{K,2}$. We write in this case the partial shift as

$$S_2 = \mathcal{S}_{2^2} \otimes \mathbb{1}_{2^{K-2}} \tag{2.43}$$

where $\mathcal{S}_{2^2}$ is the *full* shift on 2 qubits which is a matrix of dimension 2^2. But $\mathcal{S}_{2^2}$ is the simple matrix:

$$\begin{pmatrix} 1 & 0 & 0 & 0 \\ 0 & 0 & 1 & 0 \\ 0 & 1 & 0 & 0 \\ 0 & 0 & 0 & 1 \end{pmatrix}, \tag{2.44}$$

therefore we can write $B_{K,2}$ in a matrix form as

$$B_{K,2} = \begin{pmatrix} B_{2^{K-1}} & 0 \\ 0 & B_{2^{K-1}} \end{pmatrix} \begin{pmatrix} I_{2^{K-2}} & 0 & 0 & 0 \\ 0 & 0 & I_{2^{K-2}} & 0 \\ 0 & I_{2^{K-2}} & 0 & 0 \\ 0 & 0 & 0 & I_{2^{K-2}} \end{pmatrix} \tag{2.45}$$

Note that this operator is well defined if N is a multiple of 4. Where 2^K occurs above can be read as the dimensionality of the space N. In general the Schack-Caves quantum bakers exist not only in spaces of dimensions that are powers of 2. In fact $B_{K,k}$ quantization can be defined where $1 \leq k \leq K$ and where K is the largest power of 2 that divides N. Thus the optimal number of such quantizations exist when N is a power of 2, but a smaller number may exist depending on the divisibility properties of N.

Eq. (2.45) makes clear what happens classically. The matrix with the the identity matrices tells us to divide the phase space into 4 equal vertical partitions along the momentum and interchange the second and the third. Consequently the bakers take over and bake only the *first and second* partitions, and separately the *third and fourth*. But then the second partition was originally the third and vice-versa. This is completely equivalent to baking the original square. This is illustrated in Fig. (2.1). This generalizes as quite a remarkable property of the classical baker map, which to our knowledge is new.

The property is most easily verified to be true practically visually. To see this, start by dividing the square into 2^k equal vertical rectangles. Label these as $0, 1, 2, \ldots, 2^k - 1$. Then *interleave* the first half of these partitions with the rest, in an action that is the same as the riffle-shuffle action on a pack of cards [75]. This corresponds to the partial shift operator of the generalized or Schack-Caves quantum baker's map. Thus after the action, the partitions are in the order $0, (2^{k-1}), 1, (2^{k-1}+1), 2, \ldots, 2^{k-1}-1, (2^k-1)$. Now bake "locally", separately the successive rectangles pairwise $[0, (2^{k-1})]$, $[1, (2^{k-1}+1)]$ etc.. It is clear that the partitions from the second half with numbers indicated within parenthesis are boosted up in momentum by one-half, and join smoothly with the others of that

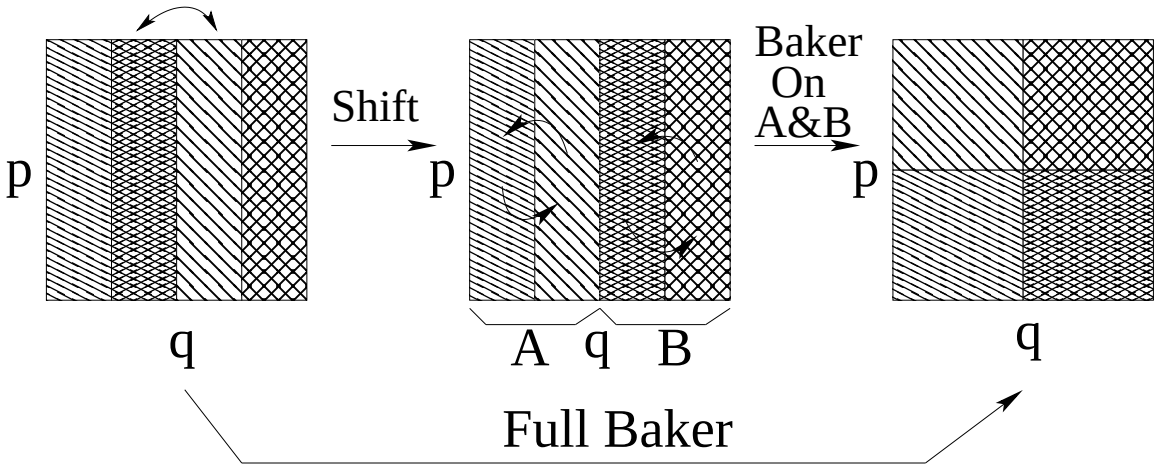

Figure 2.1: Illustrating the equivalence of the baker's map to a shift of partitions followed by "local" baker's maps. See text for details.

half. The partitions from the first half on the other hand keep to the lower half and join up smoothly. In fact it maybe said that the 2^{k-1} such local bakers restore some order that had been broken by the riffle-shuffle. These local bakers then together lead to the usual baker. This is the remarkable classical property that was alluded to. This is clearly very special for the bakers map, and we do not expect such a property for generic systems. Indeed it is this property that allows the family of quantizations found by Schack and Caves. This then provides us with the classical interpretation of $B_{K,k}$. It is clear that the classical limit will be the baker's map if k is fixed and $K \to \infty$.

Thus the family of bakers map can be thought of a riffle-shuffle followed by local bakers. The quantization of the local bakers is the diagonal block matrix with the bakers maps $B_{2^{K-1}}$ in Eq. (2.45). The generalization to $B_{K,k}$ is then immediate. It is interesting that there was an earlier study that quantized *multibaker* maps which required the quantization of many local noninteracting quantum bakers such as appears here. Lakshminarayan and Balazs [76] quantized these by considering the phase-space action as a whole and this lead to operators that did not have the block diagonal form. This then allowed for *tunneling* between the classically isolated bakers. If we use these operators here, we will get *yet more* different quantizations of the bakers map! It is quite clear that the origin of the prolificacy of the quantum baker has its roots in the stable and unstable manifolds of the bakers map being exactly aligned with the canonically conjugate directions.

2.2.6 The shift operator and the baker's map

The partial (and complete) shift operator has been introduced above in the context of Schack and Caves quantization of the baker's map. It appears along with "local bakers". In Chapter 4 we will have occasion to use the shift operator further and from symmetry adapted eigenstates of the shift operator construct an useful new orthogonal transform. We note here that the shift operator can be related to the quantum baker's map in a completely (apparently) different way [77].

In this subsection we denote the full-shift operator simply S and immediately generalize to spaces of arbitrary (even) dimension N. This is the most naive "quantization" of the one-dimensional doubling map $x \mapsto 2x\,(mod\,1)$. The action of S on the position basis (from now written simply as $|n\rangle$, rather than $|q_n\rangle$ is

$$S|n\rangle = |2n \bmod (N-1)\rangle, \tag{2.46}$$

with $S|N-1\rangle = |N-1\rangle$, rather than $|0\rangle$.

The relevance of this operator to Shor's factoring algorithm is that its generalization is the modular exponentiation. The required generalization of S, replaces the factor 2 by any integer that is coprime to $N-1$. It is the operator whose "phase estimation" leads to the solution of the order-finding problem [78]. The multiplicative order of 2 modulo $N-1$ is the smallest integer r such that $2^r = 1 \bmod (N-1)$, which is the *quantum period* also as $S^r = 1$. We are guaranteed that such a number exists as Euler's generalization of Fermat's little theorem implies that $\phi(N-1)$ is such that $2^{\phi(N-1)} \equiv 1 \bmod (N-1)$, thus r is either $\phi(N-1)$ or is a divisor of it. $\phi(n)$ is the Euler totient function, being the number of positive integers less than n and coprime to it. Finding the multiplicative order is the route of the quantum factoring algorithm of Shor. Thus it is interesting that this well-known quantum algorithm makes critical use of an operator that could be thought of as a quantization of the fully chaotic left-shift, or at least very nearly, as evidenced already by the appearance of the shift operator in the Schack-Caves quantization as well as more directly in the quantization below.

We first look at what the action of S on coherent states is, and this should make clear that its classical limit is not the bakers map. While the structure of S in the position basis is that of a permutation, its action on the momentum basis is found easily [77]:

$$\langle m'|S|m\rangle = \frac{1}{N}\frac{-\sin\left[\pi(m'+1/2)/N\right] + (-1)^{m+1}\cos\left[\pi(m'+1/2)/N\right]}{\sin\left[\pi(m-2m'-1/2)/N\right]} \tag{2.47}$$

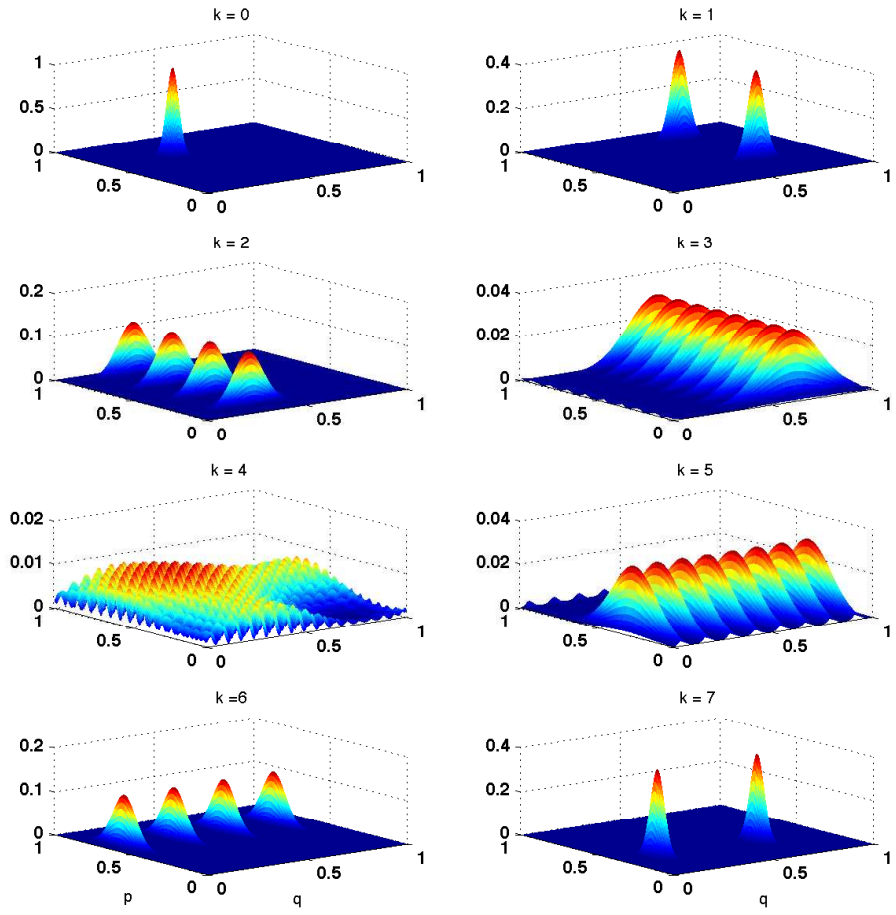

Figure 2.2: The correlation $|\langle qp|S^k|q_0, p_0\rangle|^2$ as function of (q, p) for the case of $N = 256$, where $|qp\rangle$ is a toral coherent state localized at (q, p). On further applying S to the last figure produces the first as in this case S^8 is the identity.

Here $|m\rangle$ are momentum eigenstates $|p_m\rangle$. For an initial momentum m, there are *two* momentum values around which the final state is spread, namely $[m/2]$ or $[m/2] \pm N/2$. The action of S on coherent states would be roughly a combination of its actions on position and momentum states, and therefore splits an initial state while performing appropriate scaling. Thus S creates two well-separated localized states: it takes a state localized at (q, p) to two that are localized at $(2q \bmod 1, p/2)$ and $(2q \bmod 1, (p + 1)/2)$. Repeated action by S on an initial coherent state is illustrated in Fig. (2.2), and exact revival occurs for the same reason that a deck of cards under the perfect riffle-shuffle reorders.

As S has almost the right properties of the quantum baker, it was just producing two copies of which only one was classically viable. The presence of the

other gave rise to quantum interference effects that made S exactly periodic. Thus wielding the knife of projectors we can construct the quantum baker's map with S [77]. The action of choosing the left or right vertical partition is done by the projectors P_1 and $P_2 = I_N - P_1$, where

$$P_1 = \begin{pmatrix} I_{N/2} & 0 \\ 0 & 0 \end{pmatrix}. \tag{2.48}$$

The action of stretching and compression is implemented by S. In addition though as noted above and illustrated in the picture, it produces an extra copy, shifted in momentum by one-half. Thus this is in the other horizontal partition that divides momentum into two equal halves. Thus we once again use projectors, *now in momentum space* which is $G_N^{-1} P_i G_N^{-1}$ to erase the extra copy and complete the action. Thus the full quantum baker built around S is then written as:

$$B_S = \sqrt{2}\, G_N^{-1} \left(P_1 G_N S P_1 \, + \, P_2 G_N S P_2 \right). \tag{2.49}$$

The factor of $\sqrt{2}$ is essential to restore unitarity after the projecting actions. Note that unlike the BVS quantization it does not have explicitly Fourier transforms over half the Hilbert space. However, thankfully, this is not yet another quantum baker's map since closer inspection shows that it is indeed very close to the usual baker's map in. This is seen on rewriting B_S as a matrix:

$$B_S = G_N^{-1} \begin{pmatrix} G_{N/2}^{(\frac{1}{2},\frac{1}{4})} & 0 \\ 0 & i\, G_{N/2}^{(\frac{1}{2},\frac{3}{4})} \end{pmatrix} \tag{2.50}$$

Here the superscripts refer to the phase α and β. If there are no superscripts then these are the usual values of $1/2$ each. That the usual quantum baker's map is capable of generalizations, including arbitrary phases as boundary conditions and *relative phases* between the two blocks in the mixed representation is well-known [19]. Not all of these modified baker's respect the symmetries of parity and time-reversal. The operator B_S however shows the explicit relationship between a quantum baker's map and the solvable operator S, whose action on the position basis is practically the doubling map restricted to the integers. It is worth emphasizing that even in B_S we are using anti-periodic boundary conditions. The phases of $1/4$ and $3/4$ in the $G_{N/2}$ blocks (as well as the factor of $i = \sqrt{-1}$) is a direct consequence of the structure using projection operators and are such that the operator obeys parity symmetry. This follows from the fact that R_N commutes

with G_N and that

$$R_{N/2}G_{N/2}^{(\frac{1}{2},\frac{1}{4})} = i\, G_{N/2}^{(\frac{1}{2},\frac{3}{4})} R_{N/2}, \tag{2.51}$$

which can be proved using a simple calculation [77].

Lakshminarayan then went on to invert this and write the shift operator in terms of baker's maps [79] (to be precise, two of them). This step then showed that the modular exponentiation, a subroutine of the Shor algorithm, is very closely related to this paradigmatic model of a quantum chaotic system, and led to questions of the hypersensitivity of these operators. We will study this more explicitly in the final chapter of this thesis. There has been a detailed study of the Shor algorithm's sensitivity to unitary perturbations in [63]. That the Shor algorithm was related to quantum chaotic operators was perhaps first pointed out in [80] where it was shown that the symmetry reduced Shor operator had spectral statistics that coincided quite well with that of the unitary ensembles, the GUE or the CUE.

This ends our brief survey of the construction of the quantum bakers map. Once constructed we are interested in its spectral properties. Before looking at specific states, let us first look at the statistical properties they display.

2.3 Statistical properties of eigenfunctions of the quantum bakers map

We are interested in the eigenfunctions of the quantum baker's map which preserves all the symmetries of the classical baker's map given by the Eq. (2.18). This is B of the BVS quantization. Studies by O' Connor and Tomsovic showed that the intensities of states were distributed in a manner that was close to but different from those of the eigenstates of random matrices. First we recall the results from RMT concerning the distribution of intensities of eigenstates, then show such distributions for the quantum baker's map in the case when N is a power of 2 and also when it is not. In contrast with earlier studies we concentrate on the tail of the distributions and show, apparently for the first time, that these can be heavy-tailed. Also for the first time we present results about the distribution of the extreme intensities and compare with those that are universal, and predicted by RMT.

2.3.1 Intensity Distributions

RMT requires that the states have no other correlations except those that arise from state normalization. In an arbitrary fixed orthogonal basis , $|i\rangle$ let a state by given by $|\psi\rangle = \sum_{i=1}^{N} z_i|i\rangle$. The components z_i are in general complex (case of the GUE) and if this is the case $D = 2N$, real numbers exists. Else if the state is real then $D = N$ (case of the GOE). Thus the joint probability distribution of the components is

$$P(z_1, \ldots z_N) = \frac{(D/2-1)!}{\pi^{D/2}} \delta \left(\sum_{j=1}^{D} |z_i|^2 \; - \; 1 \right). \tag{2.52}$$

Here the factorial is interpreted as the Gamma function if the argument is not an integer. Based on this j.p.d.f. a number of interesting results have been derived [81], including distribution of the extreme intensities [66].

The j.p.d.f. of $l < D$ components can be exactly calculated. If $l = 1$ this gives us the distribution of single component's intensity y as follows. First if the state is real then $y = z^2$ and $\rho(y)$ is

$$\rho_{GOE}(y) = \pi^{-1/2} \frac{\Gamma(N/2)}{\Gamma\left(\frac{N-1}{2}\right)} \frac{(1-y^2)^{(N-3)/2}}{\sqrt{y}} \tag{2.53}$$

and for the complex or unitary case $y = |z|^2$ and

$$\rho_{GUE}(y) = (N-1)(1-y)^{N-2}. \tag{2.54}$$

From unit normalization of the intensities in follows in either case that the average value of y is $1/N$. Thus it is convenient to consider the scaled intensities $x = y\,N$ which are distributed in the following simple ways for $N \to \infty$.

$$\begin{aligned} P_{GOE}(x) &= \frac{1}{\sqrt{2\pi x}} e^{-x/2} \\ P_{GUE}(x) &= e^{-x} \end{aligned} \tag{2.55}$$

The GOE distribution of intensities which is χ^2 is also known as the Porter-Thomas distribution and the GUE distribution is a simple exponential. Thus these two distributions are well distinguished from one another. These results of GOE and GUE apply the circular ensembles such as those to which the unitary operators belong.

First we look at the distribution of the eigenvalues, via the distribution of the eigen angles. In Fig. (2.3) we have shown the nearest neighbour spacing (NNS) distribution of the eigen angles for $N = 4096$ ($K = 11$), and nearby non-powers of 2, $N = 4094$ and $N = 4098$. Also shown is the RMT distribution, the Wigner surmise. We have plotted the distribution after reducing the parity to either even or odd. From the figure we can clearly see that although the distribution shows deviations from the RMT results the deviation is significantly more in the case when N is a power of 2. It is quite remarkable how the small change in the dimensionality of a large matrix, by about 0.2% in this case, can completely alter the behavior of the spectral statistics. It is perhaps worth mentioning that a similar phenomena has been observed for the quantum cat map [82]. The case when $N = 4096$ shows a rather weak level repulsion and has the appearance of the NNS of a system with a mixed phase space, or one where several weakly broken symmetries have been mixed together. The earlier study by O' Connor and Tomsovic [64] also notes the differences between N that are powers of 2 and otherwise. They have used not the NNS but other RMT measures such as the spectral rigidity.

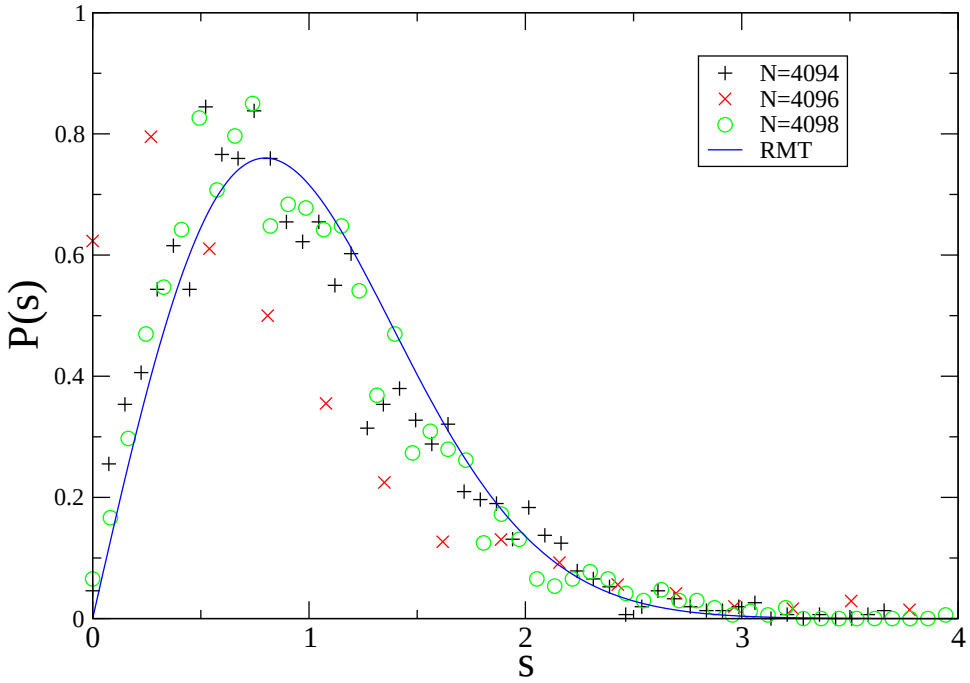

Figure 2.3: Nearest neighbour spacing distribution for the quantum baker's map along with RMT distribution (blue line), values of Hibert space dimension are denoted in the inset.

The sudden change with N is true not only for the distribution of eigenvalues but also for the eigenvector intensity distribution as well. Fig. (2.4) shows the

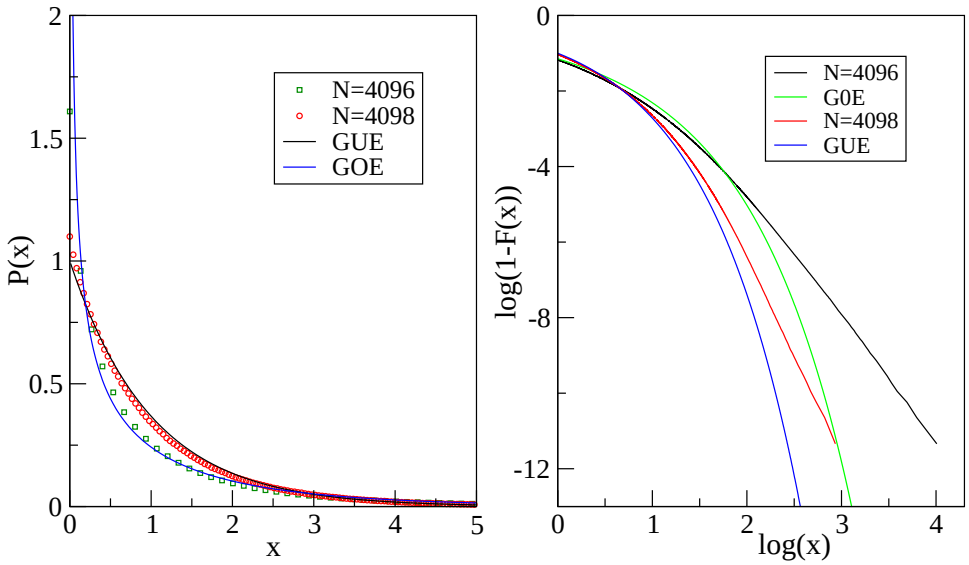

Figure 2.4: Intensity distribution of the eigenvectors for the quantum baker's map along with RMT distribution, values of Hibert space dimension are given in the inset.

intensity distribution from an ensemble containing *all* the eigenstates of the quantum baker's map for $N = 4096$, $N = 4094$ and 4098. It is clear that there are large deviations from that of the P_{GOE}, the Porter-Thomas distribution, for both these values of N. When N is not a power of 2, such as when $N = 4094, 4098$ the distribution is closer to that expected for GUE, the simple exponential. This has been noted earlier [64], and is somewhat surprising, considering that there is a time-reversal symmetry here, although the time-reversal operator is not the usual one. Note that we have not used a time-reversal adapted basis that would make the eigenfunctions real. The case when N is a power of 2 shows marked differences from either of the RMT distributions and in a log-log plot it is plausible that the tail of the distribution is a power law in this case. Thus when N is a power of 2 we observe that the intensity distribution is a *heavy tailed* power law one. It is possible that there is more than one exponent in this case.

Newman [65] has reviewed many aspects of such heavy tailed power law distributions in a very readable way. These are also known as Zipf's law or the Pareto distribution, and as he notes these arise in a wide variety of contexts, from In the context of the eigenstates of the baker's map, as indeed elsewhere, this signals that there is scale invariance, at least over some wide variety of scales. The typical intensity of eigenstates is of the order of $1/N$, and this sets the scale. However when N is a power of 2, the larger intensities are of much larger magnitude and as these form the tail of the density distribution it is interesting that there is a

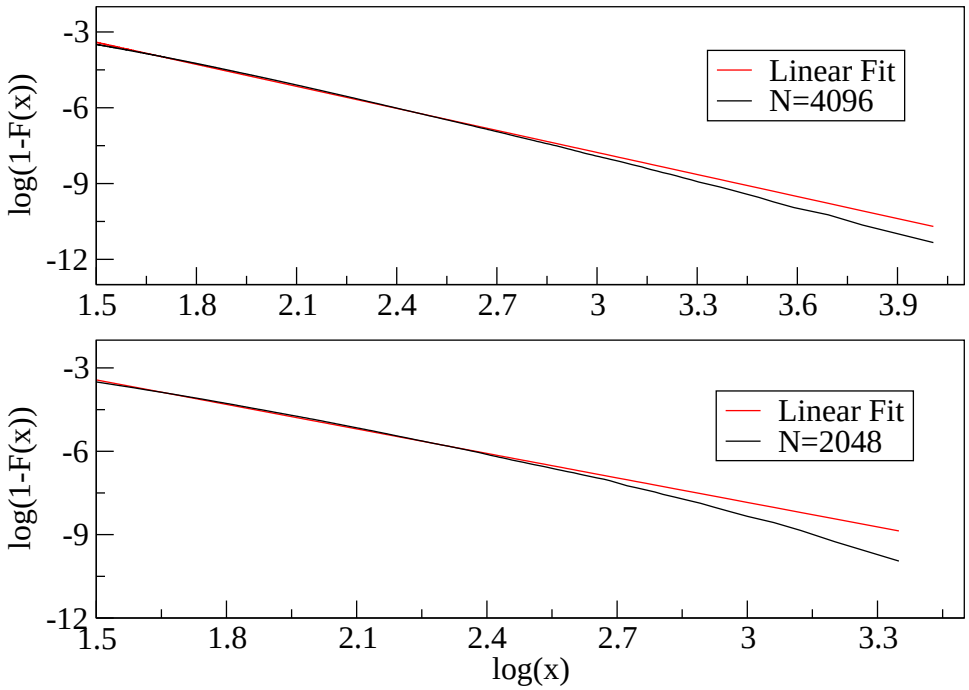

Figure 2.5: Intensity distribution of the eigen vectors for the quantum baker's map along with RMT distribution, values of Hibert space dimension are given in the inset.

power law over several decades. In Fig. (2.5) we see this illustrated for two values of N, 4096 and 2048. In both of these cases we get an approximate tail exponent of $1/x^{3.3}$. Thus the heavy tail is such that the mean, the variance and the third moment exists. This does not seem to be the case when N are non-powers of 2, although the distributions are still heavy tailed they cannot be said to have power laws. We will see in the next chapter that when N is a power of 2 the eigenfunctions are in fact multifractal.

CHAPTER 3

The Thue-Morse sequence and eigenfunctions of the quantum baker's map

The further removed from usefulness or practical application, the more important. – Axel Thue

The eigenfunctions of quantum chaotic systems, such as the hydrogen atom in a strong magnetic field, or the abstract quantum baker's maps discussed in the previous chapter are of immense interest. They carry a lot of information, yet, they are rather poorly understood even today. It maybe true that individual states may not be of that much interest as in some collective behavior of states close in some sense such as energy. This is due to the high density of states in the semiclassical limit. Nevertheless there can be classes of states that stand out in the spectrum and can be of physical significance. For example, highly scarred states occur in many systems, and these can form a series with similar properties. Short time periodic orbits that never become very unstable can support such families. For example anharmonic oscillators (hydrogen atom in a magnetic field is equivalent to such a Hamiltonian) have periodic orbits on which states can be localized and described by some adiabatic theory [83]. In completely chaotic systems such as the baker's map this seems less likely to occur.

Saraceno [20] was the first to calculate and display the eigenfunctions of the quantum baker's map. He made the observation that most of the states supported rather simple phase-space densities, that could often be associated with classical periodic orbits and their homoclinic excursions. In addition he found from autocorrelation functions some near periodicities. O'Connor, Tomsovic and Heller studied the quantum baker's map and used semiclassical methods to reconstruct autocorrelation functions and from these eigenstates. This was also a remarkably successful program, but limited in the sense that it did not give rise to any hint of the analytical structure that may underlie the states. Considering that the classical baker's map is exactly solvable, the question is, is there any simple underlying mechanism that may generate the eigenstates? As far as we know, the answer to this is still unknown, and definitely the thesis does not claim to solve this. But in this chapter we will discuss a finding that answers this definitively for a class of

states. This is itself quite interesting and provided a passage, if narrow, into the somewhat mysterious world of eigenfunctions of chaotic systems. Just as one associates the Gaussian and Hermite polynomials with the eigenfunction structure of the most ubiquitous of Hamiltonians, the harmonic oscillator, so we wish to associate an *automatic sequence* and its variants as underlying the mathematics of the eigenstates of the quantum baker's map.

An eigenstate is simplest in the eigen basis, but to know this basis is the crux of the problem. Transforms sometimes help us in coming close to the basis. It is surprising that a standard transform used in digital signal processing (for data compression, including video files such as MPEG ones), namely the Walsh-Hadamard transform is of use to the quantum baker's map eigenfunctions. This transform is also referred to sometimes simply as the Hadamard transform. It had a remarkable effect on the eigenstates of the quantum baker's map's eigenfunctions when N is a power of 2. We will assume that such is the case for the rest of this chapter.

3.1 Compression using the Walsh-Hadamard basis

Both the Fourier and the Hadamard transforms are standard tools, widely used in science and signal processing [23]. The relative importance of the two transforms may be judged to be a factor of thirty in favour of the Fourier transform if one were to go by a "google" search which returned over five million webpages for this transform. Both these transforms can be implemented with fast algorithms that reduce their implementation on N data points from N^2 to $N \log(N)$ operations. The fast Fourier transform (FFT) and the fast Hadamard transform essentially rely on the factoring of the transform into operators acting on product vector spaces. The Hadamard transform though is a real transform which only adds or subtracts the data and is therefore widely used in digital signal processing. The Fourier transform conjugate spaces are familiar ones ("time-frequency", "position-momentum") etc., while the corresponding Hadamard transforms are not so well understood. Nevertheless the Hadamard transform has also received great attention in the recent past due to its uses in quantum computing, with the Hadamard gate being a central construct [84]. Our first step in identifying special states is to Walsh-Hadamard (WH) transform [23] eigenstates.

The Hadamard transform that we use maybe written in several ways, firstly

as a tensor or Kronecker product, secondly via a recursion and finally via their matrix elements. Let N a power of 2, i.e., $N = 2^K$, for some integer K. If

$$H_2 = \frac{1}{\sqrt{2}} \begin{pmatrix} 1 & 1 \\ 1 & -1 \end{pmatrix} \tag{3.1}$$

then

$$H_{2^K} = \underbrace{H_2 \otimes H_2 \otimes \cdots \otimes H_2}_{K \text{ times}} = \otimes^K H_2. \tag{3.2}$$

Equivalently

$$H_{2^{i+1}} = \frac{1}{\sqrt{2}} \begin{pmatrix} H_{2^i} & H_{2^i} \\ H_{2^i} & -H_{2^i} \end{pmatrix}, \tag{3.3}$$

and $H_{2^0} = 1$. Also in terms of matrix elements

$$(H_N)_{m,n} = \frac{1}{\sqrt{N}} (-1)^{a \cdot b} \tag{3.4}$$

where $a \cdot b = \sum_{i=1}^K a_i \, b_i$ and $m = \sum_{i=1}^K a_i 2^{i-1}$, $n = \sum_{i=1}^K b_i 2^{i-1}$, that is a and b are vectors whose entries are the binary expansions of the matrix positions (m, n). Note that H_N is such that $H_N^2 = I$, while $G_N^4 = I$, where I is the identity, and G_N is the discrete Fourier transform introduced in the previous chapter and with either periodic or antiperiodic boundary conditions ($\alpha = \beta = 0$ or $\alpha = \beta = 1/2$). therefore the spectrum of both these transforms, Hadamard and the Fourier are highly degenerate (± 1 for H_N, $\pm 1, \pm i$ for G_N).

Also notice that we can enumerate the columns of H_N (or rows, as it is a symmetric matrix) as outer products of

$$v_0 = \frac{1}{\sqrt{2}} \begin{pmatrix} 1 \\ 1 \end{pmatrix}, \quad v_1 = \frac{1}{\sqrt{2}} \begin{pmatrix} 1 \\ -1 \end{pmatrix} \tag{3.5}$$

If $n = a_{K-1} a_{K-2} \cdots a_0$ is its binary representation ($0 \leq n \leq 2^K - 1$), the n^{th} column V_n is the outer product

$$V_n = v_{a_{K-1}} \otimes v_{a_{K-2}} \otimes \cdots \otimes v_0. \tag{3.6}$$

While the first column V_0 is simply an uniform string of 1s, the last one V_{N-1} is the K-th generation of the Thue-Morse sequence, which will be defined shortly below.

If ϕ is an eigenstate of the quantum baker's map in the position representa-

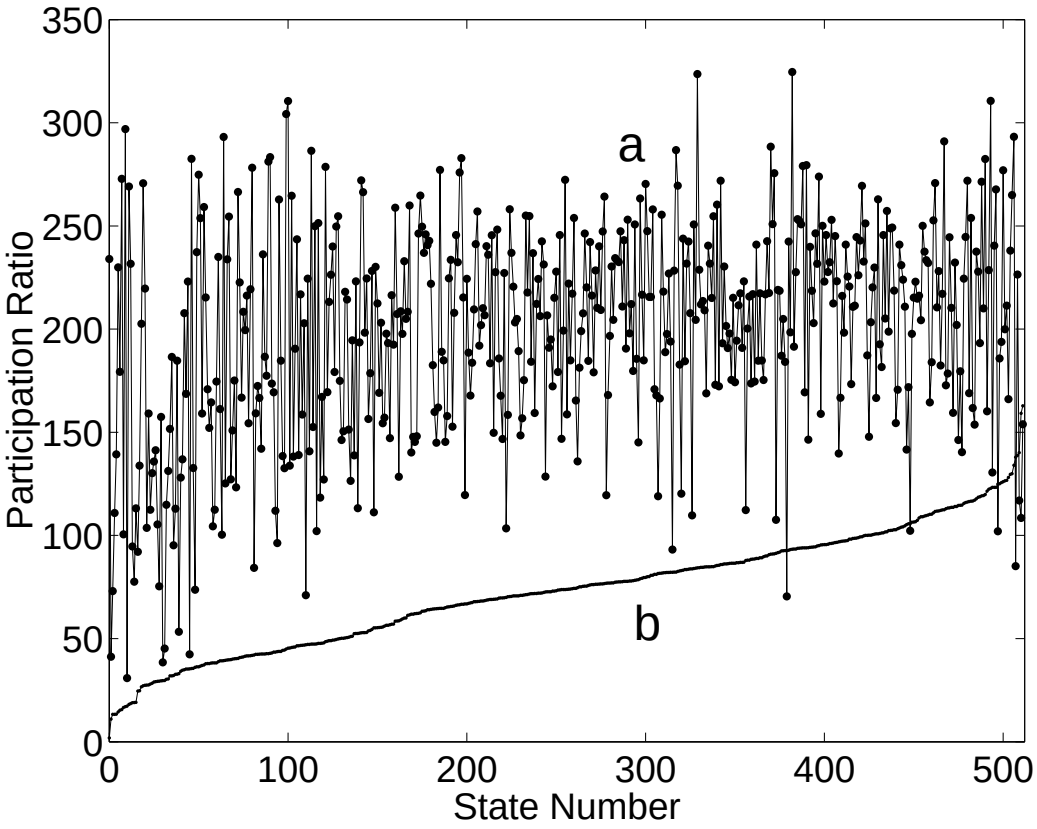

Figure 3.1: The participation ratio of the eigenstates of the quantum baker's map for $N = 512$ in the (a) position basis, and (b) Walsh-Hadamard basis. The states are arranged in increasing order of the latter number.

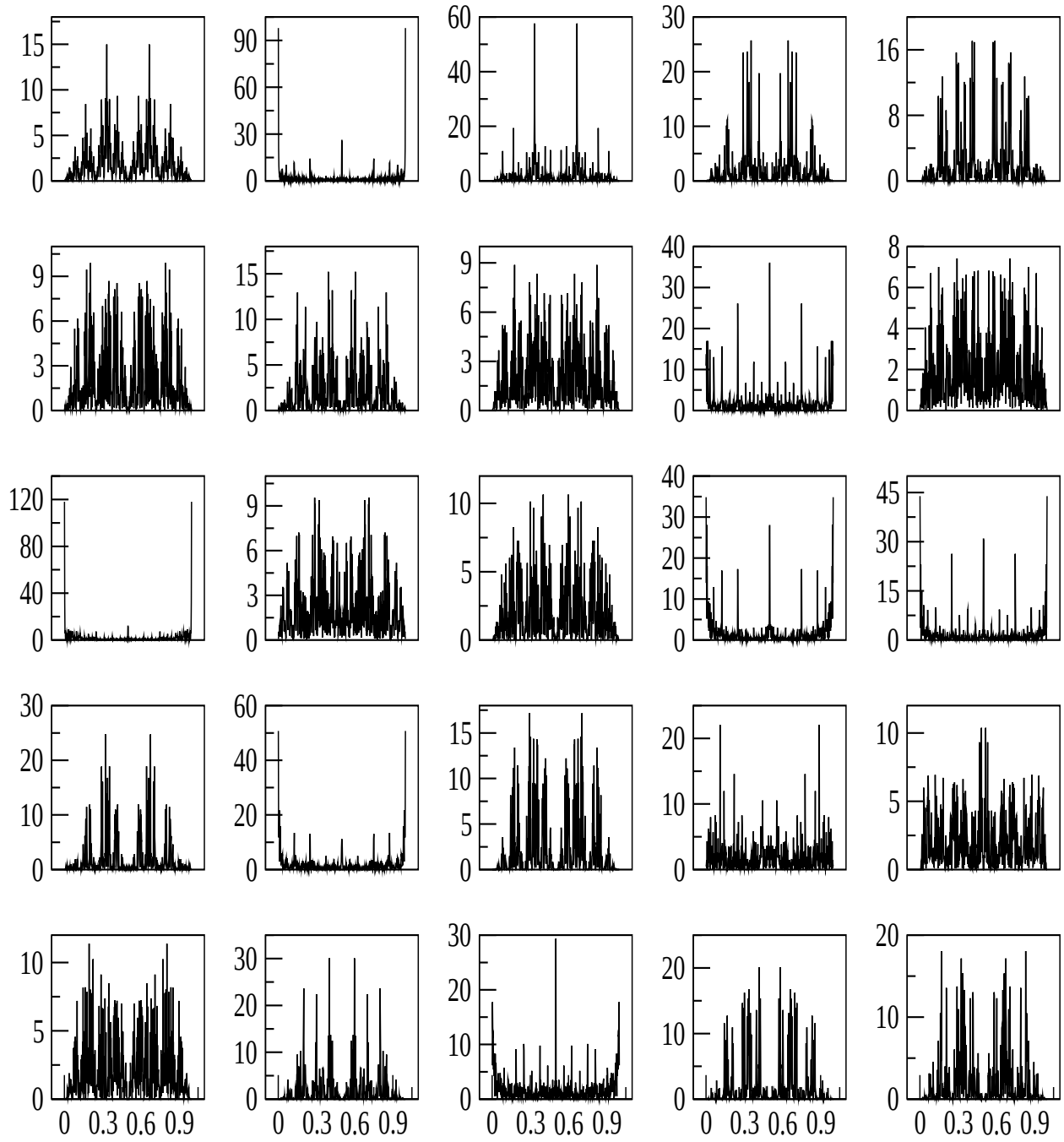

Figure 3.2: Intensities ($|\langle q_n|\phi_i\rangle|^2$) of first 25 eigenstates of the quantum baker's map for $N = 512$ in the position basis. Where $|\phi_i\rangle$ is i-th eigenstate of quantum baker's map. Intensities are multiplied by a factor of 1000 for clarity.

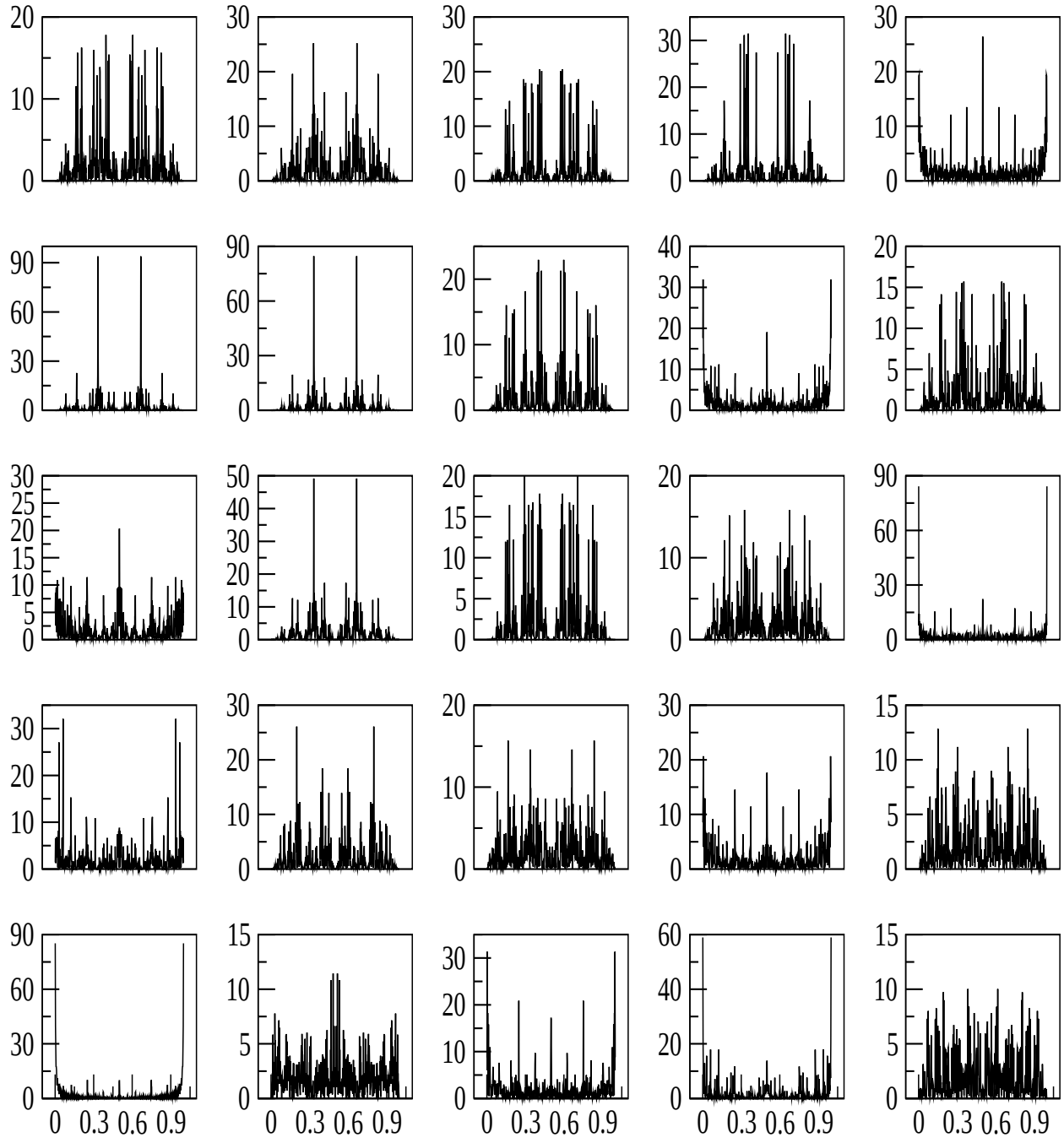

Figure 3.3: Intensities of second 25 eigenstates of the quantum baker's map for $N = 512$ in the position basis. Intensities are multiplied by a factor of 1000 for clarity.

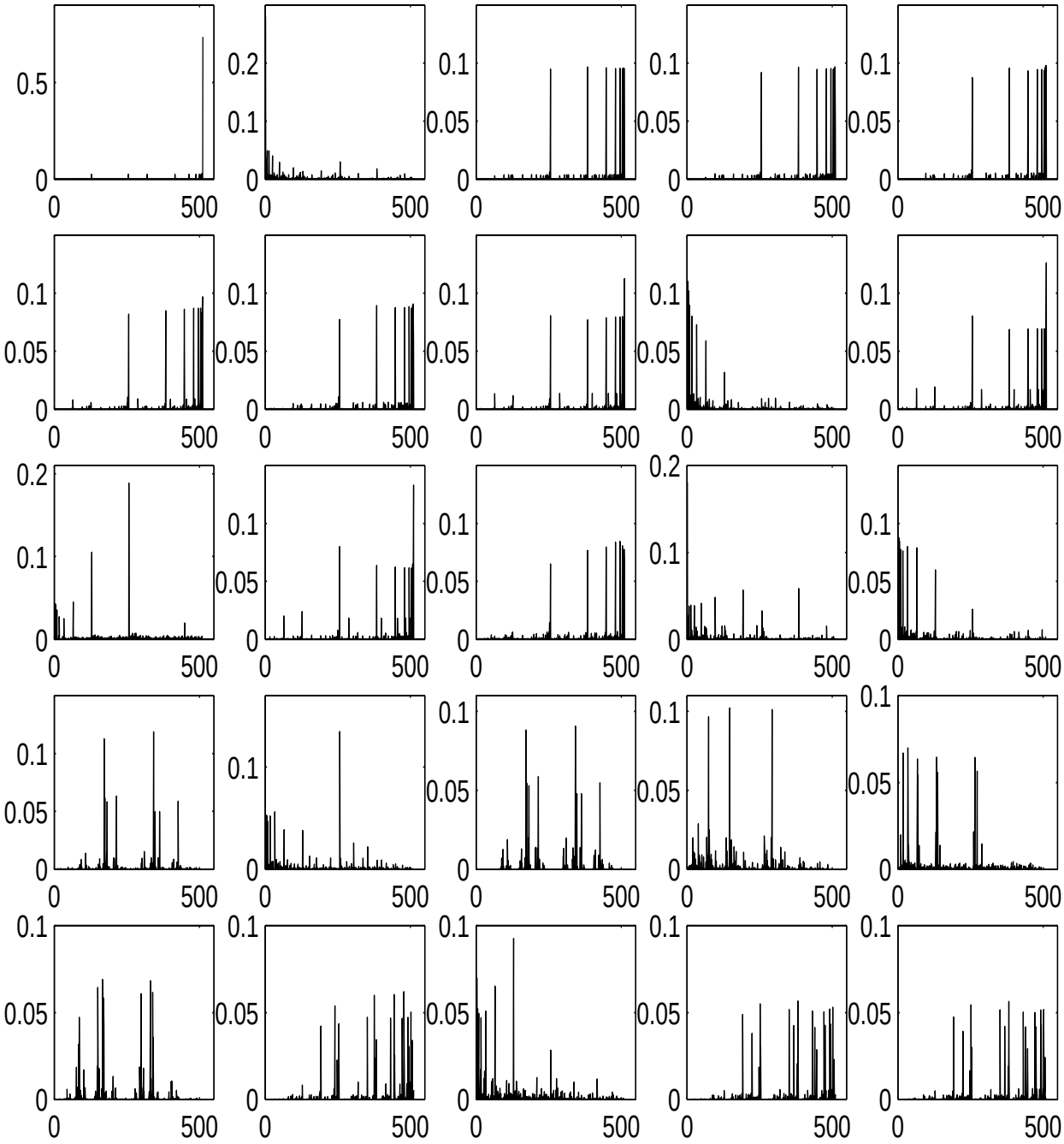

Figure 3.4: Intensities of first 25 eigenstates of the quantum baker's map for $N = 512$ in the WH basis.

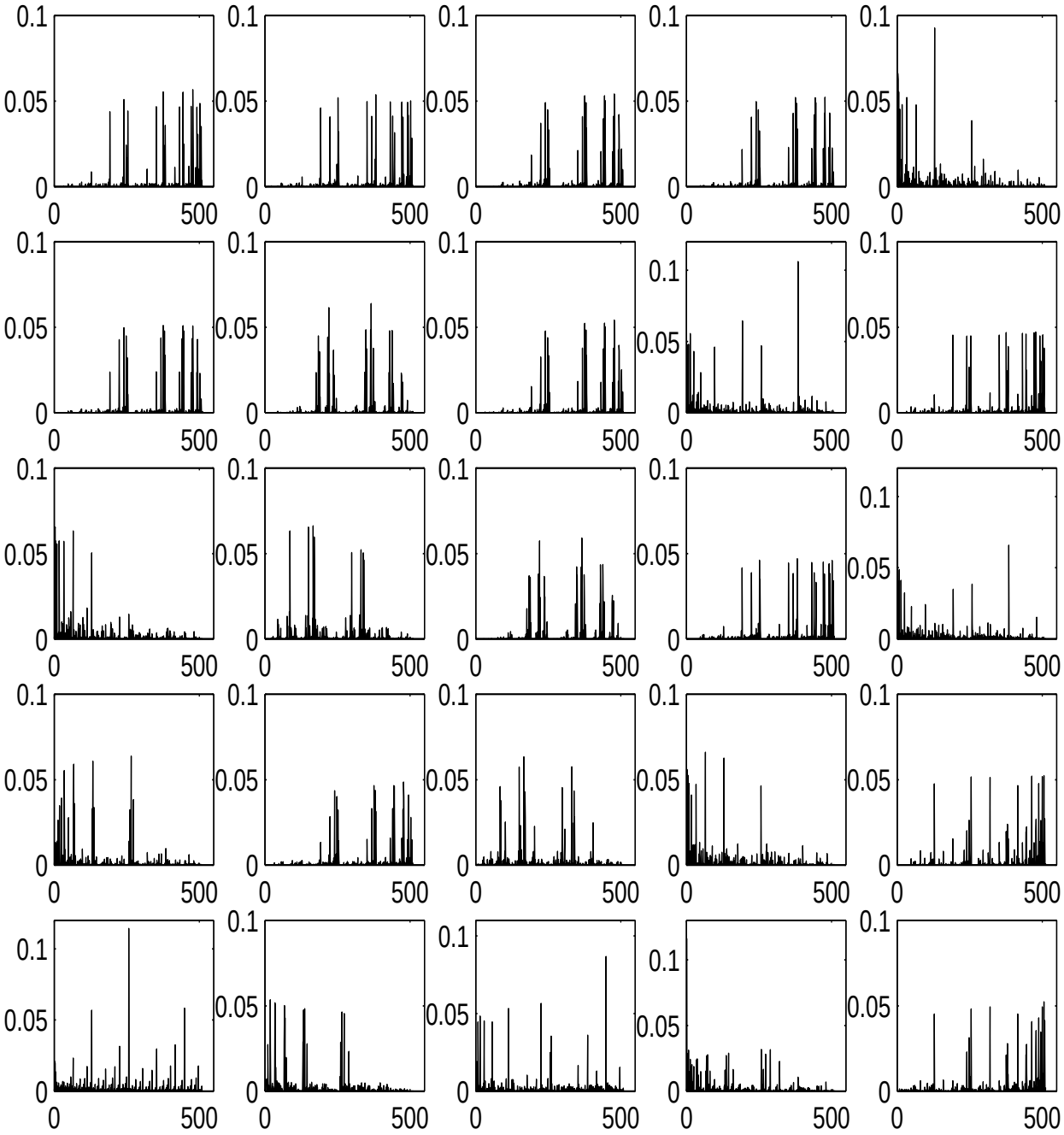

Figure 3.5: Intensities of second 25 eigenstates of the quantum baker's map for $N = 512$ in the WH basis.

tion we study it's Hadamard transform $H_N\phi$. Very significant simplifications are seen in this basis for almost all states. To quantify this "simplification" we calculate the number of principal components in the WH transform by means of the participation ratio PR_H which is

$$1/\sum_i |(H_N\phi)_i|^4 \tag{3.7}$$

In Fig. (3.1) we compare this participation ratio with that calculated in the original position basis. First 50 eigenstates of the quantum baker's map in the position basis are given in Fig. (3.2) and Fig. (3.3). Their WH transforms are shown in Fig. (3.4) and Fig. (3.5). These states are arranged according to their increasing participation ratio in the WH basis. What these figures show is the remarkable *compression* effected by the Hadamard transform on the quantum baker map's complicated eigenfunctions. If these were complex signals to be sent, it will make great sense to first Hadamard transform them. It is quite surprising that the Hadamard is effective on this quantum chaotic "signal". The amount of compression achieved is precisely the participation ratio.

3.2 The Thue-Morse state and an ansatz

For one remarkable class of states that is present for all N, PR_H is the smallest and of the order of unity, for example when $N = 1024$, $\mathrm{PR}_H = 1.96$ for this state. In contrast the participation ratio in position basis is about 427. That is a "compression" by a factor about 220! Of course this is the best case scenario. This class of states seems to have been identified by the original quantum baker's Balazs and Voros [19], as the eigenvalue is very close to $-i$. What we find is that the WH transform reveals their simplicity and beauty; also enabling an understanding in terms of automatic sequences. In Fig. (3.2) are examples of these states, for various N where we also see their near self-similarity. As N increases the states seem to limit to a distribution. If the corresponding eigenvalue is $e^{i\pi\theta_{tm}}$, the eigen angle θ_{tm} is shown in the Table 3.1. It is remarkable that the eigen angle seem to limit to $-1/2$ in the large N limit, again strongly providing evidence for convergence of this particular state. We call these set of states, ϕ_{tm} the "Thue-Morse" states, as the principal peak in the Hadamard transform corresponds to the overlap with the final column (or row) of H_K which (apart from the factor $1/\sqrt{2^K}$) is the K-th generation of the Thue-Morse sequence.

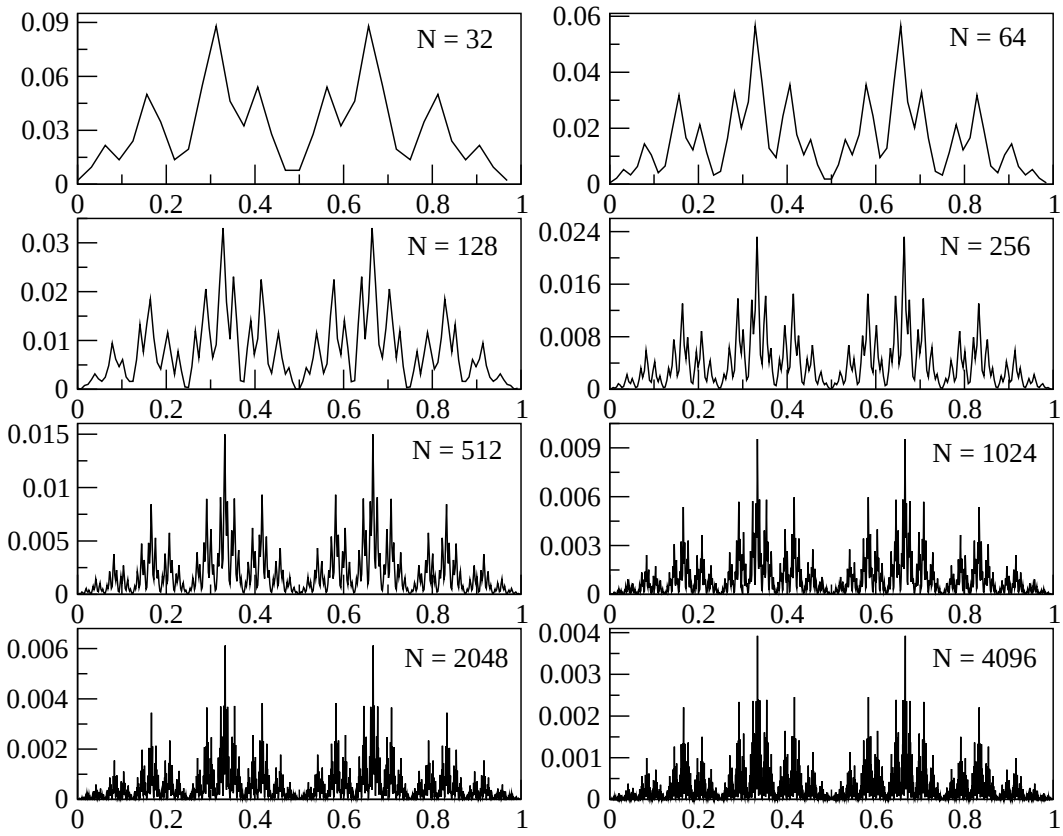

Figure 3.6: The intensities of the Thue-Morse states $|\langle n|\phi_{tm}\rangle|^2$ for $N = 2^K$ from $K = 5$ ($N = 32$) to $K = 12$ ($N = 4096$). The x-axis is the position eigenvalue n/N in all cases.

Table 3.1: Eigenangles θ_{tm} of the Thue-Morse states

N	θ_{tm}
32	-0.49985902
64	-0.50020232
128	-0.50002208
256	-0.50002275
512	-0.50000467
1024	-0.50000328
2048	-0.50000111
4096	-0.50000057
8192	-0.50000023

The Thue-Morse sequence

Sequences, especially integer sequences, have a fascinating variety in them. The interesting ones often have no apparent order, or their design is not obvious. The Thue-Morse sequence is one that is at the border of order and randomness, as we will see later. It was first studied by Axel Thue, a Norwegian mathematician, and one of the originators of the study of formal languages [85]. In 1906 he proved that there is an infinite sequence over two alphabets that did not contain three adjacent identical blocks, namely is *cube-free*. If the alphabet consists of two letters, say A and B, Thue showed that the sequence $ABBABAABBAABABBA\cdots$ is cube-free. This is the Thue-Morse sequence and can be generated as follows. Start with A, and proceed by the following substitution rules: $A \to AB$ and $B \to BA$. Thus the sequence inflates exponentially, 2^n being the number at generation n. The sequence is the infinite sequence corresponding to $n = \infty$. It is quite clear the sequence is not square-free, but Thue showed that this is cube-free, by showing that it has no overlaps. If w is any word containing a finite number of alphabets, what Thue showed was that nowhere in the sequence does the string wwa occur where a is the first letter of w, in this case one of A or B. It obviously follows then that there are no cubes. The corollary that Thue was interested in was that there exists an infinite word with three alphabets that is it is *square-free*; there is no appearance of a ww anywhere, where w is arbitrary string. Despite the complexity of the sequence, the fact that it is cube-free implies strong short and long range correlations.

This sequence of Thue was rediscovered by several people including Marston Morse in 1921 [86]. It also has a predecessor in the work of the French mathematician Prouhet who in 1851 posed an arithmetic problem whose solution involved this sequence. Thus the sequence is also called the "Prouhet-Thue-Morse" sequence and a very readable account of this is in the paper [87]. The inflation rules also make the Thue-Morse sequence a Lindenmayer or L-system. Such rules can be iterated to "grow" fractals, tilings and plant like objects [88]. The self-similar character of the sequence is best revealed by the sequence reproducing itself after striking off every other member. Replace the alphabet A by 0 and B by 1. The number

$$0.0110100110010110\cdots$$

interpreted as a binary number is called the Thue-Morse constant. This is clearly a *non-normal* number, in the sense that not all strings of 0 and 1, with a fixed length, occur with equal frequency. It has been proven by Dekking to be a transcendental

number, and is an indirect indication of the complexity of the sequence.

From the point of view of dynamical systems the Thue-Morse constant generates an interesting orbit under the shift or doubling map: $x \mapsto 2x \,(\mathrm{mod}\, 1)$. This orbit is clearly not dense on the interval $[0, 1)$ as it is not generated from a normal number. Yet it does not asymptote to a periodic orbit. It is an example of a uniformly recurrent by not ultimately periodic orbit. It is recurrent in the sense that it returns arbitrarily close to any of its orbit positions in a finite time. In fact Morse discovered the sequence as the symbolic dynamics of geodesic flows on surfaces of negative curvature that are recurrent without being ultimately periodic. This sequence indeed occurs in numerous contexts [87], and is marginal between a quasiperiodic sequence and a chaotic one. The deterministic disorder of this sequence is relevant to models of quasicrystals [89] and mesoscopic disordered systems [90], and as we show here quantum chaos. We believe that this is the first time it has emerged naturally in a quantum mechanical problem, rather than being assumed. Much more can be said of this fascinating sequence, but we will leave this for now and get back to its specific relevance to the quantum baker's map eigenfunctions.

The finite generations of the infinite Thue-Morse sequence is of interest to us. We will use as "alphabets" $1, -1$. At generation number K let the Thue-Morse sequence be the set t_k, consisting of elements $t_k(n)$ where $0 \leq n \leq 2^k - 1$. The finite generations are constructed as follows: start with $t_0 = \{1\}$ and generate $t_1 = \{1, -1\}$ by appending $\overline{t_0}$ to t_0, where the overbar is multiplication by -1, and we continue to iterate the rule $t_{k+1} = \{t_k, \overline{t_k}\}$. At stage K we get t_K a string of length 2^K, which we also treat as a column vector whose n-th element we denote as $t_K(n)$. The concatenation rule above is then equivalent to the generating rules:

$$t_K(2n) = t_{K-1}(n), \quad t_K(2n+1) = -t_{K-1}(n). \tag{3.8}$$

These generating rules will prove to be crucial below.

The Thue-Morse sequence as an approximate eigen vector

We now prove that t_K is an approximate eigen vector of the quantum baker's map. We note that while the Thue-Morse sequence is a string of 1 and -1 we would like to treat it as a normalized vector and so while using it as a vector we will normalize it with the factor of $1/\sqrt{2^K} = 1/\sqrt{N}$. However there are times when we will be sloppy and talk of this normalized vector as the Thue-Morse sequence. It is useful

to define the following:

$$\omega_{nm} = e^{2\pi i(n+1/2)(m+1/2)/N}. \tag{3.9}$$

Note that this includes the phases due to the anti-periodic boundary conditions. We have from a direct use of the definition of the BVS quantum baker that

$$(B\,t_K)_l = \frac{\sqrt{2}}{N}\left(\sum_{n=0}^{N/2-1}\omega_{ln}\sum_{m=0}^{N/2-1}\omega_{nm}^{-2}t_K(m) + \sum_{n=N/2}^{N-1}\omega_{ln}\sum_{m=N/2}^{N-1}\omega_{nm}^{-2}t_K(m)\right). \tag{3.10}$$

In the first part of the above equation as m ranges only up to $N/2-1$ $t_K(m)$ can be replaced with $t_{K-1}(m)$, as succeeding generations contain the previous. To be more precise the first half of generation K is identical to the whole of generation $K-1$. In the second part also we wish to shift the m index to the range $[0, N/2-1]$. Hence we use that $t_K(m+N/2) = -t_K(m)$ valid in this range. The second half of generation K is the *negative* of what was in generation $K-1$. After shifting the summations in the second part to the first half and using that N is an even integer we get after some algebra that

$$(B\,t_K)_l = \frac{\sqrt{2}}{N}\left(\sum_{n=0}^{N/2-1}\omega_{ln}\sum_{m=0}^{N/2-1}\omega_{nm}^{-2}t_{K-1}(m) - e^{i\pi(l+1/2)}\sum_{n=0}^{N/2-1}\omega_{ln}\sum_{m=0}^{N/2-1}\omega_{nm}^{-2}t_{K-1}(m)\right). \tag{3.11}$$

Collecting terms and writing explicitly

$$(B\,t_K)_l = \frac{\sqrt{2}}{N}(1-e^{\pi i(l+1/2)})\sum_{m=0}^{N/2-1}t_{K-1}(m)\sum_{n=0}^{N/2-1}e^{2\pi i(n+1/2)(l-2m-1/2)/N}. \tag{3.12}$$

Doing the n sum and simplifying we get

$$(B\,t_K)_l = \frac{2\sqrt{2}}{N}\times\frac{i}{2}\sum_{m=0}^{N/2-1}t_{K-1}(m)\left(\frac{1}{\sin(\frac{\pi}{N}(l-2m-1/2))}\right). \tag{3.13}$$

Till this point there has been no approximations, now we start making some crude, and uncontrolled, approximations that will serve us well. For large N, $\sin(\frac{\pi}{N}(l-2m-1/2)) \approx \frac{\pi}{N}(l-2m-1/2)$

$$(Bt_K)_l \approx \frac{\sqrt{2}i}{\pi}\sum_{m=0}^{N/2-1}\frac{t_{K-1}(m)}{(l-2m-1/2)} \tag{3.14}$$

The summand sharply peaks at $m = l/2$, or $m = (l-1)/2$ depending on if l is

even or odd. There are also significant contributions from the values of m that are neighbors, which we will ignore. Then using only the *single* term in the sum above is equivalent to the approximation that $1/(l-2m-1/2) = -2$ for $m = l/2$ and zero elsewhere when l is even and $1/(l-2m-1/2) = 2$ for $m = (l-1)/2$ and zero elsewhere when l is odd. Hence we get

$$\begin{aligned}(Bt_K)_{2m} &\approx -i\frac{2\sqrt{2}}{\pi}\, t_{K-1}(m) \;=\; -i\frac{2\sqrt{2}}{\pi} t_K(2m) \\ (Bt_K)_{2m+1} &\approx i\frac{2\sqrt{2}}{\pi}\, t_{K-1}(m) \;=\; -i\frac{2\sqrt{2}}{\pi} t_K(2m+1)\end{aligned} \tag{3.15}$$

where crucial use is made finally of the generating rules in Eq. (3.8). Thus indeed

$$(B\, t_K)_m \approx -i(2\sqrt{2}/\pi)\, t_K(m). \tag{3.16}$$

The eigenvalue we get has a modulus $\left|2\sqrt{2}/\pi\right| \approx 0.90$. We note that the numerically obtained eigenvalue of the Thue-Morse state is very close to $-i$ and seems to converge to in the semiclassical limit. That we get about $-0.9i$ for the eigenvalue using these crude approximations is quite remarkable.

The Fourier transform of the Thue-Morse sequence

The Thue-Morse sequence (of infinite length) has a Fourier spectrum that is know to be singular continuous and a multifractal. What has been studied in the literature so far is the usual Fourier transform. We are interested in the quantum baker's map to study the generalized Fourier transform (with phases, especially with $\alpha = \beta = 1/2$) and to study it for finite sequences. This will turn out to provide an alternate and complementary route. In the process we also note a very interesting difference between the usual Fourier transform and the generalized transform of the Thue-Morse sequence.

To begin with we prove a very useful product formula. Our aim is to find $G_N\, t_K$. We use yet another possible definition of the Thue-Morse sequence as the parity of integers, namely the parity of the number of 1's in the binary expansion of n is $t_K(n)$. If $n = \sum_{j=0}^{K-1} 2^j a_j$ then

$$t_K(n) \;= \frac{1}{\sqrt{N}}\, (-1)^{\sum_{j=0}^{K-1} a_j} \tag{3.17}$$

$$
\begin{aligned}
(G_N\, t_K)_m &= \frac{1}{N}\sum_{n=0}^{N-1}\omega_{mn}^{-1}(-1)^{\sum_{j=0}^{K-1}a_j} \\
&= \frac{1}{N}e^{-\pi i(m+1/2)/N}\sum_{a_{K-1}=0}^{1}\cdots\sum_{a_0=0}^{1}\prod_{j=0}^{K-1}e^{-2\pi i(m+1/2)2^j a_j/N}(-1)^{a_j}.
\end{aligned}
\tag{3.18}
$$

Now we can interchange the product and the sum and do the sums over each bit as they do not mix. This leads to

$$
\begin{aligned}
(G_N\, t_K)_m &= \frac{e^{-\pi i(m+1/2)/N}}{N}\prod_{j=0}^{K-1}\left(1-e^{-2\pi i(m+1/2)2^j/N}\right) \\
&= (-1)^{m+1}\,(i)^{K+1}\prod_{j=0}^{K-1}\sin[\pi 2^{j-K}(m+\frac{1}{2})].
\end{aligned}
\tag{3.19}
$$

As similar product formula without the additional $\frac{1}{2}$ in the phase due to the anti-periodic boundary conditions is well known to limit to a multifractal measure as $K\to\infty$. It is remarkable that such a simple trigonometric product formula has such an interesting structure. For a recent historical and mathematical review of products of sines ("duplicating sines") we refer to [91] where it is noted that while the duplicating product of cosines has this simple formula:

$$
\cos(x)\cos(2x)\cos(4x)\cdots\cos(2^n x)=\frac{\sin(2^{n+1}x)}{2^{n+1}\sin(x)},
\tag{3.20}
$$

no such simple formula exists for the product of duplicating sines.

We return to the quantum baker's map and in particular to the Thue-Morse state. We have proven that t_K is an approximate eigenstate of the map and hence is likely to be close to the Thue-Morse state $|\phi_{tm}\rangle$. For example we find numerically that when $N=2^9$, $|\langle t_9|\phi_{tm}\rangle|^2/N\approx 0.74$. We now prove that due to time-reversal symmetry $G_N\, t_K$ is as good an ansatz as t_K.

$$
G_N^{-1}|\phi_{tm}\rangle \;=\; -G_N^{-1}R_N|\phi_{tm} \;=\; \pm G_N^{-1}|\phi_{tm}\rangle
\tag{3.21}
$$

where we have used $G_N^2=-R_N$ and that $|\phi_{tm}\rangle$ is some definite parity state.

$$
\langle\phi_{tm}|G_N\, t_K\rangle=\pm\langle\phi_{tm}|G_N^{-1}|t_K\rangle=\pm\langle\phi_{tm}^*|t_K\rangle,
\tag{3.22}
$$

follows from time-reversal symmetry as $G_N|\phi_{tm}\rangle = |\phi_{tm}^*\rangle$. Since $|t_K\rangle$ is a real state it follows that the overlaps have the same modulus. Of course this is true for

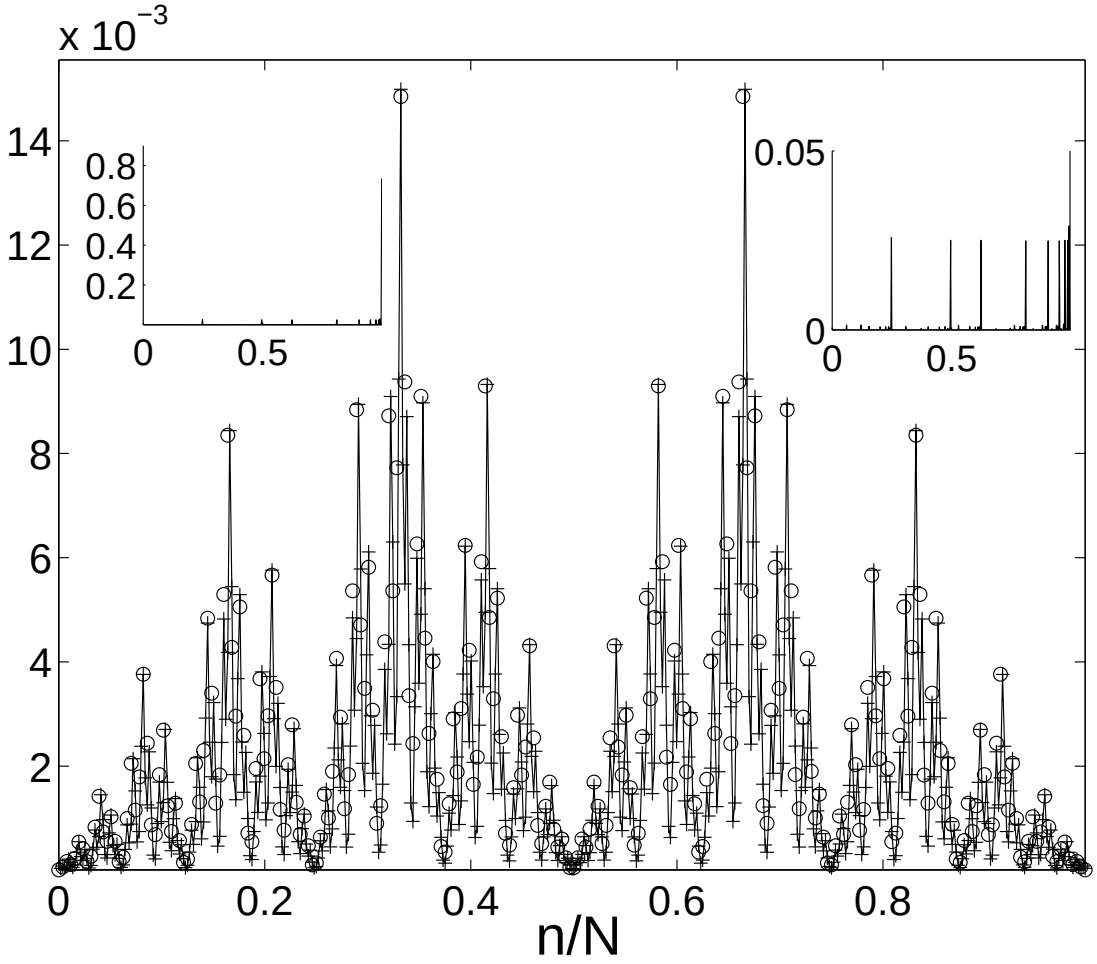

Figure 3.7: The intensity $|\langle q_n|\phi_{tm}\rangle|^2$ of the Thue-Morse state in the position representation. Shown are the states for $N = 512$ (plus) and $N = 256$ (circle) after the latter state was appropriately scaled. Also shown is the estimate ϕ^A_{tm} for $N = 512$ case (line). The left inset is the intensity of the WH transform of the Thue-Morse state for $N = 512$, while the right inset shows the same on a different scale.

any eigenstate of the quantum baker's map and is not special for the Thue-Morse state.

Also the product formula in Eq. (3.19) maybe used to prove that t_K is an approximate eigenstate using quite different approximations to get the same result. We need to prove that

$$G_N^{-1} \begin{pmatrix} G_{N/2} & 0 \\ 0 & G_{N/2} \end{pmatrix} t_K \approx \lambda\, t_K \tag{3.23}$$

for some constant λ. This implies that we need to prove that

$$\begin{pmatrix} G_{N/2}\, t_{K-1}/\sqrt{2} \\ -G_{N/2}\, t_{K-1}/\sqrt{2} \end{pmatrix} \approx \lambda G_N\, t_K \tag{3.24}$$

where use has been made of the concatenation property of the Thue-Morse sequence. The $\sqrt{2}$ factor comes from the different normalization of $t_{K-1}$and t_K. For $m \leq N/2 - 1$ we get using the product formula that

$$(G_N\, t_K)_m = i \sin\left[\frac{\pi}{2^K}\left(m + \frac{1}{2}\right)\right] \left(G_{N/2}\, t_{K-1}\right)_m . \tag{3.25}$$

The varying sin factor in the above equation forces us to make an approximation, which maybe said to be some kind of adiabatic one. The factor $\sin\left[\frac{\pi}{2^K}\left(m+\frac{1}{2}\right)\right]$ varies very slowly with m and has no oscillation as m varies from 0 to 2^{K-1}. Thus we replace this with its average value in this range:

$$\sin\left[\frac{\pi}{2^K}\left(m + \frac{1}{2}\right)\right] \approx 2\int_0^{1/2} \sin(\pi x)dx = 2/\pi. \tag{3.26}$$

We can similarly consider $m \geq N/2$ and arrive at the same result. The extra negative sign gets canceled. It then follows from Eq. (3.24) that $\lambda \approx -i\pi/(2\sqrt{2}) = -1.11i$. It is interesting that this approximation is in magnitude exactly the inverse of the one obtained previously.

The ansatz

While t_K and its Fourier transform are approximate eigenstates of the quantum baker's map, they dot have the full symmetries of the map. Taking into account these symmetries helps us do much better. It is easy to see that $R\, t_K = (-1)^K t_K$, and indeed the parity of the Thue-Morse state flips with each power of two. We note however that $G_N\, t_K \neq t_K^*$ and therefore t_K as such does not have the correct time-reversal symmetry. To take advantage of time-reversal symmetry we construct

$$\phi_0 = \gamma\, t_K + \gamma^* G_N^{-1} t_K \tag{3.27}$$

which satisfies $G_N\phi_0 = \phi_0^*$. It is straightforward to see that $G_N^{-1}t_K$ is also an approximate eigenstate of B. We determine numerically the complex constant γ such that ϕ_0 best approximates the state ϕ_{tm}. For example if $N = 512$, γ is predominantly real and just $\phi_0 = C\,(t_9 + G_{512}t_9)$ is such that $|\langle\phi_0|\phi_{tm}\rangle|^2 \approx 0.93$,

that is the state ϕ_{tm} is determined to more than 93% by the Thue-Morse sequence and its Fourier transform. C is a normalization factor and we have used that $G_{512}^{-1} t_9 = G_{512} t_9$. Thus the deterministic structural disorder of the Thue-Morse sequence is seen in a quantized model of a classically deterministic and fully chaotic system.

We note that we can improve upon the simple ansatz ϕ_0 above, by taking into account the second rung of peaks in the Hadamard transform of ϕ_{tm}, K easily identifiable peaks ($N = 2^K$), as seen for example in the right inset of Fig. (3.7). These second rung of peaks also result from the Fourier transform of the Thue-Morse sequence, but not exclusively. We introduce the notation $t_k^{(r)}$ for an 2^r-fold repetition of the Thue-Morse sequence of generation k, for example column number $2^{K-r} - 1$ of H_K is $t_{K-r}^{(r)}$. The improved ansatz for the Thue-Morse state is then

$$\phi_{tm}^A = \gamma_0 \phi_0 + \sum_{k=1}^{K} (\gamma_k \, + \, \gamma_k^* \, G_N^{-1}) S^{k-1} \, t_{K-2}^{(2)} \tag{3.28}$$

where S is the shift operator, and we again determine the complex constants γ_k numerically such that the ansatz is closest to the state.

Recall that the shift operator S, acts on the position basis as $S|q_n\rangle = |q_{2n}\rangle$ or $|q_{2n-N+1}\rangle$ depending on if $n < N/2$ or otherwise. We notice that S is "almost" B, only there is no momentum cut-off, as $\langle p_m|B|q_n\rangle = \sqrt{2}\langle p_m|q_{2n}\rangle$ for n and m both $\leq N/2-1$. Apart from other issues, discussed in the previous chapter, it does not respect time-reversal symmetry, in the sense that $G_N^{-1} S^* G_N \neq S^{-1}$. We can find γ_k such that $|\langle \phi_{tm}|\phi_{tm}^A\rangle|^2 \approx 0.998$, this is shown in Fig. (3.7). The emergence of the shift operator is unsurprising as it commutes with the Hadamard transform H_K, and is close to the quantum baker's map B. The Thue-Morse sequence t_K is an *exact* eigenstate of S and is hence a stand-alone state.

Multifractality

It is known that the support of the spectral measure of the infinite Thue-Morse sequence is a multifractal [92], thus it comes as no surprise that ϕ_{tm} has multifractal properties. We can study these either by comparing Thue-Morse states at different values of K or for a fixed K, by averaging over different sized bins. We perform a standard multifractal analysis [93] and see typical $f(\alpha)$ singularity spectrum. One simple diagnostic is the scaling of the inverse participation ratio (IPR). If ϕ_n denotes the position representation of the state ϕ, the IPR which is $\sum_{n=0}^{N-1} |\phi_n|^4$ scales as N^{-D_2}. When D_2, the correlation dimension, is such that

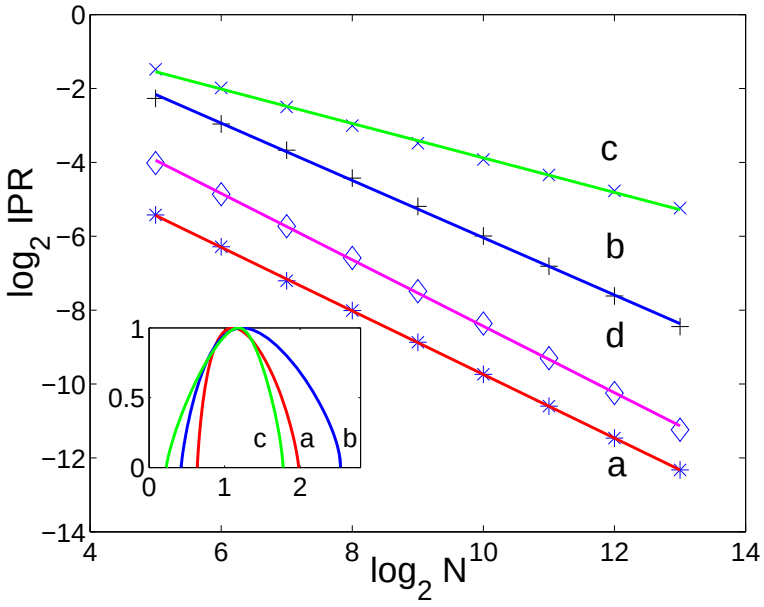

Figure 3.8: The scaling of the IPR in the position basis as a function of N. Shown as points are the numerical data, while the smooth curves are the best fit straight lines. The cases are: (a) the Thue-Morse state, (b) a period-2 scarred state, (c) fixed-point scarred state after projecting out the uniform state, and (d) average over all the states. The corresponding $f(\alpha)$ spectrums for the case $N = 8192$ are shown in the inset.

$0 < D_2 < 1$, the function is a multifractal, between localized states ($D_2 = 0$) and random states ($D_2 = 1$). This IPR and multifractal analysis is carried out in the physically relevant position basis. Either of the two procedures gives for the Thue-Morse state the dimension $D_2 \approx 0.86$, indicating its multifractal character. This scaling along with the full $f(\alpha)$ spectrum is shown in Fig. (3.8).

3.3 Other families of states

The Thue-Morse state is by far not the only one influenced by the Thue-Morse sequence. We now construct a family of strongly scarred states consisting of K members. The PR_H is low for these states also, for example when $N = 512$ $\mathrm{PR}_H \sim 15$. We identify this as a "family" based on the similarity of their PR_H and the shared position of the K principal peaks in their WH transform. For up to $N = 2^{13}$ we have verified that this family exists and has K prominent peaks, at $t^{(1)}_{K-1}$ and all its $K-1$ shifts, $S^k\, t^{(1)}_{K-1}$. Amongst this family, members are strongly scarred by period-2, period-4 and related homoclinic orbits. All the members of this family for $N = 512$ are shown in Fig. (3.9) and their WH transforms are shown

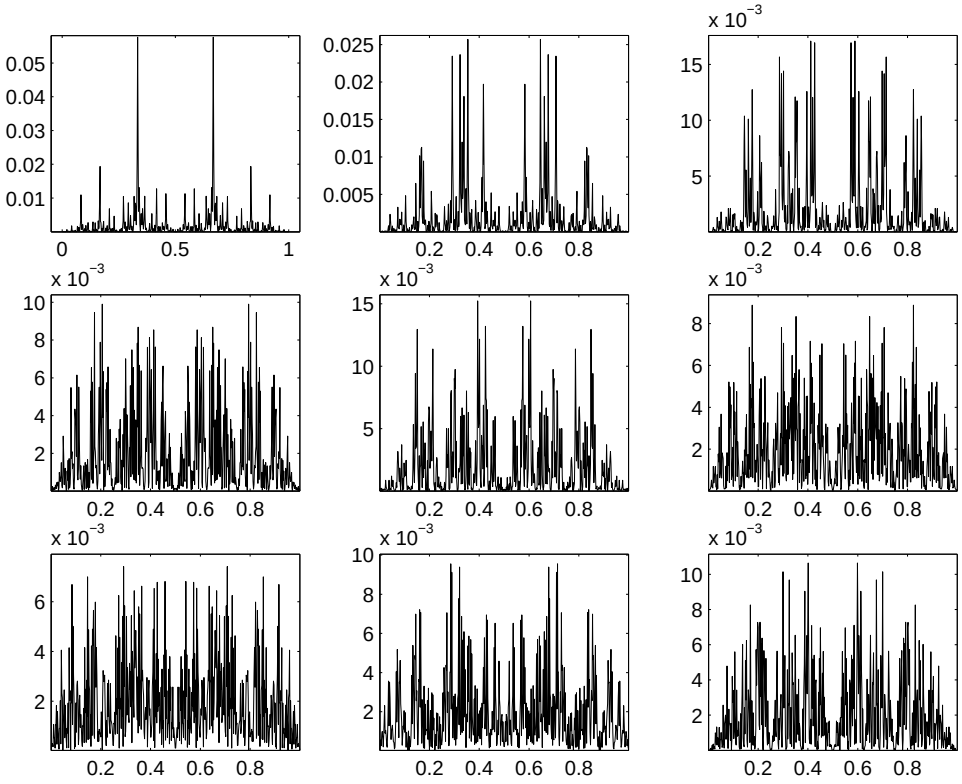

Figure 3.9: All members of the period-2 family discussed in the text for $N = 512$. Shown are the intensities in the position basis. The states in this family are scarred by the period-2 orbit, period-4 orbits and their homoclinic excursions.

in Fig. (3.10). We call these family of states as period-2 family of states since its first member of this family is strongly scarred by period-2 orbit of the classical baker's map. Taking time-reversal symmetry into account we may then write an approximate expression for this family of states based on K vectors, similar to the one above for the Thue-Morse state. For example for $N = 512$ this procedure enables us to reproduce the state strongly scarred by the period-2 orbit up to more than 95% and most of the family to similar accuracy. The existence of such families may be indicative of systematics of periodic orbit scarring.

This strongly scarred state and its family members also have multifractal properties, and indeed $D_2 \approx 0.8$ for the period-2 scarred state (Fig. (3.8)). We have identified other families, but we now turn to the state that is strongly scarred by the fixed point $(0, 0)$ and whose WH transform is strongly peaked, indeed corresponding to $t_0^{(K)}/\sqrt{2^K}$, that is simply the uniform state. This also forms a series, for different N, whose eigen angles are close to zero. Since the Fourier transform of the uniform state given above tends to a constant (independent of N) at the origin (and at 1), we expect the scarred state to be dominated by this "Bragg peak". In order to see any multifractal character even in this state we project

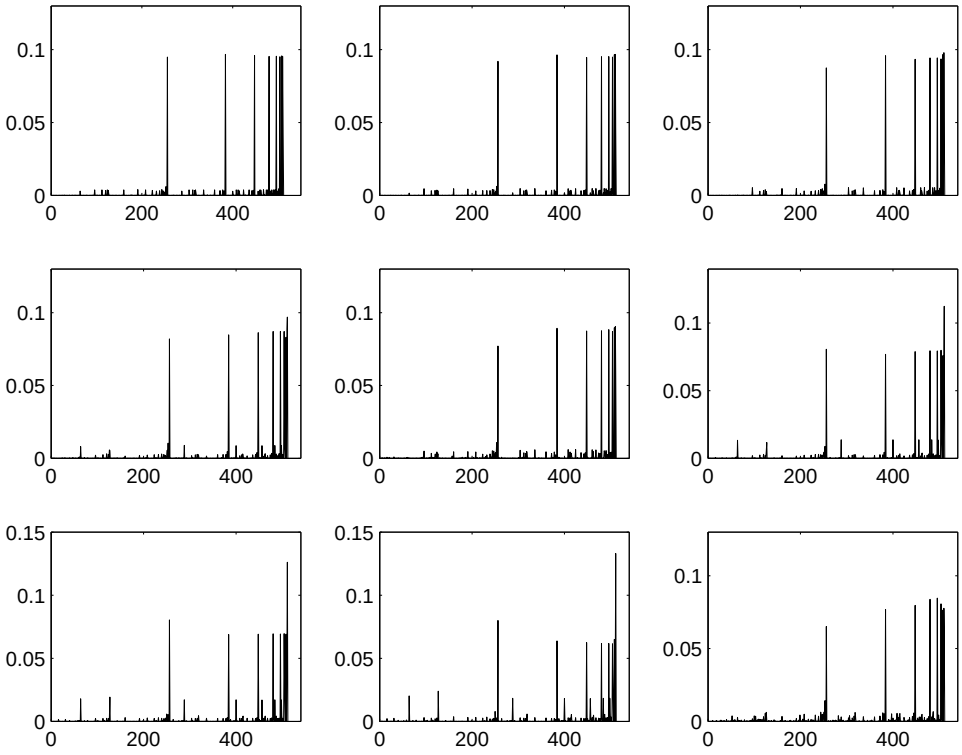

Figure 3.10: The intensities in the Walsh Hadamard basis for the family displayed in Fig. (3.9)

$t_0^{(K)}$ out of its WH transform and analyze the resultant state (after renormalizing) in the position basis. This shows that the "grass", even in this strongly scarred state, is a multifractal with a value of $D_2 \approx 0.45$, as shown in Fig. (3.8), where the $f(\alpha)$ spectrum for the fixed point and period-2 scarred states are also shown conforming to those expected of multifractals. For a gross measure of the multifractality of the entire spectrum, we averaged the IPR (in the position basis) of all the states and found a scaling with $D_2 \approx 0.9$, that is shown in Fig. (3.8).

Phase-space representations of the states

Classical structures in quantum states are clearly seen in their phase-space or coherent state representations [20] which is shown in Fig. (3.11) for the Thue-Morse states we have discussed above. Note the self-similarity of the four states shown here, the two different types of intricate structures arise from the alternating parity of these states. These states are dominated by the period-2 orbit and its associated homoclinic and heteroclinic structures. Phase-space representations for the period-2 family of states, scarred by both the period-2 and period-4 orbits along with orbits homoclinic to them, are given in Fig. (3.12).

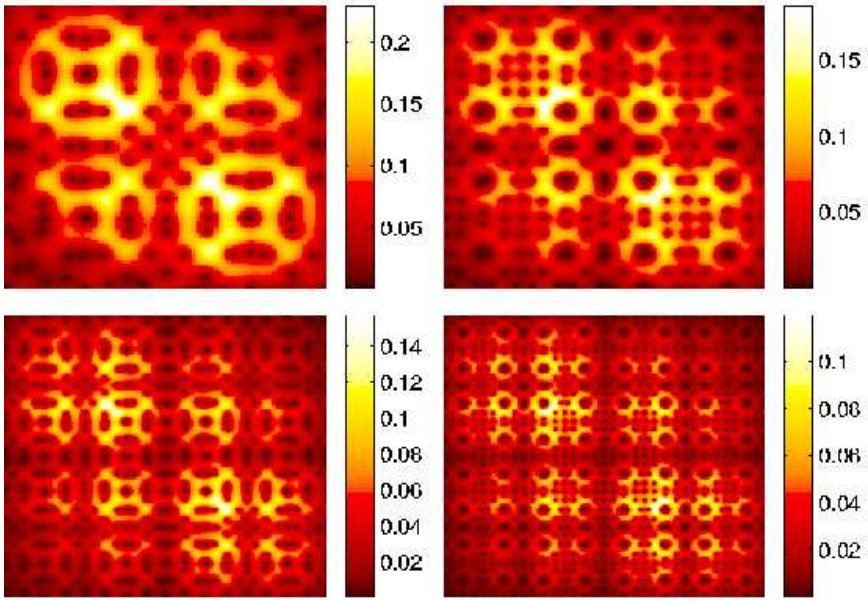

Figure 3.11: The density plots of $|\langle qp|\psi\rangle|$ on the unit phase-space square for the Thue-Morse state in the cases $N = 128$, 256, 512, and 1024 (left to right, top to bottom).

3.4 The Fourier transform of the Hadamard transform

We indicated earlier that the Fourier transform of the Thue-Morse sequence, along with the sequence itself was an excellent ansatz for a class of eigenstates in the quantum baker map, which we called the "Thue-Morse states". We also found that the Fourier transform of some *other* columns of the Hadamard transform played a crucial role in describing other states, as well as for better approximations to the Thue-Morse state itself. The Fourier transform of the Thue-Morse sequence [92, 94], or some of the other columns of H_N are not simple functions though, they could be multifractals [93]. Of course the Fourier transform of the first column V_0 is just a localized delta peak (which maybe broadened for nonzero phase factors in the generalized transform); thus we expect that the Fourier transform of the Hadamard matrix will result in a mixture of functions or measures with a range of complexity. This is our primary motivation for studying the product $G_N H_N$, the Fourier transform of the Hadamard transform. We then connect this to some further eigenstates of the quantum baker's map.

The matrix elements of $G_N H_N$ are evaluated economically as a product of K

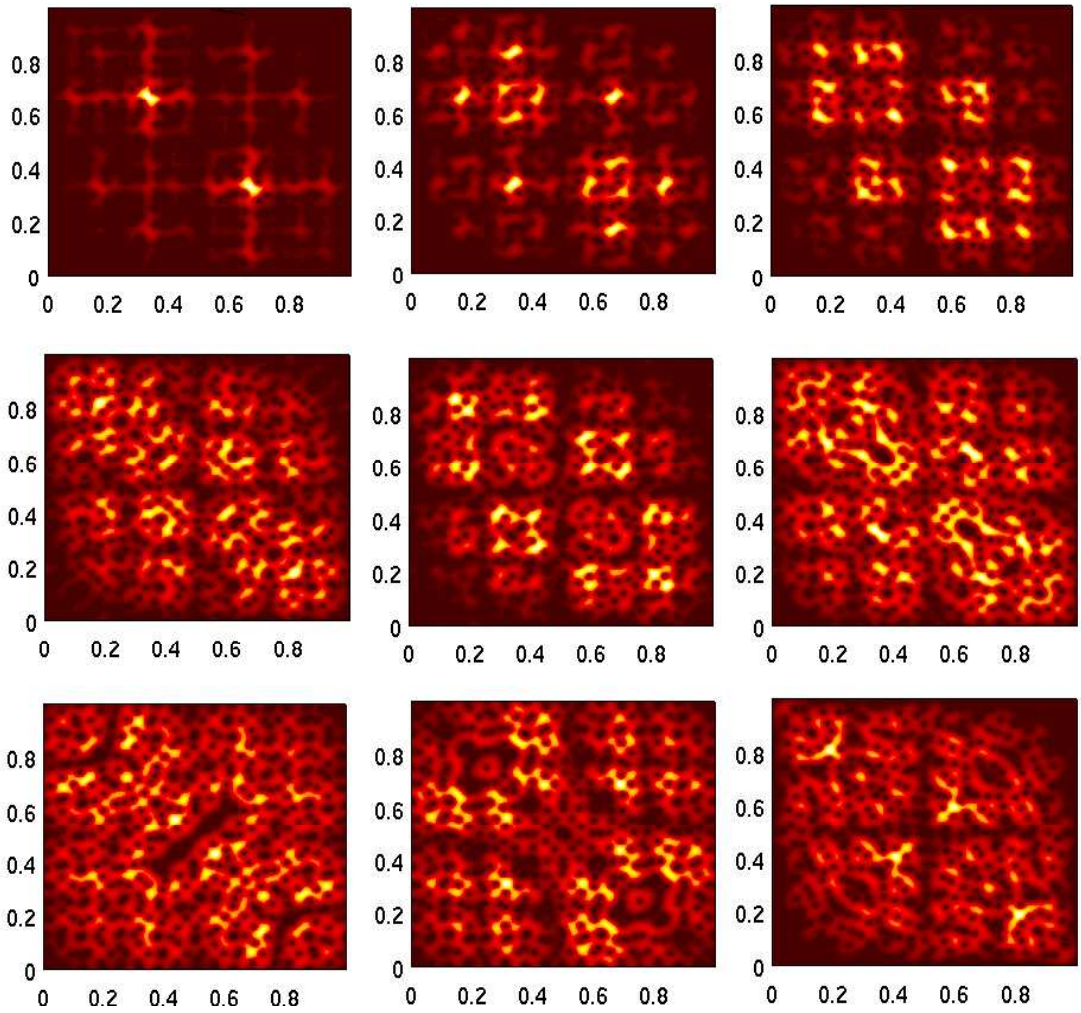

Figure 3.12: The density plots of $|\langle qp|\psi\rangle|$ on the unit phase-space square for the family of states displayed in Fig. (3.9).

trigonometric terms. Using the matrix representations of G_N and H_N we get

$$(G_N H_N)_{kn} = \frac{1}{N} \sum_{l=0}^{N-1} e^{-2\pi i (k+\alpha)(l+\alpha)/N} \, (-1)^{\sum_{j=0}^{K-1} b_j a_j} \tag{3.29}$$

where $l = \sum_{j=0}^{K-1} 2^j b_j$, and $n = \sum_{j=0}^{K-1} 2^j a_j$. Thus performing the independent sums over the b_j, and after some simplifications, we get

$$\begin{aligned} (G_N H_N)_{kn} = \quad & e^{-i\pi(k+\alpha)(N-1+2\alpha)/N} \, e^{-i\pi \sum_{j=0}^{K-1} a_j/2} \, \times \\ & \prod_{j=0}^{K-1} \cos\left[\frac{\pi}{N}(k+\alpha)2^j + \frac{\pi}{2} a_j\right] \end{aligned} \tag{3.30}$$

Thus we are led to the study of the following class of functions which are power spectra's of the columns of the Hadamard matrix: $|(G_N V_n)_k|^2 = |(G_N H_N)_{kn}|^2 \equiv f_n(k)$

$$f_n(k) = \prod_{j=0}^{K-1} \cos^2\left[\frac{\pi}{N}(k+\alpha)2^j + \frac{\pi}{2} a_j\right] \tag{3.31}$$

We view these as a function of k for a fixed $n = a_{K-1} a_{K-2} \cdots a_0$. They satisfy the normalization, that follows from the unitarity of $G_N H_N$,

$$\sum_{k=0}^{N-1} f_n(k) = 1 \tag{3.32}$$

and we will in fact treat $f_n(k)$ as a probability measure. We are interested in the limit $N \to \infty$ (or $K \to \infty$). If there exist sequences of n that lead to limiting distributions we are especially interested in these. In the following we use the notation that $(s)_m$ is an m-fold repetition of the binary string s. If n is of this form we also denote $f_n(k)$ as $f_{(s)}(k)$. For instance the case when $n = N-1 = (1)_K$ leads to the power spectrum of the Thue-Morse sequence that is well-known to limit to an multifractal measure [92]. In this case

$$f_{(1)}(k) = \prod_{j=0}^{K-1} \sin^2\left[\frac{\pi}{N}(k+\alpha)2^j\right]. \tag{3.33}$$

This has been particularly studied when $\alpha = 0$ and found to limit to a multifractal with a correlation dimension $D_2 = 0.64$ [92].

3.5 The participation ratio or the correlation dimension

To probe the limiting functions, if they exist, for multifractality we test for the scaling relation

$$P_n^{-1} = \sum_{k=0}^{N-1} f_n^2(k) \sim N^{-D_2}. \tag{3.34}$$

The left hand side of this is also interpreted as the inverse participation ratio, its inverse, P_n, being the effective spread of the power spectrum, an estimate of the number of "frequencies" (k) that participate in it. If D_2=0, the frequencies are localized (Bragg peaks of crystallography), if D_2=1, it is a situation expected of power spectra's of random sequences. In the intermediate range are multifractals, with structures at many scales.

Consider the class of functions that result as K tends to ∞ along even numbers, and $n = (01)_{K/2}$. Equivalently $n = (N-1)/3$, and the functions are $f_{(01)}(k)$. We also simultaneously consider the closely related functions $f_{(10)}(k)$. Both these tend to multifractal measures as $K \to \infty$ with $D_2 \approx 0.57$. The principal peaks of $f_{(10)}(k)$ are at $1/5, 4/5$, while those of $f_{(01)}(k)$ are at $2/5, 3/5$. Taken together these peaks constitute a *period-4* orbit of the doubling map $x \mapsto 2x \,(\mathrm{mod} 1)$. The peaks of the Fourier transform of the Thue-Morse sequence, or of $f_{(1)}(k)$ are at the period-2 orbits of the doubling map, i.e. at $1/3, 2/3$. We see these and a few other such functions in Fig. (3.13). The scaling of the participation ratio of these measures and the corresponding correlation dimension are shown in Fig. (3.14), which shows that indeed these measures are multifractals. In the case of strings of the form (001) for instance, K is taken to be multiples of 3 and so on. One interesting observation from this figure is that it appears that the more 1 there are in the string s, the more is the dimension D_2, so that the power-spectrum of the Thue-Morse sequence may have the maximum possible D_2 value in this class of multifractals. Of course the string $(0)_K$ is not a multifractal at all, and $D_2 = 0$ in this case.

For a given N, the participation ratio P_n of the Fourier transform for the various columns n, has a range of values that indicates the localization in the conjugate basis. We show in Fig. (3.15) the participation ratios for the case $N = 1024$ and $\alpha = 1/2$. We see here the intricate way in which the columns of the Hadamard matrix are arranged. The largest participation ratio occurs for the last column of the Hadamard matrix which corresponds to the Thue-Morse sequence.

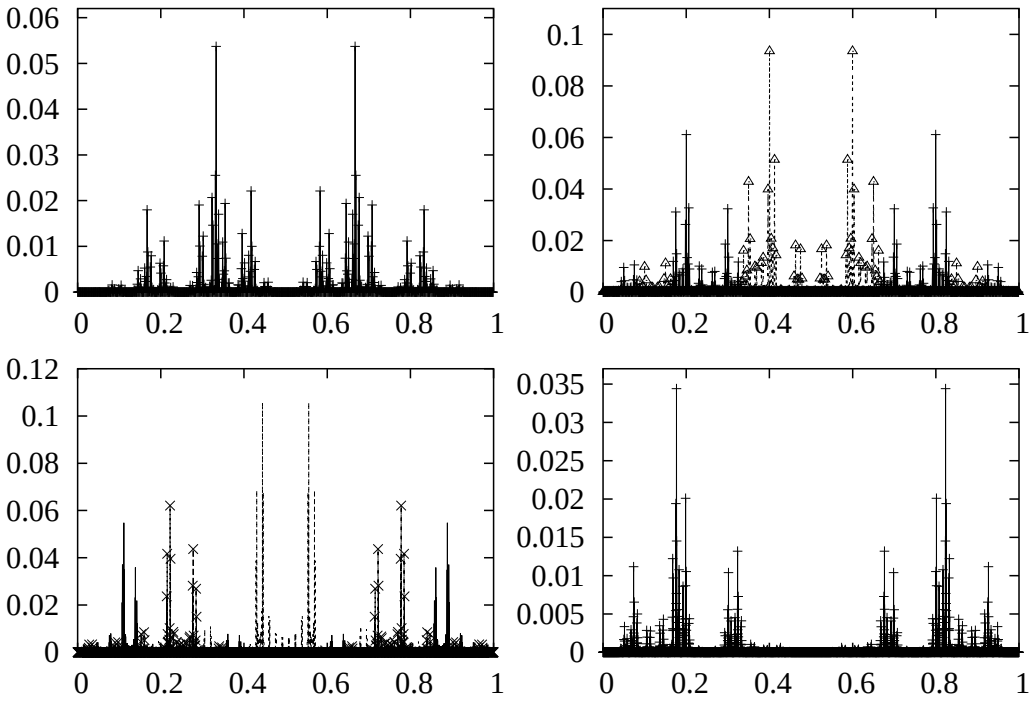

Figure 3.13: The fractal measures $f_{(1)}$, $(f_{(01)}, f_{(10)})$, $f_{(1110)}$, $(f_{(001)}, f_{(010)}, f_{(100)})$ are plotted clockwise. $K = 10$ in the first case and $K = 12$ in the others, while $\alpha = 0$ uniformly. We have grouped some functions and shown them in different styles in the figure.

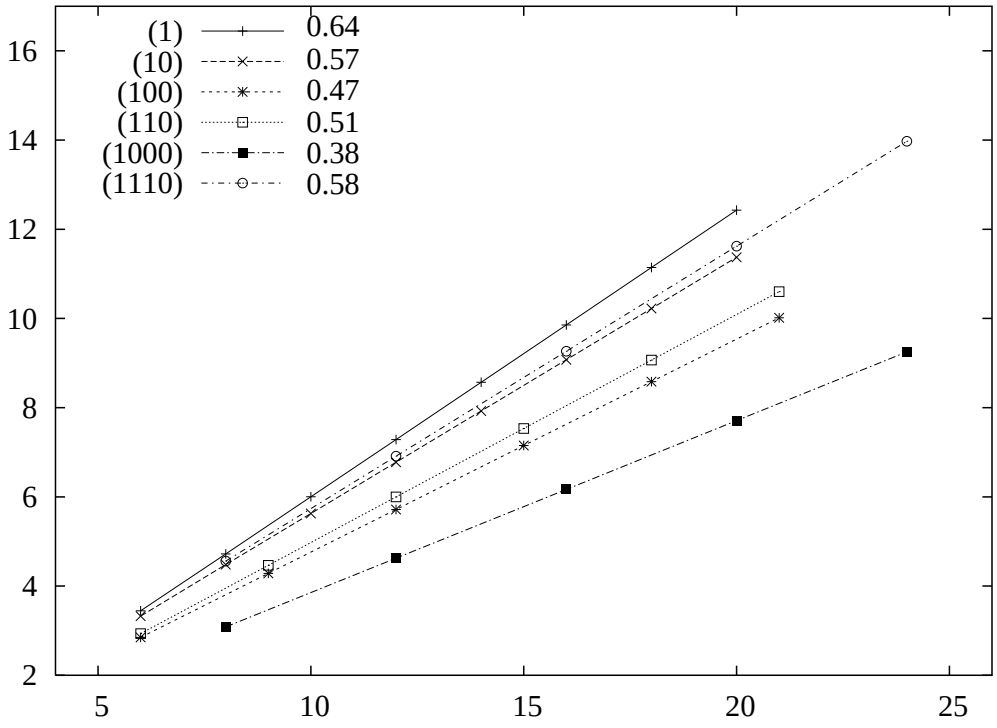

Figure 3.14: The scaling of the participation ratio P_n with N. $\log_2(P_n)$ is plotted against $\log_2(N) = K$, and $n = (s)_m$, where the string s is given in the key to the figure, and m is a whole number such that K/m is the length of the string s. The slopes of the lines are also given in the key.

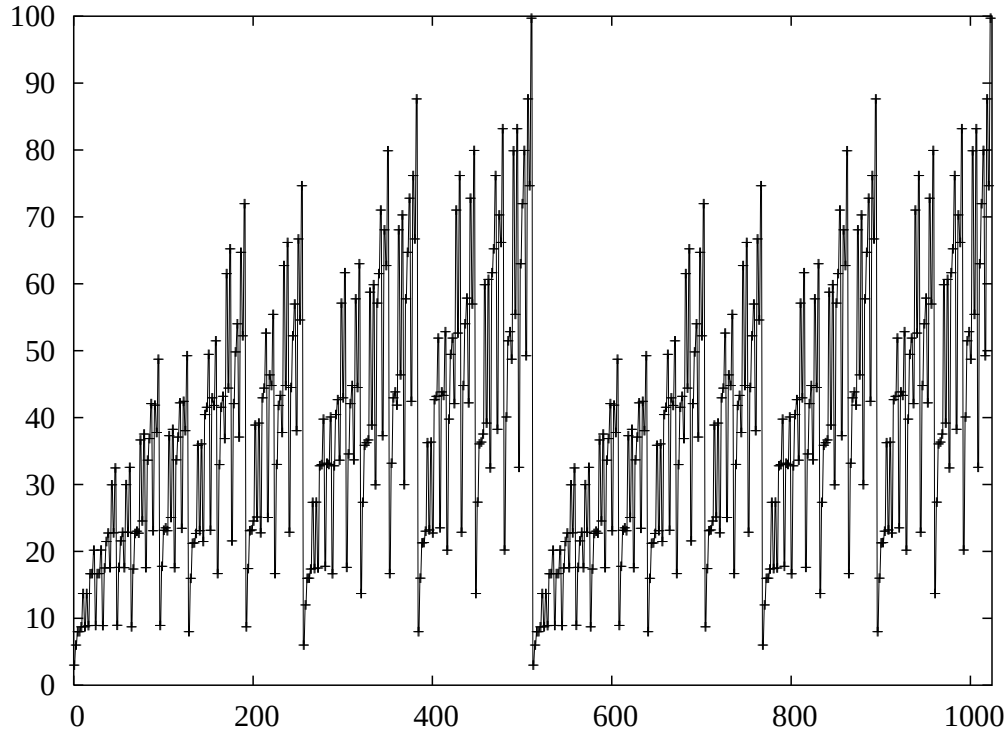

Figure 3.15: The participation ratio P_n vs n for $N = 1024$ and $\alpha = 1/2$.

We find a similar behaviour for other values of α, as well as other measures of localization such as the entropy. We include this parameter as for the application we have in mind, namely the quantum bakers map, $\alpha = 1/2$ is pertinent.

We now briefly discuss the sequence whose power spectrum is $f_{(01)}(k)$. Recall that the corresponding sequence for $f_{(1)}(k)$ was the Thue-Morse sequence $\{1, -1, -1, 1, -1, 1, 1, -1, \cdots\}$. The n-th term of this sequence is $t_n = (-1)^{\sum_{i=0}^{K-1} a_i}$ where again the a_i are bits of the binary expansion of n. Similarly the n-th term of the sequence whose power spectrum is $f_{(01)}(k)$ is

$$t_n = (-1)^{\sum_{i=0,2,\ldots} a_i}. \tag{3.35}$$

The first few terms of this sequence are $\{1, -1, 1, -1, -1, 1,$
$-1, 1, 1, -1, 1, -1, -1, 1, -1, 1, -1, 1, -1, 1, -1, 1, \ldots\}$. To write an concatenation rule we use the fact that this is formed by repeated outer product of $(1, -1, 1, -1)^T$ and get

$$S(k+1) = S(k)\overline{S(k)}S(k)\overline{S(k)} \tag{3.36}$$

Where $S(k)$ is the k-th generation of the sequence, with $S(0) = 1$, and $\overline{S(k)}$ is the complementary set where 1 and -1 are interchanged. While we found similar rules and sequences elsewhere [95], we did not find this exact one. It also appears that the inflation rules $A \to ABAB,\ B \to BABA$ produces this sequence.

3.6 Connections to quantum baker's map

So far we have introduced the measure and discussed some of their mathematical properties. Here we make explicit their relevance to quantum baker's map. Above we have proposed a few ansatz for a variety of eigenstates of quantum baker's map based upon the Thue-Morse sequence and its Fourier transform. Recall that these could sometimes reproduce states to more than 99%. Now we point to other measures such as $f_{(01)}$ that also play a role in the spectrum of the quantum baker's map.

In Fig. (3.16) we see two examples of states of the quantum baker's map in the position basis for $N = 1024$, along with their Hadamard transforms. The Hadamard transforms are particularly simple, the Thue-Morse state, ψ_{tm}, being the first. We show it here for comparison with another state whose Hadamard transform has distinct peaks at around $N/3$ and $2N/3$ implying that it is likely that the measures $f_{(01)}$ and $f_{(10)}$ discussed above are relevant for these states.

There are usually more than one such state, we show here a particularly "clean" state, in terms of its Hadamard transform, and for the purpose of this thesis call it $\psi_{(01)}$.

Indeed we can construct the ansatz

$$\phi = (\gamma_1 + \gamma_1^* G_N^{-1})\, V_{(N-1)/3} + (\gamma_2 + \gamma_2^* G_N^{-1})\, V_{2(N-1)/3} \tag{3.37}$$

where N are powers of 4. This includes both the columns at $(N-1)/3$ and $2(N-1)/3$, *along with their Fourier transforms*. The latter are included due to the presence of time-reversal symmetry. In fact they dominate the state and is the motivation for our study. This ansatz has two complex constants γ_1 and γ_2 which we determine numerically so that its overlap with the actual state $\psi_{(01)}$ is the maximum. For instance in the case $N = 64$, we were able to find γ such that the overlap $|\langle\phi|\psi_{(01)}\rangle|^2 \approx 0.75$. A comparison of the spectral measures for the Thue-Morse sequence, as well as $f_{(01)}$ and $f_{(10)}$ in Fig. (3.13) with the actual eigenfunctions in Fig. (3.16) show the similarity between them. Notice that the actual wave function is more closely related to the Fourier transforms of a linear combination of the columns of the Hadamard matrix. The peaks of this wave function can be identified with the period-4 orbit starting from $(q = 1/5, p = 4/5)$, and has been noted earlier the q part of this corresponds to the peaks in the measures $f_{(01)}$ and $f_{(10)}$.

We have concentrated on convergent measures as $n = (s)_m$ tends to infinity and s is a bit string repeated m times. We can have other sequences of n that lead to convergent measures, in particular those whose binary expansions ends in a string of 1 or 0. In the former case we have already used such measures to describe a family of states of the bakers map that are scarred by period-2, period-4 and associated homoclinic orbits. As spectral measures they are different depending on the finite string that precedes the infinite string of 1; however their correlation dimension D_2 seems to be the same as that of the spectrum of the Thue-Morse sequence, namely 0.64. As we noted earlier this seems to be consistent with our view that more the 1, more the dimension D_2. If the string a_i is itself not periodic, say when n is tending to infinity such that $n/2^K$ tends to an irrational number, there does not seem to be any convergent measures.

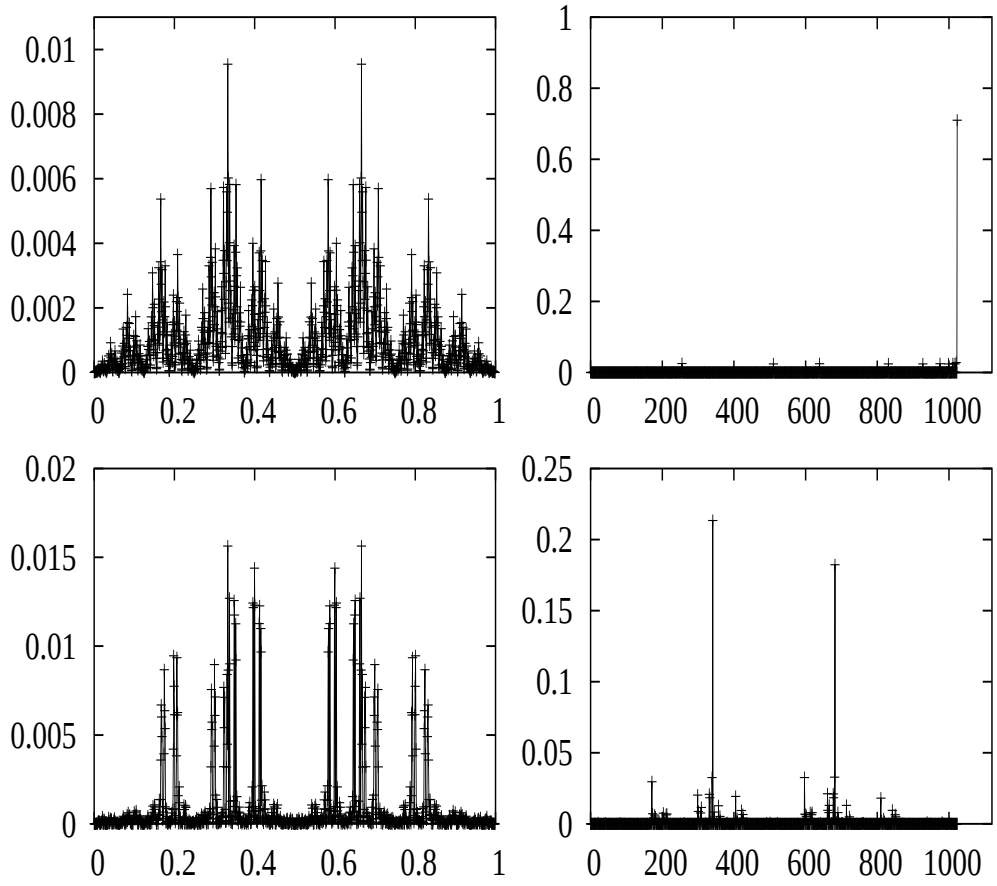

Figure 3.16: The Thue-Morse state ψ_{tm} (top left) and a state called in the text $\psi_{(01)}$ (bottom left), along with their corresponding Hadamard transforms (right). In this case $N = 1024$ and the peaks of the Hadamard transform of $\psi_{(01)}$ occur at $(N-1)/3$ and $2(N-1)/3$.

CHAPTER 4

A new transform nearly solving the Quantum baker's map

4.1 Introduction

We have pointed out in the last chapter that the Walsh-Hadamard (WH) transform (or simply the Hadamard transform) [23] simplified the eigenstates of the quantum baker's map considerably, the so-called "Thue-Morse" state being a particularly good, even spectacular, example of this. Further, it has been shown that the exactly solvable shift permutation operator, viewed as the quantization of cyclic shifts, was useful in constructing a relevant basis [77], especially for cases when N is *not* a power of 2. We connect these two observations here and explicitly point out the rationale for the emergence of the Hadamard transform in the context of the quantum baker's map, and therefore are able to *go beyond* by constructing a transform based on the Hadamard that simplifies the eigenstates of the quantum baker's map much more significantly. It is quite likely that the new unitary transform finds use in broader contexts since it combines the widely used discrete Fourier transform and the Hadamard transform in a novel manner.

Lakshminarayan studied S, zero-th order operator for the quantum baker's map, although there is no classical integrable "zero-th order" system for the baker's map [77]. As described in Chapter 2 it was also shown here how one can construct a quantum baker's map B_S that is very closely allied to the BVS quantum baker B, using S, thereby explaining this closeness. It may therefore be expected that the eigenstates of S form a basis in which the eigenstates of the quantum baker's map appear simple. Thus we seek to diagonalize the shift operator and use this as a basis to expand the eigenstates of the quantum baker's map.

However the spectrum of S is typically highly degenerate, especially when N is a power of 2, therefore we have multiple choices for the eigenstates. In [77] the N values studied were such that this lead to the smallest degeneracy possible. Specifically those N whose order modulo 2 is the largest possible value, $N-2$, have a nondegenerate spectrum save for two states with unit eigenvalues. The case when N is a power of 2 is however very interesting, as the eigenfunctions are well

simplified in light if the findings described in Chapter 3. Therefore it is natural that we seek to understand this case from the point of view that uses the shift operator essentially. To do this we make use of the symmetries of the shift operator especially the parity and time-reversal to "reduce" the eigenstates. The use of quantum symmetries is of course natural, and we note that in the case of quantum cat maps [15] the complete use of all quantum symmetries results in exactly solvable states that are ergodic and these have been called Hecke eigenfunctions [96].

4.2 Eigenfunctions of the Shift operator

We will denote the position eigenkets $|q_n\rangle$ simply as $|n\rangle$ and use this as a basis unless otherwise stated. We recall some properties of the shift operator S. By definition, it acts on the position basis as

$$S|n\rangle = \begin{cases} |2n\rangle & 0 \leq n < N/2 \\ |2n - N + 1\rangle & N/2 \leq n \leq N - 1. \end{cases} \tag{4.1}$$

Let $n = a_{K-1}a_{K-2}\cdots a_0$ be the binary expansion of n, so that

$$|n\rangle = |a_{K-1}\rangle \otimes |a_{K-2}\rangle \otimes \cdots |a_0\rangle, \tag{4.2}$$

where now the "qubit" states $|0\rangle$ and $|1\rangle$ are orthonormal basis states. In the standard representation

$$|0\rangle \doteq \begin{pmatrix} 1 \\ 0 \end{pmatrix}, \quad |1\rangle \doteq \begin{pmatrix} 0 \\ 1 \end{pmatrix}. \tag{4.3}$$

Of course the state $|0\rangle$ is not to be confused with the state $|n = 0\rangle$ which is actually $\otimes^K|0\rangle$. In the following we will not work with individual qubits states as such for this confusion to arise.

The action of the shift operator is then transparent:

$$S|n\rangle = |a_{K-2}\rangle \otimes |a_{K-3}\rangle \cdots |a_0\rangle \otimes |a_{K-1}\rangle. \tag{4.4}$$

Thus the quantum operator S embodies the left-shift action, by cyclically shifting the states from one qubit to its left "neighbour". It however re-injects the most significant bit at the least significant position, due to periodic boundary conditions, which ultimately naturally leads to periodicity. It is also helpful to think of S as

acting on the space $\{0,1\}^K$ consisting of binary strings of length K, which we denote generically by σ: $S(a_{K-1}a_{K-2}\cdots a_0) = a_{K-2}a_{K-3}\cdots a_0 a_{K-1}$.

The parity operator R introduced earlier, can be written as a pure K-fold tensor product on this space, so that it can be thought of as local action on the individual qubits.

$$R = \otimes^K \mathcal{R}, \quad \text{where} \quad \mathcal{R} = \begin{pmatrix} 0 & 1 \\ 1 & 0 \end{pmatrix}. \tag{4.5}$$

Thus the action on individual qubits is that of a flip. When considered as action on binary strings, $R(a_{K-1}a_{K-2}\cdots a_0) = \overline{a}_{K-1}\overline{a}_{K-2}\cdots\overline{a}_0$, where $\overline{0} = 1$ and $\overline{1} = 0$ are bit-flips. It is easy to see that S commutes with R. While there are uncountably many operators that commute with S (any operator of the form $\otimes^K \mathcal{A}$, where $\mathcal{A}$ is a 1-qubit operator, will commute with S), R also commutes with the usual quantum baker's map B, and is thus an important symmetry for constructing a basis that is close to that of the eigenfunctions of the quantum baker's map. The classical limit of the unitary operator S has been discussed earlier [77] and summarized in Chapter 2. It can also be thought of as quantizing a *multivalued* mapping that is hyperbolic [77], similar interpretations have been proposed for toy models of open bakers in [27]. However we continue to use it here only in so far as it enables us to understand the eigenstates of B.

It is particularly simple to diagonalize S in the case when $N = 2^K$. Let d be a divisor of K (including 1 and K). Let $\sigma = s_1 s_2 \cdots s_d$ be a *primitive* binary string of length d, representing strings consisting of all its cyclic shifts. For example there are 12 primitive strings of length 4, consisting of three cycles. We represent these three cycles with the strings $0001, 0011$, and 0111, chosen for convenience, to be the smallest when the cycle elements are evaluated as numbers. Let $\overline{\sigma}$ denote the string σ repeated K/d times and its value evaluated as a binary representation be k.

Then one set of eigenstates of S constructed from these cycles are:

$$|\tilde{\phi}_l^k\rangle = \frac{1}{\sqrt{d}} \sum_{m=0}^{d-1} e^{-2\pi i l m/d}\, S^m |k\rangle, \;\; 0 \le l \le d-1 \tag{4.6}$$

and the corresponding eigenvalue is $e^{2\pi i l/d}$ [77]. If there are $p(d)$ such primitive representative strings of length of d, then $\sum_{d|K} d\, p(d) = 2^K$, hence using the

Mobiüs inversion formula,

$$p(n) = \frac{1}{n} \sum_{k|n} \mu\left(\frac{n}{k}\right) 2^k. \tag{4.7}$$

Here $\mu(n)$ is the Mobiüs function [97], $\mu(n) = 0$ if n has a repeated prime in its prime factorization, otherwise it is $(-1)^r$, where r is the number of primes in its factorization, and $\mu(1) = 1$. Thus $|\tilde{\phi}_l^k\rangle$ form a complete and orthonormal set. Clearly there is degeneracy and this set is not unique. There is also freedom in the choice of the representative string σ, we will choose this to be the smallest integer when treated as a binary expansion. The eigen vectors arranged in columns of a matrix constitute an unitary transform which consists of direct sums of $p(d)$ Discrete Fourier Transforms (DFTs) of dimension d each. It may be written as:

$$T_f = \bigoplus_{d|K} \bigoplus_{p(d)} F_d \tag{4.8}$$

where F_d is a DFT of dimension d. For example if $K = 3$, the divisors are only 1 and 3, there are two subspaces of dimension 1 and two of dimension 3 corresponding to the cycles $\overline{0}$, $\overline{1}, \overline{001}, \overline{011}$. If the basis is arranged in the order 000, 001, 010, 100, 011, 110, 101, 111, we have chosen the first member of the cycle to be the smallest, the others are got by consecutive left-shifts, $T_f = F_1 \bigoplus F_3 \bigoplus F_3 \bigoplus F_1$.

4.2.1 Simultaneous eigenstates of parity and the shift operator

The vectors $|\tilde{\phi}_l^k\rangle$ are however not eigenstates of parity R. In order to construct this we find an unitary operator H of the form $\otimes^K \mathcal{H}$, so that it commutes with S, and such that $\mathcal{H}$ diagonalizes $\mathcal{R}$. This fixes

$$\mathcal{H} = \frac{1}{\sqrt{2}} \begin{pmatrix} 1 & 1 \\ 1 & -1 \end{pmatrix}, \tag{4.9}$$

and H as the Walsh-Hadamard transform. It follows that

$$RH = Ht, \quad t = \mathrm{diag}(1, -1, -1, 1, \ldots), \tag{4.10}$$

t is a diagonal matrix whose entries are the Thue-Morse sequence. We recall that its n-th term is $t_n = (-1)^r$, where $r = \sum_j a_j$ and a_j are the bits in the binary

expansion of n, and they satisfy the iterative rule:

$$t_{2n} = t_n, \;\; t_{2n+1} = -t_n, \;\; t_0 = 1. \tag{4.11}$$

Stated otherwise, the columns of the Walsh-Hadamard matrix H have parities that are arranged according to the Thue-Morse sequence.

Consider the orthonormal complete set $|\phi_l^k\rangle = H|\tilde{\phi}_l^k\rangle$. Since S and H commute, this is clearly an eigenstate of the shift S. That it is also a parity eigenstate follows from:

$$R|\phi_l^k\rangle = \frac{1}{\sqrt{d}} \sum_{m=0}^{d-1} e^{-2\pi i l m/d} \, S^m RH|k\rangle \; = \frac{1}{\sqrt{d}} \sum_{m=0}^{d-1} e^{-2\pi i l m/d} \, S^m Ht|k\rangle \; = t_k |\phi_l^k\rangle. \tag{4.12}$$

where we have used that R commutes with S and t_k is the k^{th} member of the Thue-Morse sequence. Thus:

$$S|\phi_l^k\rangle = e^{2\pi i l/d}|\phi_l^k\rangle, \;\; R|\phi_l^k\rangle = t_k|\phi_l^k\rangle, \tag{4.13}$$

We will also presently adapt these eigenstates to "time-reversal", however before that we notice that the plain Walsh-Hadamard transform shares some common rows with $\langle\phi_l^k|n\rangle$. For instance when $k = 0$ ($\sigma = (0)$) and when $k = N-1$ ($\sigma = (1)$) the rows $\langle\phi_0^0|n\rangle$ and $\langle\phi_0^{N-1}|n\rangle$ consisting of all ones, and the row with the Thue-Morse sequence respectively are common to the Hadamard matrix. Indeed since the Thue-Morse and closely allied sequence dominate the eigenfunctions of the quantum baker's map, the Hadamard transform works well in this context.

To be more explicit about the proposed transform we again illustrate with the case $K = 3$. Using the ordering described above, the structure of the transform is $1/\sqrt{2^3 \times 3} \times$

$$\begin{pmatrix} 1 & 1 & 1 & 1 & 1 & 1 & 1 & 1 \\ 1 & -1 & 1 & 1 & -1 & 1 & -1 & -1 \\ 1 & 1 & -1 & 1 & -1 & -1 & 1 & -1 \\ 1 & -1 & -1 & 1 & 1 & -1 & -1 & 1 \\ 1 & 1 & 1 & -1 & 1 & -1 & -1 & -1 \\ 1 & -1 & 1 & -1 & -1 & -1 & 1 & 1 \\ 1 & 1 & -1 & -1 & -1 & 1 & -1 & 1 \\ 1 & -1 & -1 & -1 & 1 & 1 & 1 & -1 \end{pmatrix} \begin{pmatrix} \sqrt{3} & & & & & & & \\ & 1 & 1 & 1 & & & & \\ & 1 & \omega & \omega^2 & & & & \\ & 1 & \omega^2 & \omega & & & & \\ & & & & 1 & 1 & 1 & \\ & & & & 1 & \omega & \omega^2 & \\ & & & & 1 & \omega^2 & \omega & \\ & & & & & & & \sqrt{3} \end{pmatrix}$$

where $\omega = e^{2\pi i/3}$. The second matrix is what we called T_f, the first is essentially

the Walsh-Hadamard matrix, *but for the rearrangement of the columns according to cycles*. Thus this transform which appears to be new, combines the DFT and the Hadamard transforms in an interesting way.

4.2.2 Time-reversal adapted states of the shift operator

The time-reversal symmetry of the quantum baker's map [20] is not the same as that of the shift S as $G_N S G_N^{-1} \neq S^{-1}$. Therefore we cannot have the eigenstates of S to be such that its Fourier transform is identical to its complex conjugate. However there is an analogous symmetry:

$$\mathsf{b}_0 S \mathsf{b}_0 = S^{-1}, \;\; \mathsf{b}_0 \left|a_{K-1}a_{K-2}\cdots a_0\right\rangle = \left|a_0 a_1 \cdots a_{K-1}\right\rangle. \tag{4.14}$$

Here b_0 is the bit-reversal operator, it reverses the significance of the bits in a binary string. Clearly $\mathsf{b}_0^2 = 1$. Its emergence is linked to the fact that the periodic points of the baker's map, are such that the position and momentum are bit-reversals of each other. Its connection to the Fourier transform is made even more closer in the context of the baker's map when we note that

$$B = (G_N^{-1})_0 \left(\mathbb{1} \otimes (G_{N/2})_1\right) \tag{4.15}$$

where the additional subscripts on the Fourier transform refer to the number of most significant bits that are left out while performing the transform, which is therefore a "partial Fourier transform" as defined by [60]. In particular $(G_N)_0$ is the full transform all the qubits and is therefore of dimensionality $N = 2^K$, while $(G_{N/2})_1$ transforms the $K-1$ least significant bits and has the dimensionality $N/2 = 2^{K-1}$, the first qubit is left unaltered. Analogously it is easy to see by acting on bit strings that

$$S = \mathsf{b}_0 \left(\mathbb{1} \otimes \mathsf{b}_1\right) \tag{4.16}$$

where b_k bit reverses the $L-k$ least insignificant bits, for example b_0 reverses the whole string.

The time-reversal symmetry of S then implies that eigenstates $|\psi\rangle$ of S may be chosen such that $\mathsf{b}_0|\psi\rangle = |\psi^*\rangle$, where the complex conjugation is done in the standard position basis. Now the state $|\phi_l^k\rangle$ need not be of this kind, therefore it is necessary to multiply by suitable phases or take appropriate linear combinations of them. Towards this end we define two bit strings σ and σ' shift-equivalent ($\sigma \sim \sigma'$) if one is the result of repeatedly applying the cyclic shift operator S to the other. There are two kinds of binary strings, we label them type-A and

type-B. If σ is a string of type-A then $\mathsf{b}_0\sigma \sim \sigma$, and it is otherwise of type-B. It is somewhat surprising that the smallest binary string of type-B is of length 6 and that there are only 2 of them: $110010, 110100$, apart from their cyclic shifts. It is easy to see that if σ is of type-B then $S^m\sigma$ is also of type-B for any integer m.

If σ (value k) is a string of type-A then there exists an integer p such that $S^p\sigma = \mathsf{b}_0\sigma$. Also we note that b_0 commutes with the Hadamard matrix H. Using these facts, a short calculation shows that if

$$|\psi_l^k\rangle = e^{i\pi lp/d}|\phi_l^k\rangle, \text{ then } \mathsf{b}_0|\psi_l^k\rangle = |\psi_l^{k\,*}\rangle. \tag{4.17}$$

Thus type-A strings give rise to states that are time-reversal adapted up to multiplication by a phase. If σ is of type-B, and its bit-reversal $\mathsf{b}_0\sigma$ evaluates to k', we note that $\mathsf{b}_0|\phi_l^k\rangle = |\phi_l^{k'\,*}\rangle$ and $\mathsf{b}_0|\phi_l^{k'}\rangle = |\phi_l^{k\,*}\rangle$. Therefore we can construct the linear combinations:

$$|\psi_l^{k\pm}\rangle = \frac{e^{-i\alpha_\pm}}{\sqrt{2}}\left(|\phi_l^k\rangle \pm |\phi_l^{k'}\rangle\right), \tag{4.18}$$

where $\alpha_+ = 0$ and $\alpha_- = \pi/2$, which are orthogonal and such that $\mathsf{b}_0|\psi_l^{k\,\pm}\rangle = |\psi_l^{k\,\pm\,*}\rangle$. Thus this way we can construct a transform whose elements are $\langle\psi_j|n\rangle$, where j labels all the parity and time-reversal adapted states of the shift-operator S. In practice we order binary strings in the following way: $0, 1, 10, 100, 110, 1000, 1100, 1110, 10000, 10100, \ldots$, such that if σ and σ' are two members on the list then σ or $\mathsf{b}_0\sigma$ are not shift-equivalent to σ'. Among the possible representatives we choose that which is *largest* when treated as a binary representation of an integer. Choosing the largest, as opposed to the smallest as in the previous case, gives us an unique increasing sequence that appears to be new. Given any $N = 2^K$, we choose from this list strings whose length are divisors of K. These would include strings of both type-A and type-B, in either case we construct a set of states based on the algorithm outlined above, finding p by inspection in the case of type-A strings.

In Fig. (4.1) we show ten of these states for the case $N = 32$, showing the simplest uniform state, the Thue-Morse sequence and eight other states that involve appropriate combinations of Fourier transforms of the columns of the Hadamard matrix.

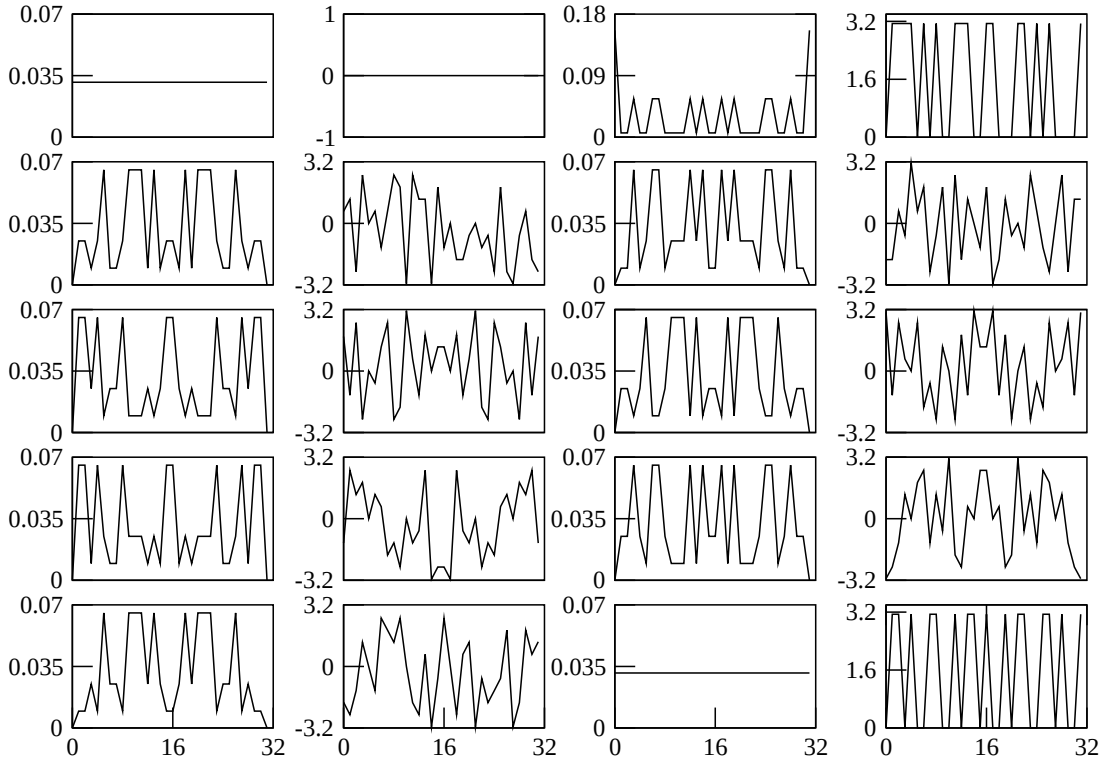

Figure 4.1: Ten basis states $|\psi\rangle$ that are simultaneous eigenfunctions of the shift operator, parity (bit-flip) and time-reversal (bit-reversal) for the case $N = 32$. Shown in the first and third columns are the intensities ($|\langle n|\psi\rangle|^2$) while the second and fourth columns have the corresponding phases. The first state is the uniform state, while the last has the Thue-Morse sequence as the components.

4.3 The eigenstates of the quantum baker's map in the new basis

If $|\Phi_k\rangle$ is an eigen vector of B then we refer to its representation in the position basis as **basis-0** ($\langle n|\Phi_k\rangle$), in the Hadamard basis as **basis-1** ($\langle n|H|\Phi_k\rangle$), in the parity adapted basis of the shift operator as **basis-2** ($\langle\phi_l^\sigma|\Phi_k\rangle$), in the parity and time-reversal adapted basis of the shift operator as **basis-3** ($\langle\psi_j|\Phi_k\rangle$).

In Fig. (4.2) we show 10 most simplified eigenfunctions for $N = 2^9 = 512$ using the new representations. For comparison we show the states in both basis-0 (position) and in basis-2. We found that for these states basis-3 did not yield further significant simplifications, we will presently quantify the degree of simplification across the spectrum. The state that is most simplified continues to be the Thue-Morse state which we have discussed in the previous chapter. Its transformation whether using the Hadamard or the new transformations continues to be dominated by the Thue-Morse sequence t_k. As we have pointed out earlier this state is well described by the ansatz $t_K + G_N\, t_K$, where t_K is the normalized Thue-Morse sequence of length $2^K = N$ treated as a vector. In other words the Thue-Morse sequence and its Fourier transform dominates the state.

The structure of the eigenstate is dominated by the Fourier transform of the Thue-Morse sequence, the peaks being much larger than $1/\sqrt{N}$. The peaks occur at the period - 2 orbit of the doubling map at $(1/3, 2/3)$ and at points corresponding to homoclinic orbits of this point. Since the Thue-Morse states form a sequence for increasing N, and $N \to \infty$ is the classical limit, it maybe expected that the Thue-Morse state is related to some classical invariant measure of the classical baker's map. We now show that this is indeed the case.

Since we are dealing with the position representation of the states, and since the baker's map is such that its position coordinate evolves (in the forward direction) independently of the momentum according to the doubling map ($x \mapsto 2x \,(\mathrm{mod}\, 1)$), the invariant density is simply that of this one-dimensional map. If $\rho(x)$ is an invariant density of this map, we must have that:

$$\rho(x) = \frac{1}{2}\,\rho\left(\frac{x}{2}\right) + \frac{1}{2}\,\rho\left(\frac{x+1}{2}\right). \tag{4.19}$$

If $\rho(x) = \sum_{k=0}^{\infty} t_k \exp(2\pi i k x)$ then it is easy to see, using the recursion relation we have stated earlier namely $t_{2k} = t_k$, that it satisfies the requirement of an invariant density. Since the Thue-Morse state is close to the Fourier transform of the Thue-

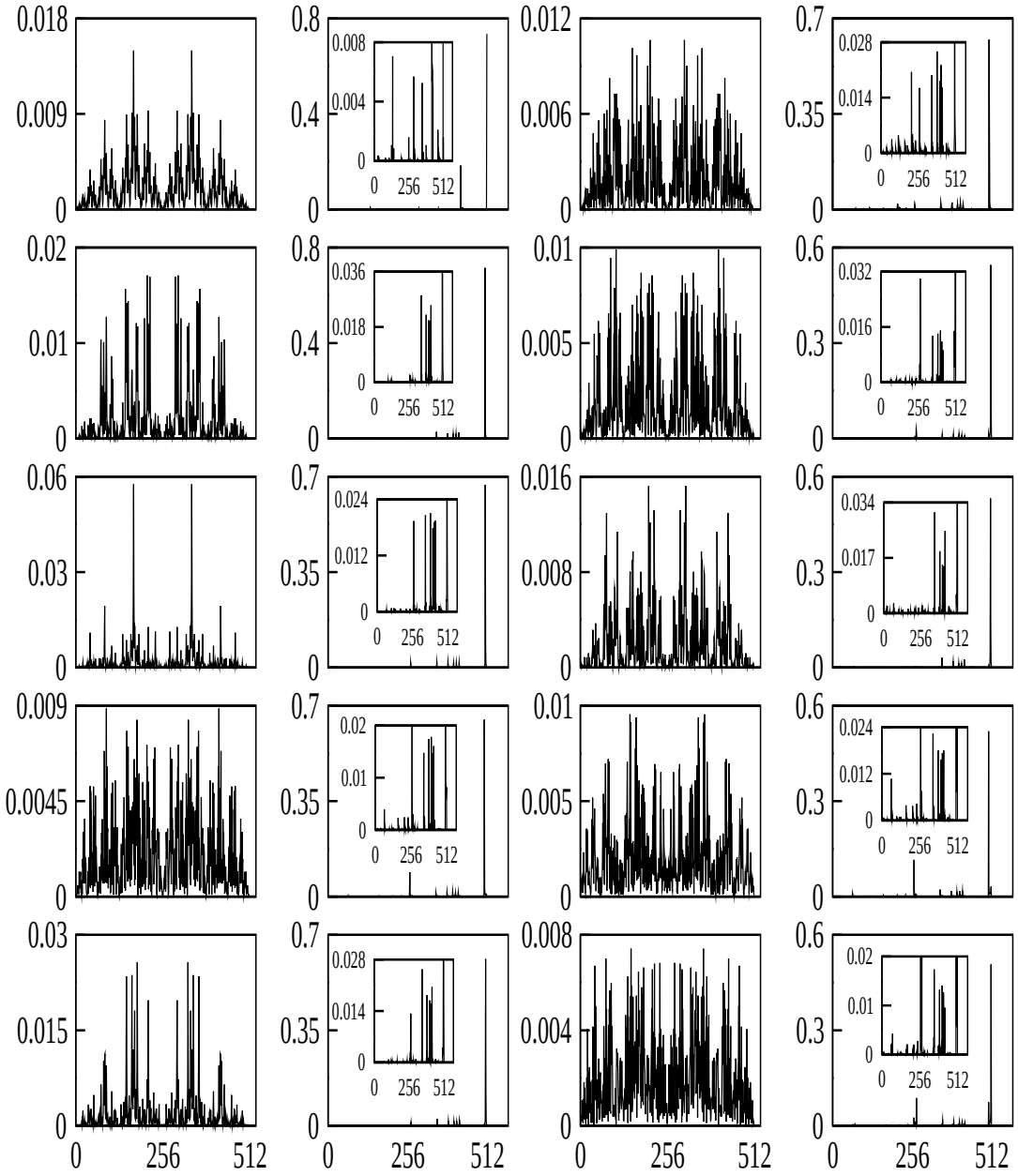

Figure 4.2: Ten eigenstates of the quantum baker's map for $N = 512$ that are most simplified on using basis-2 or basis-3. Shown in columns 1 and 3 are the intensities of the states in the position basis. Columns 2 and 4 show the corresponding intensities on using basis-2 (along with the "grass" in the insets), this basis having states that are simultaneous eigenstates of the shift operator and parity. The Thue-Morse state is the first one.

Morse sequence, it is suggestive that $\rho(x)$ is relevant to the classical limit of such states. Thus we believe we have a concrete example of a set of states of a quantum chaotic system that limits to a classical invariant measure that is not the ergodic measure, which would be uniform in this case. Instead it is a multifractal measure that is strongly peaked at period - 2 periodic orbits and all their homoclinic excursions. This is opposed to known examples where the limit is either ergodic or have delta-peaks corresponding to classical periodic orbits [18, 98]. While we have given evidence of this without establishing it rigorously, this is an interesting deviation from quantum ergodicity that is allowed by Schnirelman's theorem [25]. It is very likely that many other eigenstates of the quantum baker's map are also of this kind, limiting to classical invariant measures that are non-ergodic and are multifractal. That the eigenfunctions are multifractal we have already indicated in the previous chapter.

It is pertinent here to connect with the works of Nonennmacher and co-workers, who have studied the quantum cat maps [18, 98] and the Walsh-quantized baker's map [99], which is an exactly solvable toy model of the bakers map. Among other things they have found two types of states in the Walsh-quantized bakers map, the first which they call "half-scarred" has in the semiclassical limit part of its measure on classical periodic orbits and part is equidistributed in the Lebesgue measure. Such states have also been constructed by them for the quantum cat maps [18, 98]. The tensor-product states found for the Walsh-quantized bakers map [99] have semiclassical measures that are singular Bernoulli measures and were constructed as tensor products of states of the underlying "qubit" space (when N is a power of 2 as in this thesis, but have been generalized to other powers). The Thue-Morse states of the quantum bakers map ("Weyl" quantized) under discussion seem to be closer to the tensor-product states than the "half-scarred" ones. For one, there is strong evidence that the measure is multifractal in the semiclassical limit, and also the scarring can be unambiguously associated with short period periodic-orbits and homoclinic ones. Moreover the Thue-Morse state is "close" to the simple tensor product $\otimes^K(|0\rangle - |1\rangle)/\sqrt{2}$ for $N = 2^K$, which indeed is the finite Thue-Morse sequence. This can be measured in terms of the modulus of the inner-product and while this does decrease with N, it does so slowly. Numerical calculations not shown here indicate a decay of $N^{-0.1}$. Note that typical inner-products with random states will scale as $N^{-0.5}$. A more accurate representation of the Thue-Morse state as a superposition of the above product and its Fourier transform is such that their inner product decays even more slowly to zero (as $N^{-0.08}$). We must however say that the resolution of the semiclassical measure of the Thue-Morse state and in general other states of the quantum bakers map into

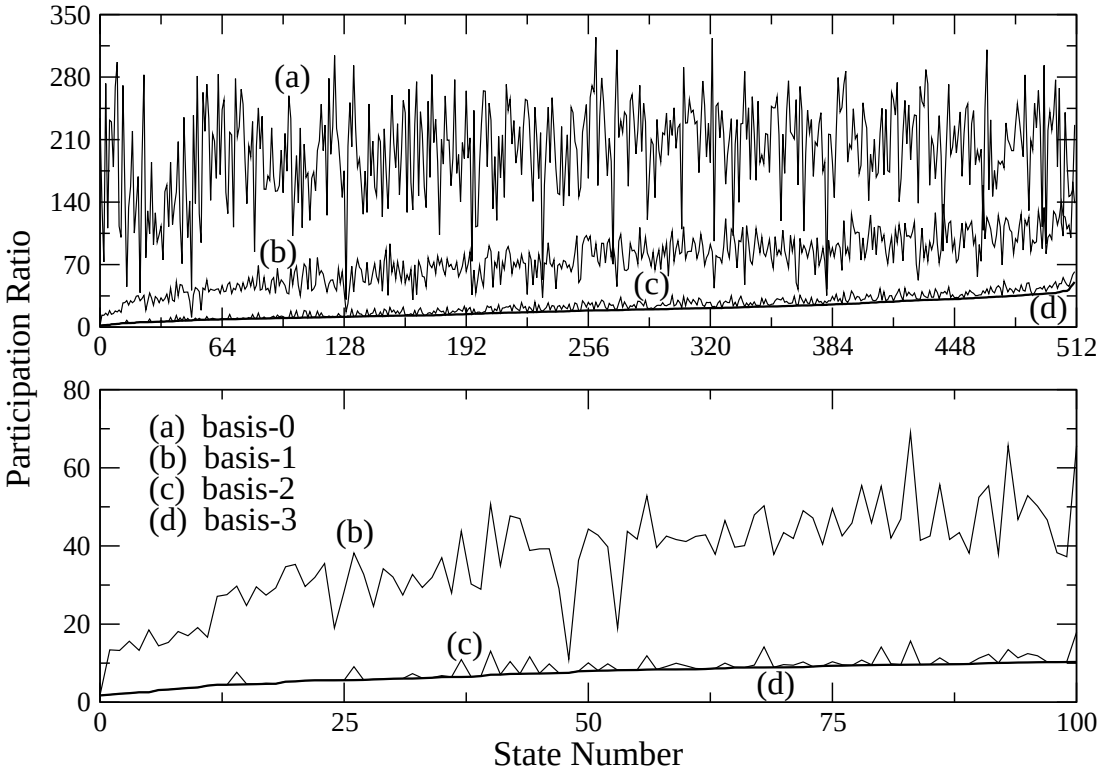

Figure 4.3: The participation ratio of the eigenstates of the baker's map in the position basis (basis-0), the Walsh-Hadamard basis (basis-1), the basis that is parity reduced eigenstates of S (basis-2), and in the basis that is also time-reversal symmetry adapted (basis-3). The states are arranged in the increasing order of the PR in basis-3. This is for the case $N = 512$, and the lower figure is a magnification of details for the first hundred states.

singular-continuous, pure-point and continuous components is not yet clear.

To quantify the extent to which the eigen vectors $|\Phi_k\rangle$ of B are simplified we evaluate the participation ratios (PR). Recall that when a complete orthonormal basis $\{|\alpha_i\rangle,\, i = 0, \ldots, N-1\}$ is used the PR is defined as

$$\left(\sum_{i=0}^{N-1} |\langle \alpha_i | \Phi_k \rangle|^4 \right)^{-1}, \tag{4.20}$$

and the PR is an estimate of the number of $|\alpha\rangle$ basis states needed to construct the vector $|\Phi_k\rangle$, here chosen to be one of the eigenstates of B. We calculate the PR in (1) the position basis (basis-0, $|\alpha\rangle = |n\rangle$), (2) the Hadamard basis (basis-1, $|\alpha\rangle = H|n\rangle$), (3) the basis that consists of parity reduced eigenstates of S (basis-2, $|\alpha\rangle = |\phi_l^k\rangle$), and (4) the basis that has both parity and time-reversal symmetry reduced eigenstates of S (basis-3, $|\alpha\rangle = |\psi_j\rangle$).

From Fig. (4.3) we indeed see that the eigenstates of S, properly symme-

try reduced simplify the eigenstates of the quantum baker's map B significantly. This does considerably better than the previously used Walsh-Hadamard transform. The difference is only however marginal for the Thue-Morse state, as the last column of the Walsh-Hadamard transform, the Thue-Morse sequence of finite generation, is anyway a parity and time-reversal symmetric eigenstate of the shift operator S. We see from the figure that for $N = 512$, there are about hundred states that can be constructed from ten or fewer eigenstates of the shift operator as we have constructed them above. We also notice that while there is considerable difference between using the basis-2 and the Hadamard basis (basis-1), there is not that much simplification due to the use of basis-3 over basis-2. This is understandable as parity symmetry (R) is the same for both S and B, while the time-reversal symmetries are different. In Fig. (4.4) we have given the magnitude of the B in WH basis and basis-2 for $N = 64$. In the position representation the magnitude of B has structure similar to that of the doubling map ($x \mapsto 2x \,(\mathrm{mod}\, 1)$). In the WH basis the baker operator has a similar structure, indicating that this is still far from diagonal. However in basis-2, we can see a block diagonal form for the matrix element which implies that the basis-2 almost diagonalizes the baker operator.

Due to the simplicity and efficacy of basis-2, we will discuss this further. We first point out that the dual or momentum basis $G_N|\phi_l^k\rangle$ is exactly as effective as the original basis for studying the eigenfunctions of the baker's map, due to time-reversal symmetry. To prove this notice that

$$G_N|\phi_l^k\rangle = -G_N^{-1}\, R\,|\phi_l^k\rangle = -t_k G_N^{-1}\,|\phi_l^k\rangle \tag{4.21}$$

where we have used $G_N^2 = -R$ (for example see Saraceno in [20]), and Eq. (4.13). Using time-reversal of the eigenstates of B ($G_N|\Phi\rangle = |\Phi^*\rangle$) implies that

$$\langle\Phi|G_N^{-1}|\phi_l^k\rangle = \left(\sum_n \langle\Phi|n\rangle\langle n|\phi_l^k\rangle^*\right)^* = \langle\Phi|\phi_{l'}^k\rangle^* \tag{4.22}$$

where $l' = d - l$ unless $l = 0$, in which case $l' = 0$ as well. Hence finally

$$\langle\Phi|G_N|\phi_l^k\rangle = -t_k\langle\Phi|\phi_{l'}^k\rangle^*. \tag{4.23}$$

Thus while the overlaps of the eigenstates of the quantum baker's map in a basis which is the the Fourier transform of the basis-2 are not the same as originally, they are upto a sign, complex conjugates of overlaps with some other basis states with a different value of l in general. Clearly this leads to identical participation

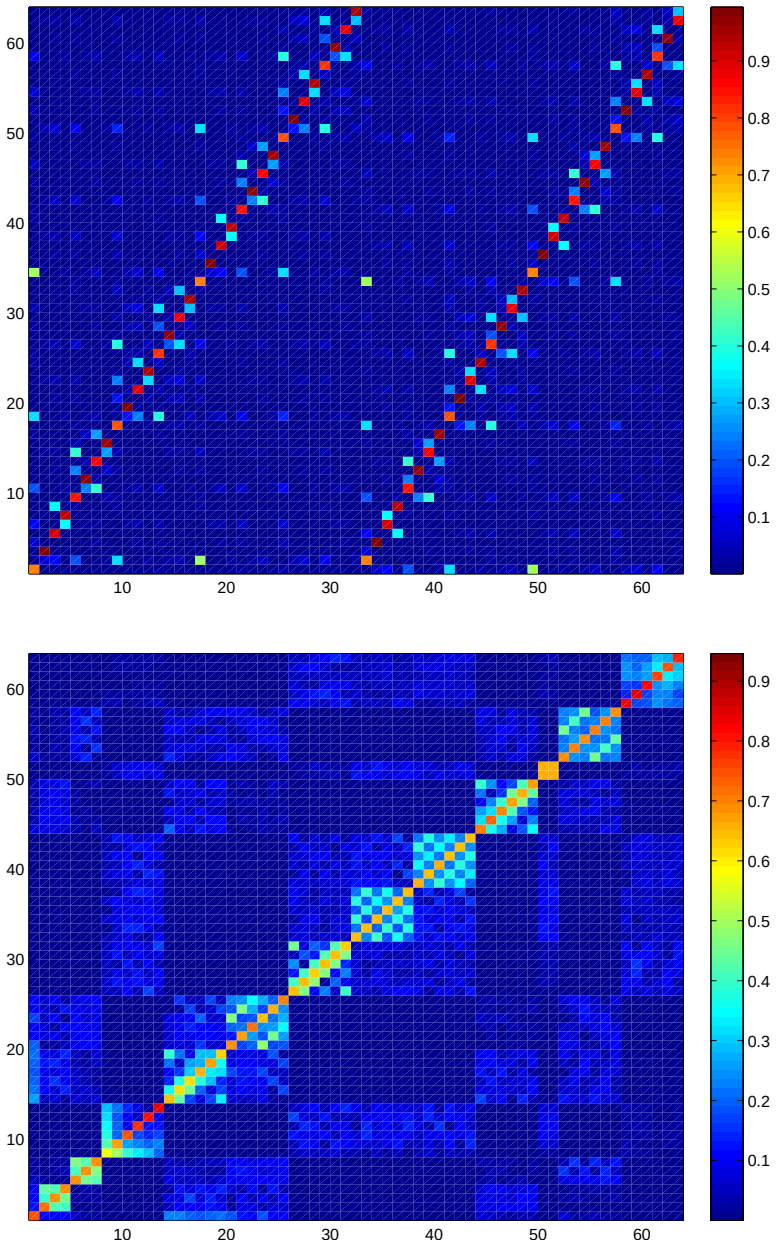

Figure 4.4: Magnitude of the matrix elements of B ($|\langle n'|HBH|n\rangle|$) in WH basis and basis-2 ($|\langle\phi_{l'}^{k'}|B|\phi_l^k\rangle|$) for $N = 64$(top to bottom).

ratios. Thus the Fourier transform of basis-2 is also of interest, indeed as we have already indicated, many of the eigenstates of the baker's map look like them, the foremost being the Thue-Morse state where the momentum representation of $|\phi_0^{(N-1)}\rangle$ is of relevance. Thus we have a natural way of generalizing this class of functions. We do not pursue this further here, but note that the other Fourier transforms are also of relevance to the spectrum of the quantum baker's map, and they also have multifractal characters. A few related functions have been studied

by us as the "Fourier transform of the Hadamard transform" and presented in the previous chapter. It is also reasonable to expect that a combination of basis-2 and its Fourier transform maybe even closer to the actual eigenstates of the quantum baker's map than even basis-2. For instance in the case of the Thue-Morse state, such a combination does better than either the Thue-Morse sequence or its Fourier transform taken individually as shown in the previous chapter.

To summarize, in this chapter we have constructed eigenfunctions of the shift operator that have additional symmetries of bit-flip or parity and bit-reversal or time-reversal. Using these we have seen why the Walsh-Hadamard transform simplifies states of the quantum baker's map, as well as shown that these transforms are capable of doing significantly better. The use of these transforms in other contexts, other than the quantum baker's map, is possible. It combines elements of both the Fourier and the Hadamard transforms in an interesting way. Using these transforms helps us study the eigenfunctions of the baker's map in a more detailed manner, and further work on this is warranted. Operators akin to the shift operator have been used as toy models of open quantum bakers to study fractal Weyl laws [27]. It is also interesting that the same cocktail of the shift operator, the Fourier transform and the Hadamard transform appears essentially in Shor's quantum algorithm for factoring, a fact also previously pointed out in [77]. A very recent work makes a significant contribution by constructing suitable basis sets for N that are not powers of 2 [26].

CHAPTER 5

Application of the transforms to other quantum baker's maps

In this chapter we discuss the applications of transforms using basis-1 (Walsh Hadamard, or WH, basis) and the transform we developed in the previous chapter and called "basis-2" on the eigenfunctions of a few generalized quantum baker's maps. These generalizations are selected to include first a closed map that still has dimensions of powers of 2, and stable and unstable manifolds parallel to the canonically conjugate directions, namely the quantization of a tetradic baker's map. Secondly we will still have two partitions but choose a map whose stable and unstable manifolds are not uniformly parallel to only one of the conjugate directions, and has in it the geometric action of *rotation* in addition to hyperbolicity, although the map remains fully chaotic. This is one of the so-called lazy baker's map [100]. Finally we study quite a different kind of system, one which is an *open* quantum map. The classical limit of this corresponds to a dissipative system, with a fractal hyperbolic repeller.

The nature of this chapter is exploratory and largely numerical and we limit its scope to mainly studying how effective the Hadamard and basis-2 transforms are in contexts other than the standard dyadic quantum baker's map. In particular, we do this by calculating the participation ratios (PR) of the eigenfunctions of the generalized quantum baker's maps mentioned above in the position basis (basis-0) and comparing it with the participation ratios calculated in the basis-1 and basis-2. We only touch upon some details of the nature of the eigenfunctions.

5.1 A closed tetradic baker

Generalized closed, area-preserving, baker's maps with many vertical rectangular partitions of different sizes undergoing pure stretch in the horizontal and compression in the vertical directions to horizontal rectangular partitions constitute Bernoulli systems, fully chaotic deterministic systems. Balazs and Voros [19] showed how the methodology of quantizing the standard dyadic baker's map can be carried over to these cases practically by visual inspection. In fact actions

other than stretching can also be accommodated easily. For instance if there are rotations of some rectangles then this can also be quantized. We will discuss this case further below. Here we consider the simplest generalization that still has Hilbert space dimensions that are powers of 2, as the transforms we are interested in are defined only in these cases. Note that this rules out the triadic bakers with three partitions. The next simplest is the "tetradic baker".

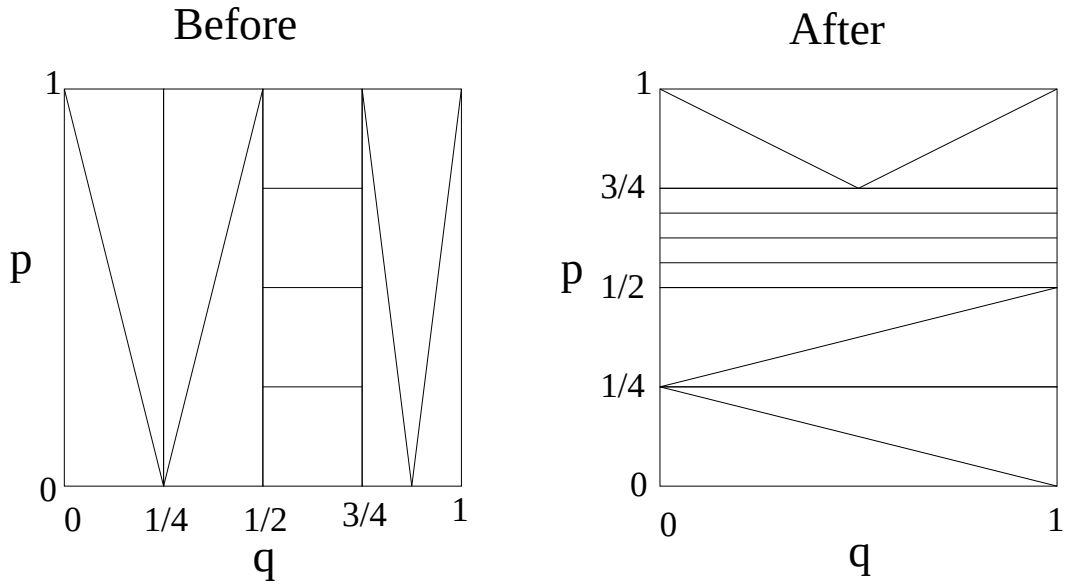

Figure 5.1: Pictorial representation of classical tetradic baker's map.

The classical tetradic baker's map we study is defined as follows

$$T_{tetradic}(q,p) = \begin{cases} (4q, \frac{p}{4}) & \text{if} \quad 0 \le q < 1/4 \\ (4q-1, \frac{p+1}{4}) & \text{if} \quad 1/4 \le q < 1/2 \\ (4q-2, \frac{p+2}{4}) & \text{if} \quad 1/2 \le q < 3/4 \\ (4q-3, \frac{p+3}{4}) & \text{if} \quad 3/4 \le q < 1 \end{cases} \tag{5.1}$$

The phasespace of the tetradic baker's map is an unit square and it is a transformation of the unit square onto itself. Unlike the usual baker's map now the unit square is divided into four partitions and they are stretched along the position direction by a factor of 4 and compressed along the momentum direction by a factor of 4 in compensation and portions exceeding the unit square is cut and brought back to the unit square. The action of the map is given in Fig. (5.1). It clearly has uniform hyperbolicity and its (positive) Lyapunov exponent is log(4). Thus this map has twice as much chaos as the dyadic baker's map. We note that there is a close connection between the standard baker's map iterated two times

and this tetradic baker's map, however they are different. We will say more on this presently.

Its quantization with anti periodic boundary conditions is given by[19]

$$B_{tetradic} = G_N^{-1} \begin{pmatrix} G_{N/4} & 0 & 0 & 0 \\ 0 & G_{N/4} & 0 & 0 \\ 0 & 0 & G_{N/4} & 0 \\ 0 & 0 & 0 & G_{N/4} \end{pmatrix} \tag{5.2}$$

The quantum map exists for all values of N which are divisible by 4 by construction. We consider the case $N = 2^K$ with K taking values from 4 to 11. In Fig. (5.2) we show participation ratios in the position basis, WH basis and basis-2 for the values of N mentioned above for the eigenstates of the quantum map $B_{tetradic}$. The states are arranged according to increasing participation ratio in the basis-2. From the figure we can clearly see that whenever N is 2^{2K} ($K = 2, 3, 4$ and 5, left column) , basis-2 simplifies almost all the eigenstates significantly. When N is 2^{2K+1} ($K = 2, 3, 4$ and 5, right column) basis-2 simplifies the eigenstates marginally well in comparison to WH basis.

Again we pay attention to the states that are most compressed by the WH or basis-2 transforms. We could identify special class of eigenstates for $B_{tetradic}$ whenever N is 2^{2K+1}, that is an odd power of 2. There are two family of eigenstates, one which has convergence towards the eigenvalue $-i$ and other one which has convergence towards the eigenvalue -1. We identified these two family of states by calculating the ratio between PR in position basis and WH basis. These convergent states are the ones which are maximally compressed in the WH basis, and hence have the largest values of such a ratio. In Fig. (5.3) and Fig. (5.4) we show these family of states for various values of N.

The family which has convergence towards eigenvalue $-i$ has the principal peak in the WH basis at $(2N-1)/3$. This column of the Hadamard transform does not correspond to the Thue-Morse sequence. The sequence is found by noting that in base 2 the number $(2N-1)/3$ is

$$\left(\frac{2N-1}{3}\right)_2 = \underbrace{1010\cdots10}_{2K}1 \tag{5.3}$$

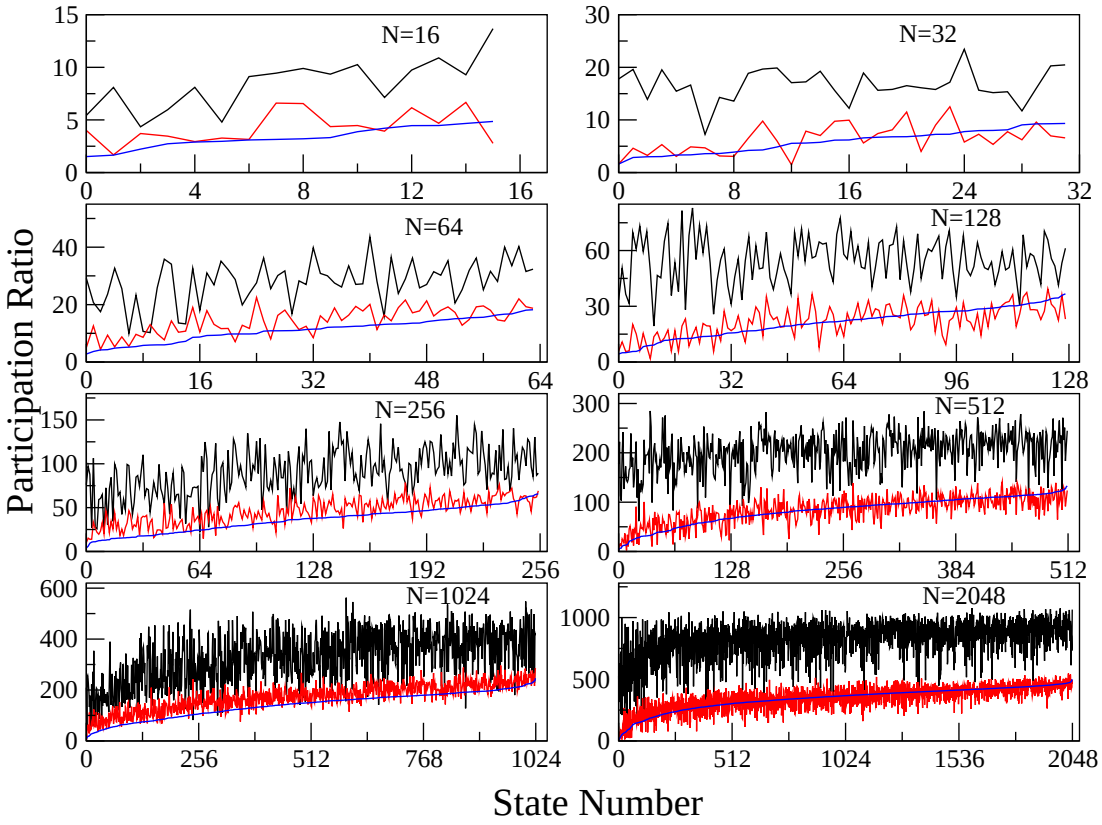

Figure 5.2: Participation Ratio vs. State Number for $B_{tetradic}$ for various values of N. The values of N are given as legends. Participation ratios in the position basis, WH basis and basis-2 are given by the curves in black, red and blue color respectively. The states are arranged in increasing order of PR in the basis-2.

which then implies that the sequence is

$$\overset{K}{\bigotimes} \begin{pmatrix} 1 \\ 1 \\ -1 \\ -1 \end{pmatrix} \bigotimes \begin{pmatrix} 1 \\ -1 \end{pmatrix}. \tag{5.4}$$

This sequence is quite different from the Thue-Morse sequence. We expect the eigenfunction to again be well approximated by the sequence along with its Fourier transform. Such sequences were also studied in chapter 3 where the Fourier transform of the Hadamard transform is discussed.

The family which has convergence towards eigenvalue -1 (See Fig. (5.4)) has principal peak in the WH basis at $N-1$. This implies that these states are dominated by the Thue-Morse sequence, as in the Thue-Morse states of the usual baker's map. In fact though this state looks different from the Thue-Morse state they are quite akin to each other. This is reasonable as the tetradic baker we are

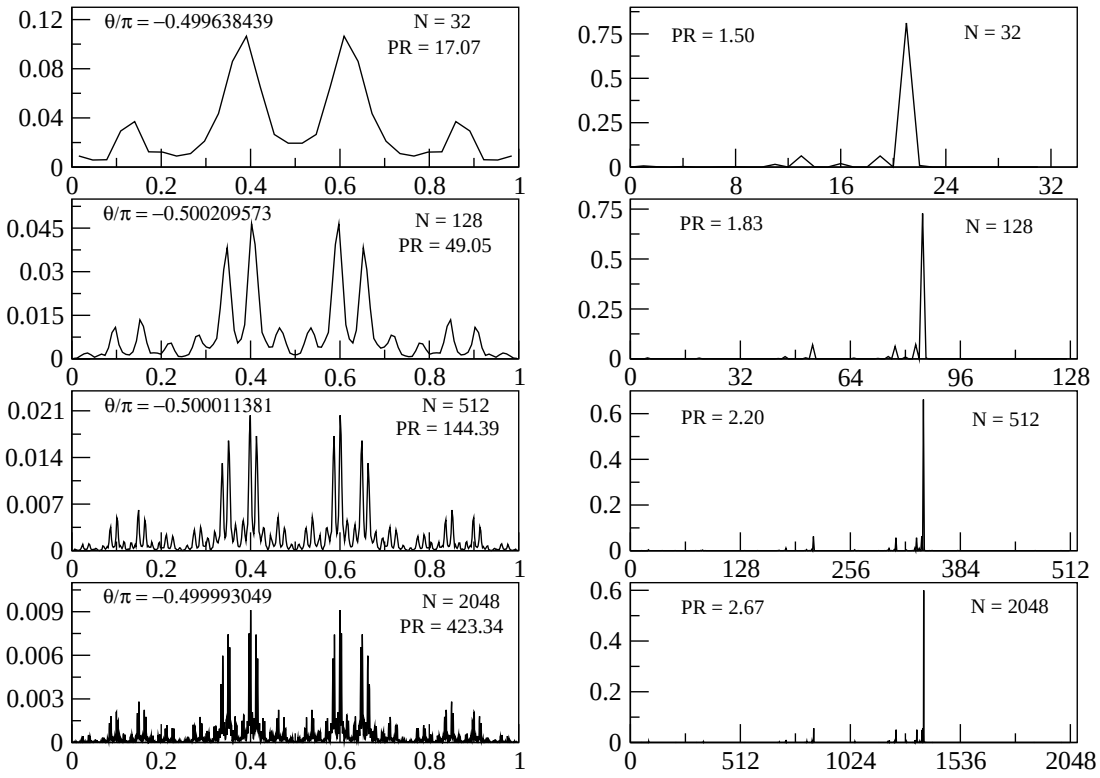

Figure 5.3: A family of eigenstates of the $B_{tetradic}$ which converges to the eigenvalue $-i$. Intensities in the position basis are given in the left column along with their eigenangle, PR and the Hilbert space dimension N, their corresponding WH transform are given in the right column along with their PR and N.

considering if sightly rearranged is another tetradic baker whose quantization is a semiquantum baker's map [19, 57, 101], which is the quantization of the dyadic baker map after two time steps. This corresponds to interchanging the partitions 2 and 3 in the Fig. (5.1) after the baking. In fact the eigenvalue is very close to the square of the eigenvalue of the usual Thue-Morse state, recall that the eigenvalue there was $-i$ while here it is -1.

We note a curious fact that we found for many baker's maps, that $N = 128$ is somewhat anomalous. For instance for the tetradic quantum baker' map under current discussion, the eigenstate with eigenvalue close to -1 shows deviation from other members of the family in terms of the PR in the WH basis (which is of the order of 6 while for other members of the family it is of the order of 2 or 3) as well as in terms of the nature of the intensities in the position basis.

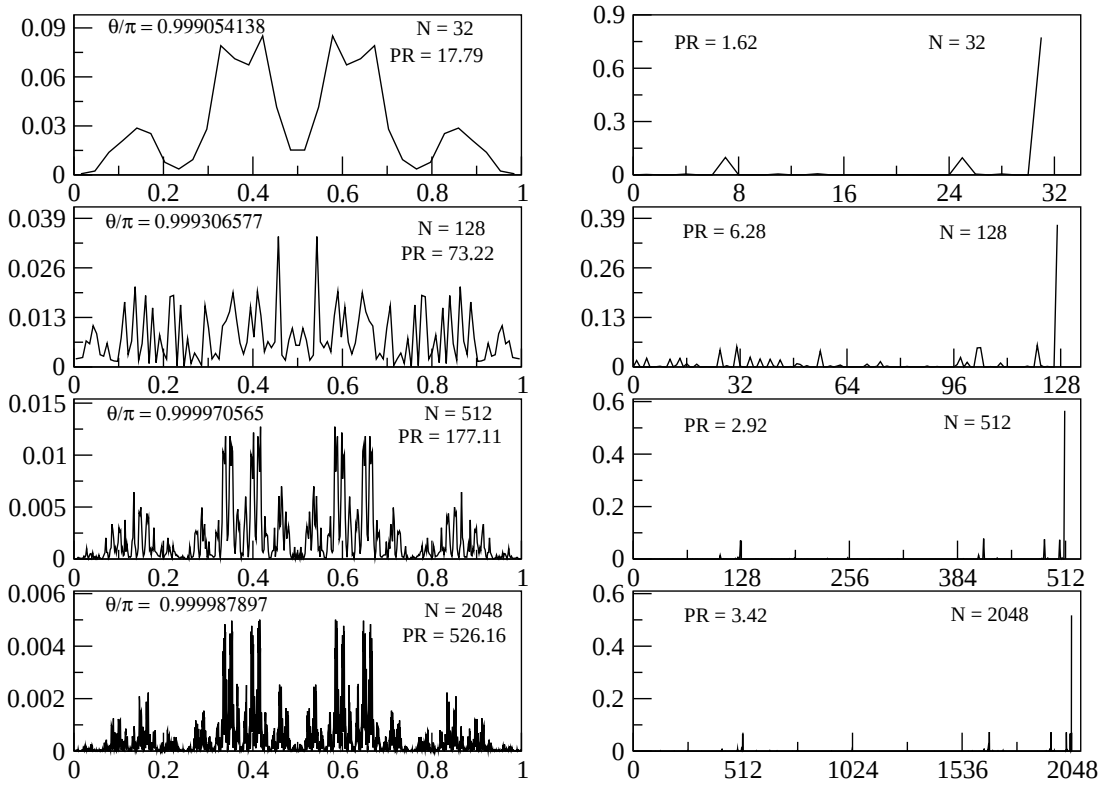

Figure 5.4: A family of eigenstates of the $B_{tetradic}$ which converges to the eigenvalue -1. Intensities in the position basis are given in the left column along with their eigen angle, PR and the Hilbert space dimension N, their corresponding WH transform are given in the right column along with their PR and N.

5.2 A lazy baker

Now we turn to a closed baker's map which involves stretching as well as *rotation* about the center of the square. Several families of these have been studied under the epithet "lazy" baker's map as they were to be the simplest models of mixed system, systems with both regular and chaotic orbits[100]. Actually they can range from maps with a cantor set of chaotic orbits of measure zero to fully chaotic maps through mixed phase spaces. The example which we consider is a fully chaotic system called the SR map[100]. For this map baking of the square in the left vertical rectangle is same as that of the usual classical baker's map with stretching and compression by a factor of 2 along position and momentum direction respectively. This is the map from L to B in Fig. (5.5). The action on the right half (R to T) is a rotation with respect to the center of the square by ninety degrees, as in Fig. (5.5). This map does not possess parity symmetry. The

evolution of the map is defined as follows

$$T_L(q,p) = \begin{cases} \left(2q, \frac{p}{2}\right) & \text{if} \quad 0 \le q < 1/2 \\ \left(1-p, q\right) & \text{if} \quad 1/2 \le q < 1 \end{cases} \tag{5.5}$$

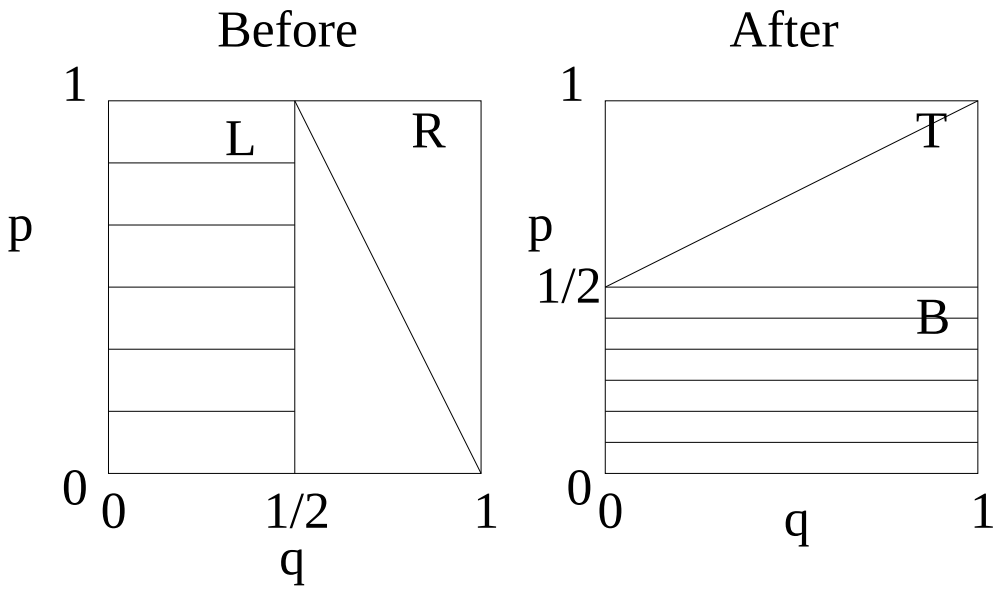

Figure 5.5: Pictorial representation of lazy baker's map.

Some classical properties of this map are that it is an ergodic and mixing system on the whole unit square. The positive Lyapunov exponent is log(2)/2, half that of the usual baker's map (hence lazy). The dynamics has been shown to be one of a subshift on *three* symbols. The Markov partitions are the left vertical rectangle and the bottom and top halves of the right vertical rectangle [102]. The topological entropy is about log(1.46), which is slightly larger than the Lyapunov exponent as the map is non-uniformly hyperbolic. Note that for the usual baker's map these numbers all coincide with log(2). In terms of symmetries, while it possesses time reversal symmetry, it does not have parity symmetry.

Its quantization is given by

$$B_L = G_N^{-1} \begin{pmatrix} G_{N/2} & 0 \\ 0 & I_{N/2} \end{pmatrix} \tag{5.6}$$

This follows as rotation by 90° in the mixed $p-q$ representation is the identity matrix.

The quantum map exist for all even values of integer N. In Fig. (5.6) we show

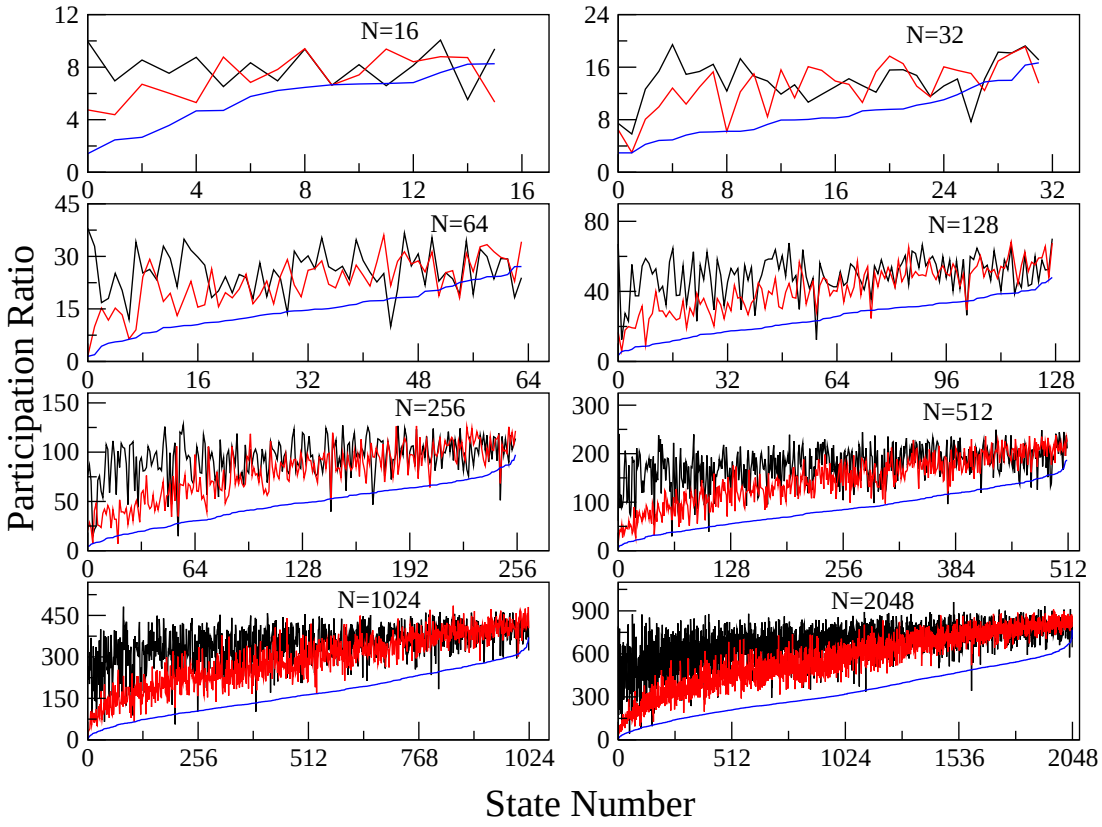

Figure 5.6: Participation Ratio vs. State Number for B_L for various values of N. The values of N are given as legends. Participation ratios in the position basis, WH basis and basis-2 are given by the curves in black, red and blue color respectively. The states are arranged in increasing order of PR in the basis-2.

participation ratios in the position basis, WH basis and basis-2 for the values of N mentioned above for the eigenstates of the quantum map B_L. From the figure we can clearly see that the basis-2 simplifies almost all the eigenstates. Unlike the quantum version of the tetradic baker's map where the basis-2 is marginal in comparison to the WH basis in simplifying the eigenstates, here it does much better than that of the WH basis, as in the case of the usual dyadic baker's map.

Like the usual baker's map which has a remarkable family of eigenstates (the Thue-Morse state) which has eigenvalue convergence towards $-i$ whenever N is power of two, for the SR lazy baker's map also we could find a similar family which has convergence to the eigenvalue $-i$. However they are occurring only when N is power of 4 and even among them there are two families based on whether the power of 4 is an even or odd integer. We have verified these for the values of N equal to $16, 64, 256$ and 1024. Since the classical map does not possess parity symmetry these family of eigenstates does not have parity symmetry in comparison to that of the usual quantum baker's map. In Fig. (5.7) and Fig. (5.8) we show these

family of states for N which is 4 power an even integer or odd integer respectively. We identified these states based on their maximal compression in the WH basis,

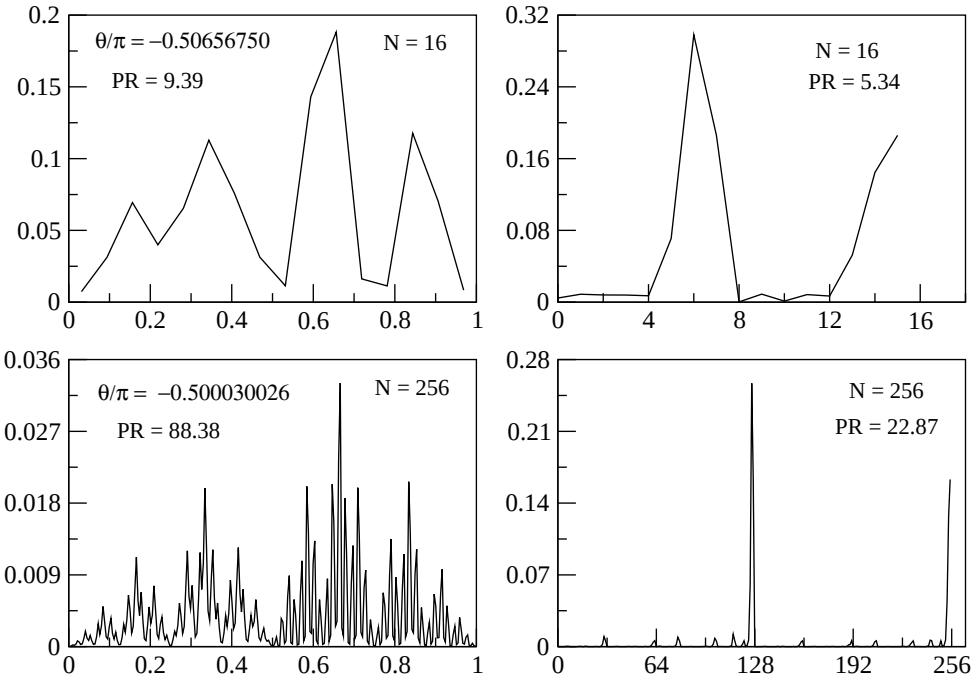

Figure 5.7: Intensities of eigenstates of B_L with eigenvalue close to $-i$ for $N = 16$ and 256. Intensities in the position basis is given in the left column along with their eigenangle, PR and the Hilbert space dimension N while their corresponding WH transform is given in the right column along with their PR and N.

by means of calculating the ratio between PR in position and WH basis. When N is an even power of 4 ($N = 2^K$, with K being multiples of 4) the principal peak in the WH basis occurs at $(N-4)/2$, apart from another major but smaller peak at $N-1$. In contrast the Thue-Morse state in the usual quantum baker's map has only one major peak which is at $N-1$.

The peak at $(N-4)/2$ corresponds to the following sequence. As

$$\left(\frac{N-4}{2}\right)_2 = 0\underbrace{11\cdots1}_{K-2}0, \tag{5.7}$$

the sequence is

$$\begin{pmatrix} 1 \\ 1 \end{pmatrix}^{\bigotimes K-2} \begin{pmatrix} 1 \\ -1 \end{pmatrix} \bigotimes \begin{pmatrix} 1 \\ 1 \end{pmatrix} = \begin{pmatrix} t_{K-2} \\ t_{K-2} \end{pmatrix} \bigotimes \begin{pmatrix} 1 \\ 1 \end{pmatrix}. \tag{5.8}$$

Thus the sequence is the twofold repetition of padded Thue-Morse sequences of length 2^{K-2}. The padding duplicates every 1 and -1. This is similar to but not

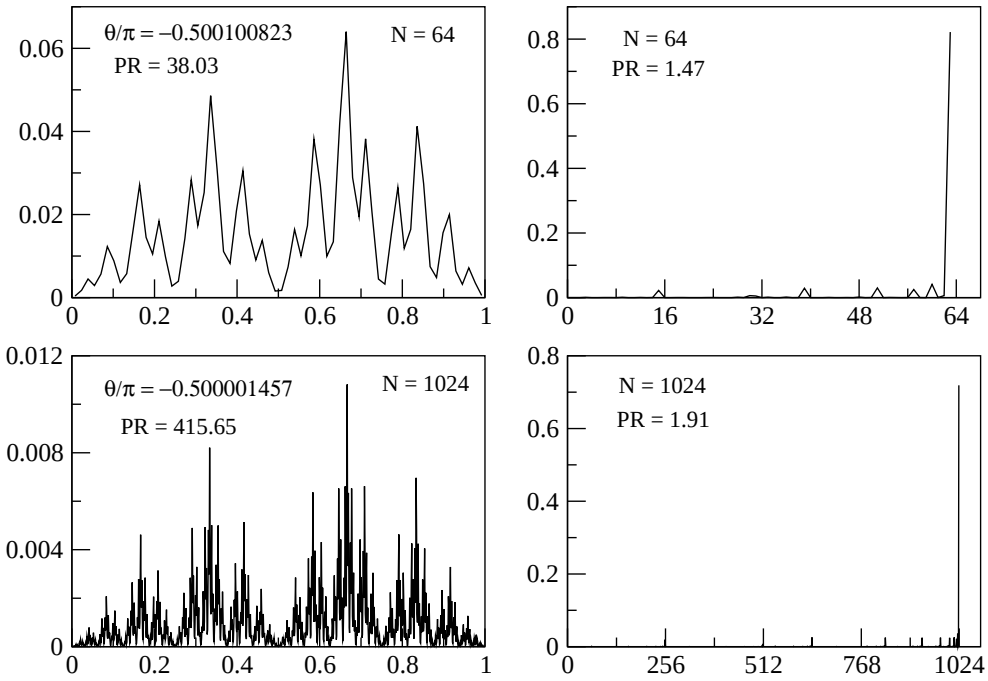

Figure 5.8: Intensities of eigenstates of B_L with eigenvalue close to $-i$ for $N = 64$ and 1024. Intensities in the position basis is given in the left column while their corresponding WH transform is given in the right column along with their PR and N.

identical with the secondary peaks of the Thue-Morse state.

However when N is 4 power an odd integer the principal peak in the WH basis occurs at $N-1$, corresponding to the Thue-Morse sequence, and indeed the states resemble very much the Thue-Morse states except for the symmetry, which must be broken due to contributions from the secondary peaks, with conflicting parities.

5.3 An open tetradic baker

We turn now to a quite a different kind of system, where the quantum map is *non-unitary*. This corresponds to classical *open* systems. Phase space points "escape" or are annihilated. In any case the remaining phase space trajectories are of successively smaller measure and model scattering or dissipative systems with shrinking phase-space volume. In the presence of chaos it is well known that usually the limiting attractor or underlying repeller, depending in whether the system is dissipative or scattering is a fractal. The models we consider are more like scattering systems where trajectories escape to infinity except for a strange set of measure zero. For example a three-disk scatterer is such a system[103, 104]. Thus

the quantum systems have "resonances" in place of eigenstats and the eigenvalues which are inside the unit circle are related to the lifetime of these resonances.

The first study of such quantum systems, to our knowledge, was by Vallejos and Saraceno [105] when they studied a quantization of the Smale horseshoe map[13] using a simple modification of the baker's map quantization of Balazs and Voros. They have been extensively used in the recent past, especially to study the conjecture about fractal Weyl law stemming from the works of Sjostrand[106] and Zworski[107]. Recall that Weyl's law semiclassically associates each bound quantum state with a phase space volume of $(2\pi\hbar)^d$ where d is the number of degrees of freedom of the system. Thus if H is the classical Hamiltonian, the number of levels between E_1 and E_2 is semiclassically

$$N(E_1, E_2) = \frac{\mathrm{vol}(E_1 \leq H \leq E_2)}{(2\pi\hbar)^d}. \tag{5.9}$$

For an open, scattering system the trajectories at energy E escape except possibly a set of measure zero, the fractal repeller K_E. The fractal Weyl law states that the scaling of the the density of resonances with Planck's constant is determined not by the actual number of degrees of freedom, but by the fractal dimension $D(K_E)$ of K_E. To be more precise, if the resonances are $E - i\gamma$, then the number of these with $E_1 < E < E_2$ and $0 < \gamma < \hbar$ scales as $\hbar^{-(D(K_E)+1)/2}$. Note that if the system limits to a closed one, $D(K_E) = 2d-1$, the dimension of the energy shell and this reduces to the usual Weyl law. The fractal Weyl law has been extensively studied, for example there is evidence of it in a scattering system with a potential consisting of three Gaussians[108, 109]. The study of this law will require a knowledge of the quantum resonances as well as the classical invariant set. Naturally simple models such as open baker's maps are then attractive models for this, and there has been studies on this, for example [27, 110, 111, 112, 113]

We restrict ourselves to a somewhat superficial and cursory look at what the Hadamard and basis-2 transform do to the resonances of an open tetradic quantum baker's map. Recall that the nature of structures of open chaotic systems in phase-space is characterized by the forward and backward trapped sets, namely the trajectories which are trapped on the fractal sets in the far future and the distant past respectively, and their intersection is the classical repeller. In the present study we consider an open version of the tetradic baker map we studied first in this chapter. This is obtained by removing second and third vertical strips of the baker's map with 4 partitions $T_{tetradic}$. In Fig. (5.9) we give a pictorial representation of the map, the horizontal middle two partitions are *removed* after the

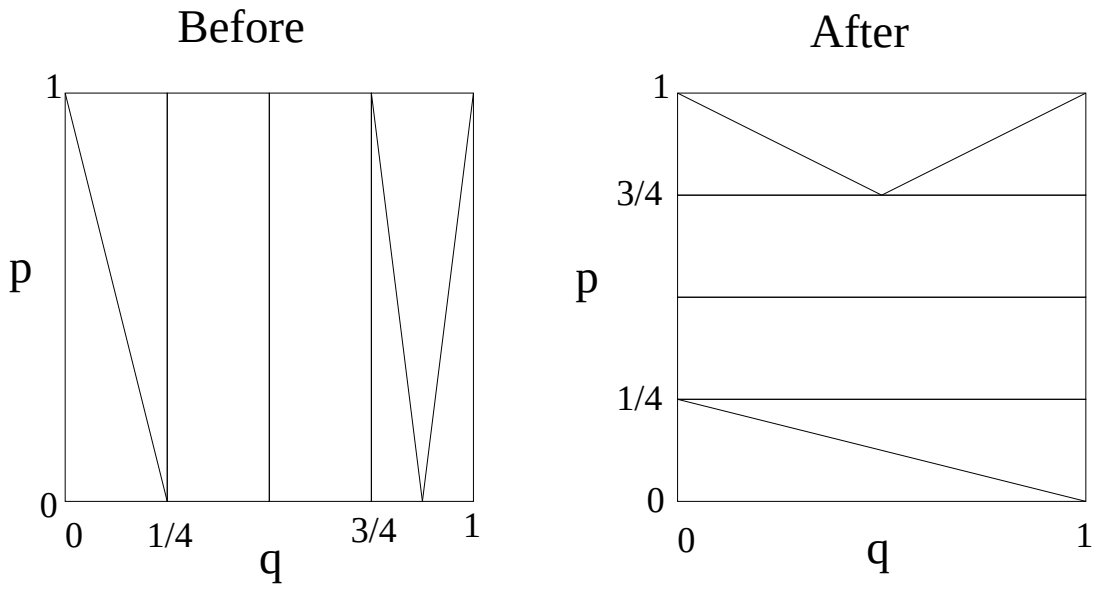

Figure 5.9: Open tetradic baker's map with second and third vertical stripes being removed.

iteration, the trajectories have scattered to never reappear again. The forward trapped set for this map is given by $C_{1/2} \times [0,1)$ and backward trapped set is $[0,1) \times C_{1/2}$ [27]. Where $C_{1/2}$ denotes the cantor set obtained by iteratively removing the central half of each line segment, just as the standard one-third Cantor set is obtained by removing the middle-thirds. The fractal dimension of $C_{1/2}$ is $\log(2)/\log(4) = 1/2$. The Lyapunov exponent on the trapped set is $\log(4)$. We study this rather than the often used open triadic baker's map as we wish still to deal with spaces that have dimensions that are powers of 2.

The evolution equations are given as follows

$$\tilde{T}_{tetradic}(q,p) = \begin{cases} \left(4q, \frac{p}{4}\right) & \text{if} \quad 0 \leq q < 1/4 \\ \left(4q-3, \frac{p+3}{4}\right) & \text{if} \quad 3/4 \leq q < 1 \end{cases} \tag{5.10}$$

Its quantization is given by

$$\tilde{B}_{tetradic} = G_N^{-1} \begin{pmatrix} G_{N/4} & 0 & 0 & 0 \\ 0 & 0 & 0 & 0 \\ 0 & 0 & 0 & 0 \\ 0 & 0 & 0 & G_{N/4} \end{pmatrix} \tag{5.11}$$

The open quantum system is obtained by setting the second and third block of the diagonal matrix of $B_{tetradic}$, corresponding to the two openings equal to zero. The

quantum system is now non- unitary, the left and right eigenstates are neither equal nor orthogonal. The eigenvalues λ_i are complex with modulus less than or equal to one. $|\lambda_i|^2 = e^{-\Gamma_i} \leq 1$, Γ_i is the decay rate. There are 'short-lived' and 'long-lived' eigenstates which are differentiated in terms of decay rates. The long-lived eigenstates are concentrated on the classical repeller in the semiclassical limit[110].

There are $N/2$ exact null eigenvalues and the corresponding eigenstates are position eigenstates belonging to the interval $[1/4, 3/4)$. Being of a trivial nature these are ignored. The kinematics of the open tetradic baker's map is such that position representation of the right eigenstates is same as that of the momentum representation of the left eigenstates. The long-lived right eigenstates are characterized by the backward trapped set and long-lived left eigenstates are characterized by the forward trapped set for the open baker's map[110]. Thus momentum representation of the long-lived right eigenstates and position representation of the left eigenstates has support on the Cantor set $C_{1/2}$ in the semiclassical regime.

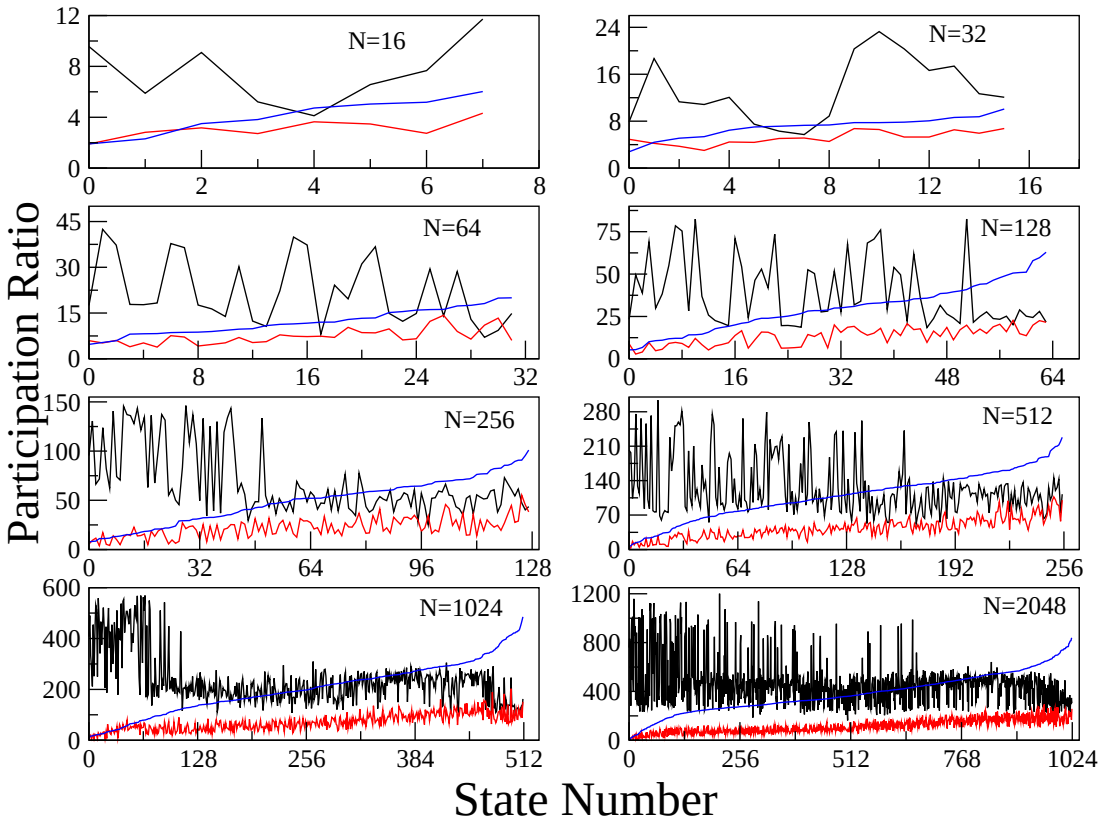

Figure 5.10: Participation Ratio vs. State Number for $\tilde{B}_{tetradic}$ for various values of N. Participation ratios in the position basis, WH basis and basis-2 are given by the curves in black, red and blue color respectively. The states are arranged in increasing order of PR in the basis-2.

We consider the position representation of the right eigenstates of the open tetradic baker's map in order to see whether it simplifies after the Hadamard as well as the new transform developed in the previous chapter. The plot of participation ratio versus state number is given in Fig. (5.10). From Fig.(5.10), we can see that the Hadamard transform simplifies almost all the right eigenstates of $\tilde{B}_{tetradic}$. Surprisingly the plain Hadamard transform does better than the basis-2, which incidentally was comparable or marginally better off than the Hadamard transform for the closed tetradic baker map, see Fig. (5.2). It is not clear to us presently why this must be so. We now turn to see the structure of the most compressed resonances.

In Fig. (5.11) we show first eight right eigenstates (or resonances) in the position representation which are arranged according to the ratio of the participation ratios between the position basis and basis-2 in descending order. This ratio is a measure of the efficiency of the transforms to compress the states.

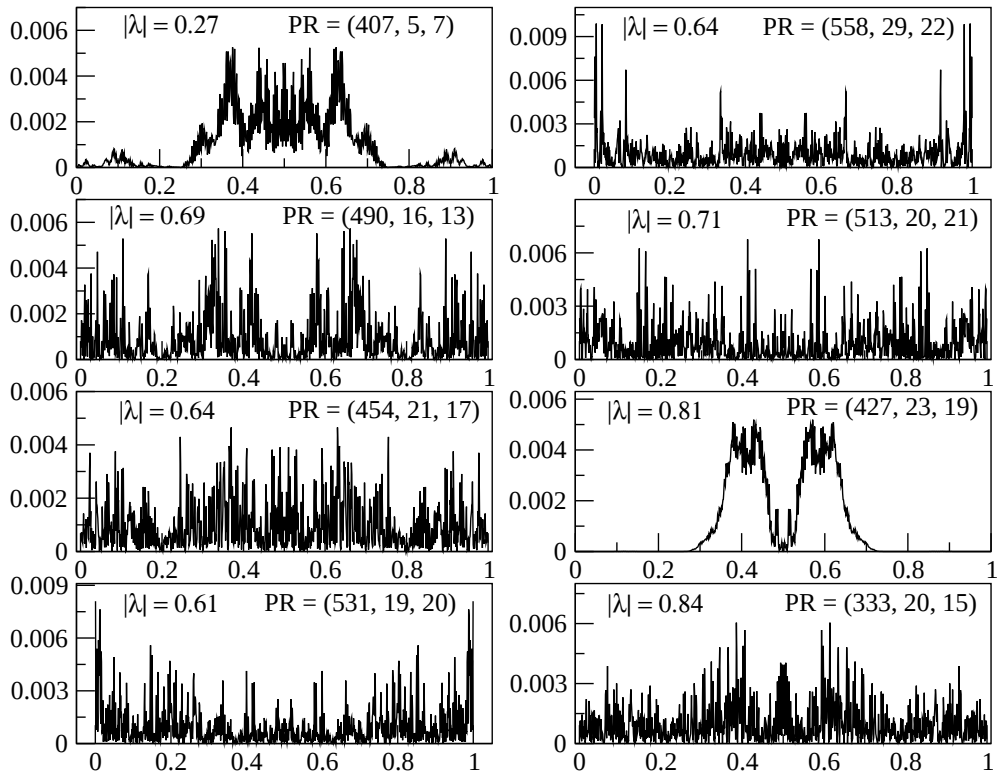

Figure 5.11: Intensities in the position basis for eight right eigenstates, which are arranged according to descending order of ratio between PR in position basis (PR_q) and basis-2 (PR_2). The modulus of eigenvalue ($|\lambda|$) and PR_q, PR_H (PR in WH basis) and PR_2 are given as legends.

We see the optimally compressed states are pretty long-lived, and the new transforms can compress by factors ranging from about 80 to 15 in this range.

Thus it is very interesting that these transforms continue to do quite a good job even for these open quantum maps and resonances. However these open baker's maps offer us an interesting possibility that was not present for the maps studied hitherto in this thesis. This is the fact that the momentum and position representations are *essentially different*. This means that the much used Fourier transform is now going to produce something very different. Thus in Fig. (5.12) we show their intensities in the momentum basis. For the usual quantum baker's map(B) because of the time-reversal property position and momentum representation of the eigenstates are just complex conjugates thus participation ratios in momentum and position are same. But for the open baker's map the momentum representation of the right eigenstates are not same as that of the position representation of the right eigenstates and they are supported (semiclassically) on a cantor set.

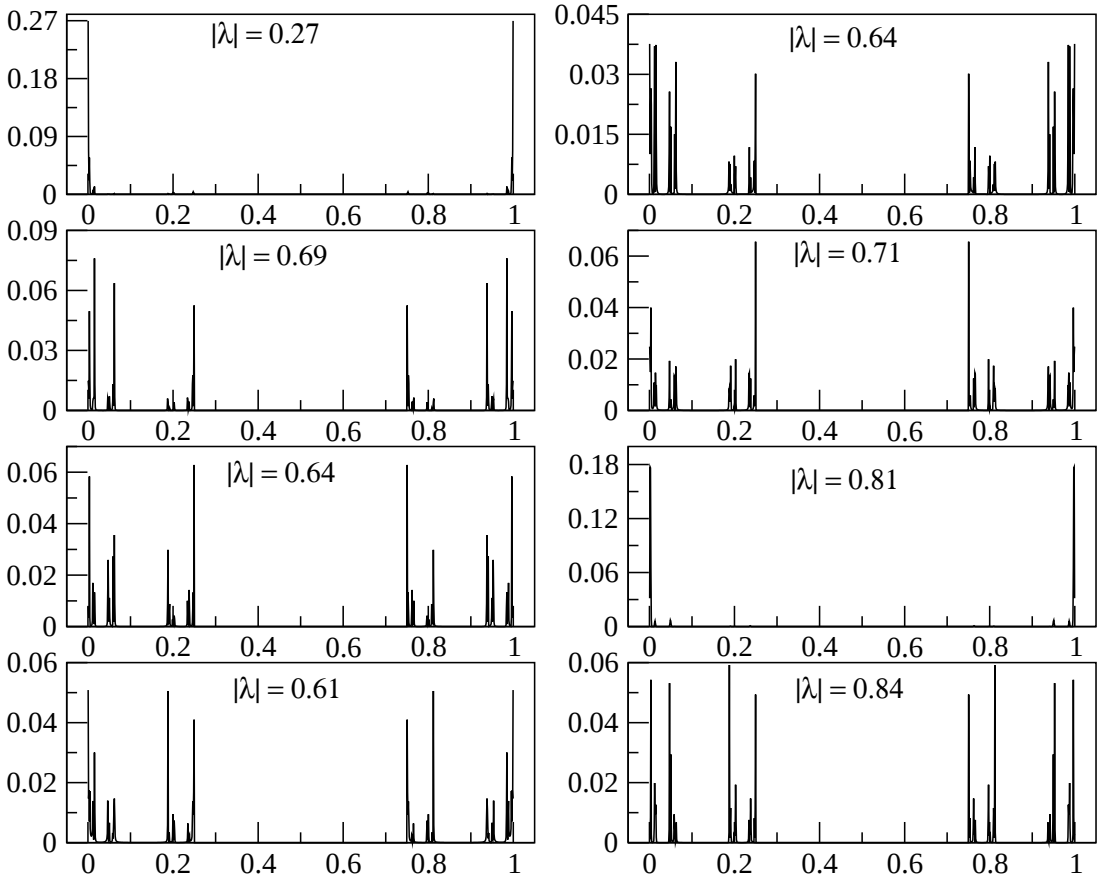

Figure 5.12: Intensities in the momentum basis for the right eigenstates shown in Fig. (5.11)

Thus one would expect that participation ratios of the right eigenstates in their momentum representation to be small in comparison to that of the position basis. In Fig. (5.13) we show the participation ratio of the right eigenstates in

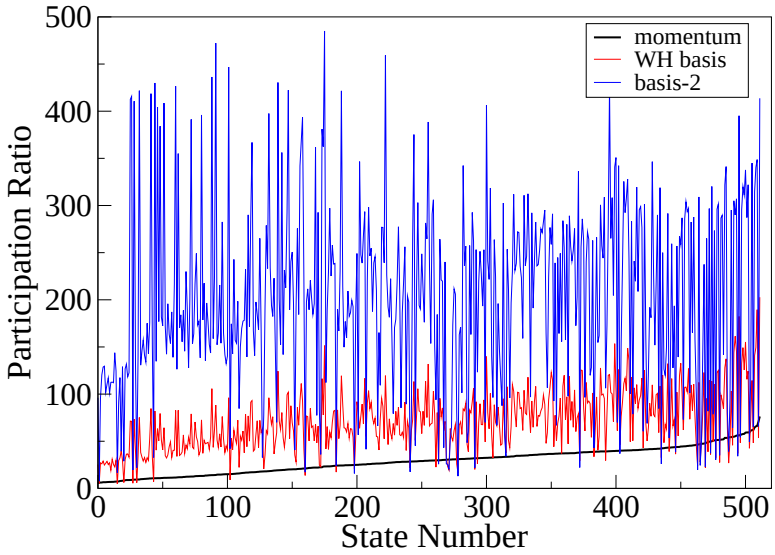

Figure 5.13: Participation Ratio vs. State Number for $\tilde{B}_{tetradic}$ for $N = 1024$. The states are arranged in increasing order of PR in momentum basis.

momentum basis, WH basis and basis-2 for the right eigenstates of $\tilde{B}_{tetradic}$ for $N = 1024$. From the figure we see clearly that the participation ratio of the right eigenstates is compressed most in the momentum basis in comparison to that of WH basis and basis-2 except for few exceptions. What is interesting is that the Hadamard transform does comparably well with the momentum representation. This begs the question of if there is a physical interpretation of the Hadamard transform which we have so extensively used here.

In this chapter we have studied the applicability of the new transform (basis-2) which we discussed in the last chapter as a transformation for simplifying the eigenstates or resonances of generalized quantum baker's map both open and closed. We have done this by means of calculating PR for the eigenstates of the generalized quantum baker's maps in position basis, WH basis and basis-2. In the process we found several special family of states based on their maximal compression in WH basis or basis-2, with which we could associate sequences akin to the Thue-Morse one. More work on these states has to be done, and it is possible that the transforms will shed further light on especially the structure of resonances in open systems.

CHAPTER 6

Hypersensitivity to perturbation

The usual markers of classical chaos, such as the Lyapunov exponent, Komogorov-Sinai or topological entropy etc., are not of use in quantum chaos, as the very arena of phase-space does not exist. Therefore the *independent* characterization of quantum chaos is one of the important challenges present. Many systems do not have obvious classical limits, such as spin systems, but can have spectral properties that are those of RMT [114]. Thus from a statistical point of view they are quantum chaotic. Hypersensitivity [115] is an interesting attempt at characterizing quantum chaos, using concepts from information theory. In this chapter, which is again exploratory and numerical in nature, hypersensitivity to perturbations for the operators related to quantum baker's map and Shor's factoring algorithm has been studied. These are precisely the main players in this thesis so far, namely the Fourier and Hadamard transforms, the combined Fourier of Hadamard transform and the shift operator. We have already noted in chapter 2 that the close link between the shift operator and the baker's map, implies a close link between Shor's algorithm and the quantum baker's map, as the shift operator is a special case of the modular exponentiation operator.

The physics of information plays an important role in current times with the very active developments in quantum information and computation [84]. The roots of this are to be found in the Maxwell's demon [116] and its resolution by Szilard [117] and Bennett [118] using notions of information stored in the demon's mind. This in turn has made use of the Landauer principle which states that for every bit of information that is erased the entropy of the universe increases *at least* by $k_B \log(2)$ [119] (with an equal decrease in the system entropy that can be converted to useful work), where k_B is Boltzmann's constant. Hypersensitivity to perturbations implies that this erasure cost is much higher than the consequent reduction in the system entropy. Schack and Caves found using several model systems, including the baker's map and the lazy baker's map that quantum chaotic systems qualified as being hypersensitive. As the notions of entropy play a crucial role in classical chaos, this approach is very interesting.

6.1 Description of the algorithm

We will first describe the algorithmic definitions of hypersensitivity as developed by Schack and Caves. Given an unitary operator U, whose hypersensitivity we are going to find, the procedure is as follows. An initial state $|\psi_0\rangle$ is at $U^n|\psi_0\rangle$ after time n in the absence of perturbation. We assume that after each time step one of the two possible perturbations ($\hat{\Pi}$ and $\hat{\Pi}^{-1}$, both unitary operators close to identity), occurs randomly with equal probability. Then at time n there are $N = 2^n$ possible perturbation histories, which are vectors of the set $\{|\psi_1\rangle, |\psi_2\rangle, \cdots |\psi_N\rangle\}$. In the absence of any information about the perturbation, these perturbation histories are assigned equal *apriori* probability and the state at time n is the mixture:

$$\hat{\rho}_s = \frac{1}{N}\sum_{i=1}^{N} |\psi_i\rangle\langle\psi_i|. \tag{6.1}$$

The entropy of this mixture is $\Delta H_s = -\mathrm{T}r(\hat{\rho}_s \log_2 \hat{\rho}_s)$. Now we try to reduce this entropy by *gaining information* about the perturbation sequence. We do this by grouping the vectors $\{|\psi_i\rangle\}$ according to their distance from each other defined in terms of the Hilbert space angle

$$\phi = \cos^{-1}(|\langle\psi_i|\psi_j\rangle|)\,,\ [0 \leq \phi \leq \pi/2]. \tag{6.2}$$

We bin the interval $[0, \pi/2]$ into intervals of width $\Delta\phi$. Each interval has N_r vectors and there are $\left[\frac{\pi}{2\Delta\phi}\right]$ such groups , $r = 1, 2, \cdots \left[\frac{\pi}{2\Delta\phi}\right]$. $\Delta\phi$ is a measure of how finely we resolve the state and hence get information about the environment's perturbation. The conditional entropy of the r^{th} group is $\Delta H_r = -\mathrm{T}r(\hat{\rho}_r \log_2 \hat{\rho}_r)$ where

$$\hat{\rho}_r = \frac{1}{N_r}\sum_{i=1}^{N_r} |\psi_i^r\rangle\langle\psi_i^r| \tag{6.3}$$

and the average conditional entropy is

$$\Delta H = \sum_r \left(\frac{N_r}{N}\right)\Delta H_r = \sum_r p_r \Delta H_r\,,\ p_r = \frac{N_r}{N}. \tag{6.4}$$

The entropy reduction due to the process of grouping is $\Delta H_s - \Delta H$. This is accomplished by *gaining information* about the perturbation histories. This is equal to $\Delta I = -\sum_r p_r \log_2 p_r$. In the extreme case $\Delta\phi = \pi/2$, minimum resolution case, $N_r = N$ and $p_r = 1, \Delta I = 0$, $\Delta H = \Delta H_s$. When $\Delta\phi = 0$, the perturbing environment is known exactly and $p_r = 1/N, \Delta I = \log_2 N$ and $\Delta H = 0$, the state

is one of the possible 2^N *pure states* (whose Von-Neumann entropy is zero). Schack ad Caves [115] then defined hypersensitivity to be the condition $\frac{\Delta I}{\Delta H_s - \Delta H} \gg 1$, which is to be interpreted as the information required for a reduction in the entropy is much greater than the change in entropy itself. By determining the entropy ΔH and the information ΔI as functions of the resolution angle ϕ, a detailed picture of how the vectors are distributed in the Hilbert space emerges. The distribution $g(\phi)$ of Hilbert space angles ϕ between all pairs of vectors is calculated as an additional criterion.

6.2 Hypersensitivity study for the operators G_N, H_N and $G_N H_N$

We now subject the Fourier transform G_N, the Hadamard transform H_N, and their product $G_N H_N$ to the test of hypersensitivity. In fact an earlier study of Braun [28] involved hypersensitivity calculations for Grover's algorithm and for the Fourier transform. He concluded that the Fourier transform had signatures of integrable dynamics, which indeed is to be expected as it can be treated as a ninety degree rotation in the classical limit. To our knowledge this has not been done for H_N which is so crucially applied in all of quantum computation. The classical limit of H_N is far from clear, if such a limit indeed exists. Its square is the identity, yet its effect of coherent states (treating H_N as a unitary quantum map) is quite disruptive. This can well be imagined as the "zero" state $|00\cdots0\rangle$ is mapped to an equal superposition of *all* states. In fact our study will show that where H_N can be replaced by the Fourier F_N this will be more robust to perturbations.

Coming to the particulars of the calculation, to investigate if a quantum system shows hypersensitivity to perturbations or not, we first compute a list of vectors corresponding to different perturbation histories. Then, for about 50 values of the angle ϕ ranging from 0 to $\pi/2$ we group the vectors in the nearly optimal way as described in the introduction. For each grouping and thus for each chosen angle ϕ, we compute the information $\Delta I(\phi)$ and $\Delta H(\phi)$. We also compute the angles between all pairs of vectors in the list and plot them as a histogram approximating the distribution function $g(\phi)$. As a preliminary step we used the perturbation operator used by Schack and Caves [115] and reproduced the results obtained by them for the quantum baker's map. We have taken the initial state to be a coherent state centred at the origin. We made use of the same perturbation

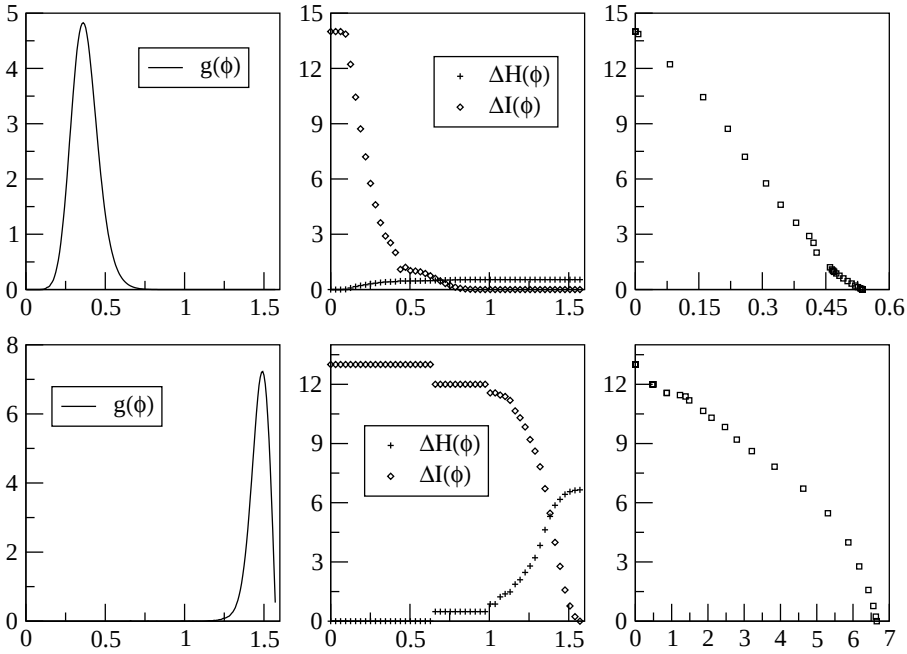

Figure 6.1: Plot of $g(\phi)$ vs. ϕ, $\Delta I(\phi), \Delta H(\phi)$ vs. ϕ and $\Delta I(\phi)$ vs. $\Delta H(\phi)$ for the quantum baker's map with an initial coherent state $|\psi_0\rangle = |1/2D, 1/2D\rangle$. $D = 16$, $\alpha = 0.005$, all 2^{14} vectors after 14 steps.(top) $D = 256$, $\alpha = 0.005$, all 2^{13} vectors after 13 steps.(bottom)

operator and initial state to investigate the hypersensitivity to perturbation for the operators G_N, H_N and $G_N H_N$. The perturbation operator(Π) in the position basis is given by

$$\Pi_{kj} = \begin{cases} \delta_{kj} e^{2\pi i j \alpha} & \text{if} \quad 0 \leq j < D/2 \\ \delta_{kj} e^{2\pi i (D-j-1)\alpha} & \text{if} \quad D/2 \leq j < D \end{cases} \tag{6.5}$$

Here, $\alpha \geq 0$ is the magnitude of the momentum shift ($D\alpha$ is the magnitude of momentum shift in units of the separation between momentum eigenstates). We restrict ourselves to Hilbert spaces with an even dimension D. A perturbed time step consists of first applying the unperturbed time-evolution operator T, followed either by the perturbation operator Π or by its inverse Π^{-1} both representing a momentum shift, chosen randomly. After n perturbed time steps, the number of different perturbation histories equals to 2^n, all occurring with equal probability.

By comparing Fig. (6.1) with Figs. (6.2, 6.3, 6.4) we can make the following observations. In the case of the quantum baker's map and $G_N H_N$ the distribution function $g(\phi)$ has no stharp peaks, except for the bunching around $\pi/2$ indicating a random distribution of vectors [115], where typical vectors are nearly orthogonal.The $\Delta I(\phi)$ vs. $\Delta H(\phi)$ curve has a steep slope near ΔH_S, a signature

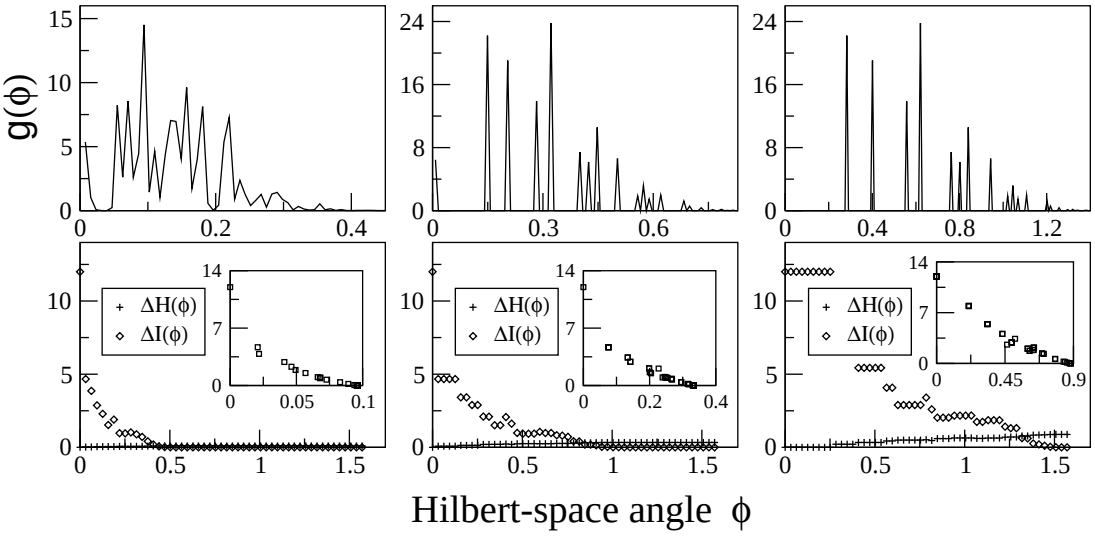

Figure 6.2: Plot of $g(\phi)$ vs.ϕ (first row), $\Delta I(\phi)$, $\Delta H(\phi)$ vs. ϕ (second row) for the Fourier transform with an initial coherent state $|\psi_0\rangle = |1/2D, 1/2D\rangle$. $\Delta I(\phi)$ vs. $\Delta H(\phi)$ is plotted in the inset (second row). $\alpha = 0.005$, all 2^{12} vectors after 12 steps. $D = 16, 64$ and 256 from left to right.

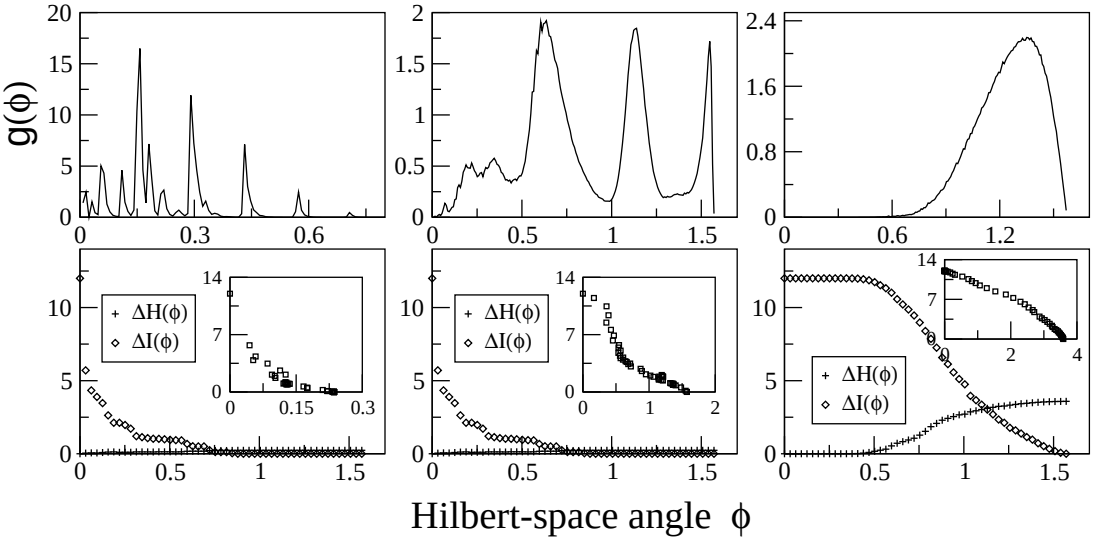

Figure 6.3: Same as Fig. (6.2) but for the Hadamard transform. $D = 16, 64$ and 256 left to right, all 2^{12} vectors after 12 steps.

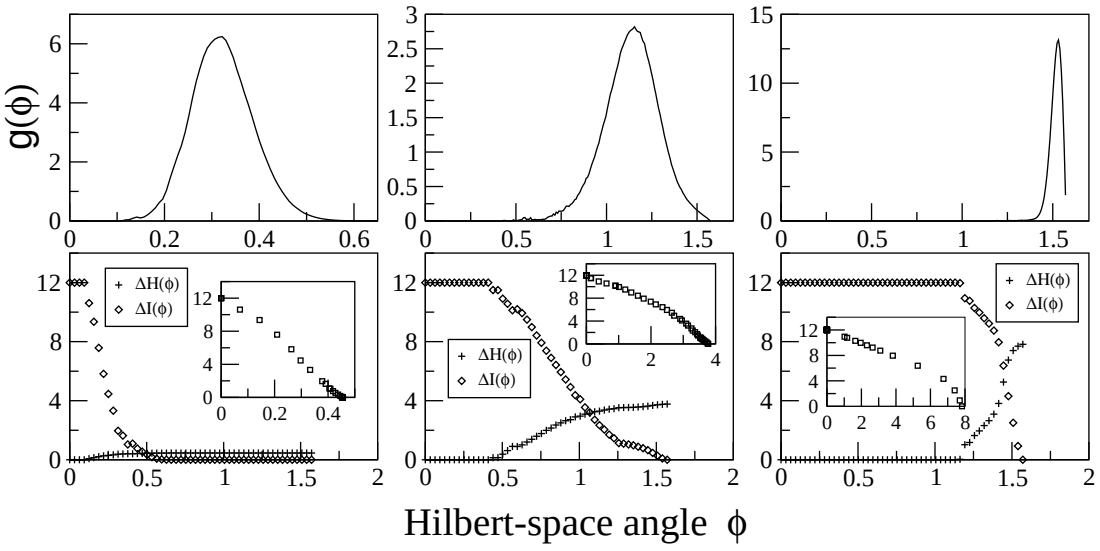

Figure 6.4: Same as Fig. (6.2) but for the Fourier transform of the Hadamard transform. $D = 16, 64$ and 256 from left to right, all 2^{12} vectors after 12 steps.

of hypersensitivity to perturbation. The hypersensitivity of the quantum baker's map is well known. The hypersensitivity of the $G_N H_N$ is consistent with the observation that its spectrum has RMT fluctuations[80]. This operator was studied by Maity and Lakshminarayan as it is part of a symmetry decomposition of the Shor algorithm unitary operator (before the measurement step). They concluded that its spectral statistics was close to that the CUE (or GUE). Just as there is no known classical limit of H_N there is no classical limit known for $G_N H_N$.

For the Fourier transform which represents ninety degree rotation in the phase space, the $g(\phi)$ distribution has many pronounced peaks indicated a propensity of vectors to bunch rather than explore available Hilbert space freely. Also ΔH_S is always less than 1 irrespective of the Hilbert space dimension D. We do not see any smooth relationship between $\Delta I(\phi)$ and $\Delta H(\phi)$. We conclude that it is not hypersensitive to perturbation and believe this is consistent with the previous study [28] and the fact that its classical limit is integrable.

In the case of the Hadmard transform,H_N, we do not see hypersensitivity to perturbation for $D = 16, 64$ from both the $g(\phi)$ distribution as well as $\Delta I(\phi)$ vs. $\Delta H(\phi)$ plots. But for $D = 256$, the $g(\phi)$ distribution has a peak that is tending to $\pi/2$, but the width of the distribution is broad in comparison to that of quantum baker's map. The $\Delta I(\phi)$ vs. $\Delta H(\phi)$ curve shows a steep slope near ΔH_S, a signature of hypersensitivity. Thus we conclude that the Hadamard transform is more sensitive than the Fourier to perturbations, but is not as sensitive as chaotic maps such as the quantum baker's map.

6.3 Hypersensitivity of the shift operator

In Shor's factoring algorithm [78], given an integer M, we try to find another integer p between 1 and M that divides M. The algorithm consists of two parts. A reduction of the factoring problem to the problem of order-finding, which can be done on a classical computer, and a quantum algorithm to solve the order-finding problem. The crucial ingredient in the order-finding part of the algorithm is the modular exponentiation operator which is defined as follows

$$\begin{aligned} U_x|k\rangle &= |xk \mod M\rangle \quad \text{for} \quad 0 \leq k \leq M-1 \\ U_x|k\rangle &= |k\rangle \quad \text{otherwise} \end{aligned} \tag{6.6}$$

Here M is the integer we wish to factor and x is an integer that is co-prime to it. If we take $x = 2$ and M to be an odd integer, we are guaranteed that an integer r exists such that $2^r = 1 \mod M$, where r is the order we are seeking. Note that when $M = 2^K - 1$ it is the full-shift operator S for which the order is equal to K, where K is an integer.

The unitary part of Shor's factoring algorithm when desymmetrized in terms of the eigenstates of S is known have signatures of quantum chaos and the desymmetrized operators are relevant to the usual quantum baker's map [80]. In order to study hypersensitivity of U_2 (since $x = 2$), which is what we studied earlier as the shift operator, we use binary perturbations of the form $\Pi_G = G_N \Pi G_N^{-1}$ and $\Pi_G^{-1} = G_N \Pi^{-1} G_N^{-1}$ which models a shift in the position basis. We use this particular operator since U_2 shifts the position basis states. The shift operator treats position states specially as it permutes them. Therefore perturbations that are diagonal in the position basis are bound to be special. Thus to restore some semblance of a generic perturbation we chose to study the momentum space representation of the original perturbation used in the previous section.

The initial state is taken as $|\psi_0\rangle = |1\rangle$ which is relevant to the Shor's factoring algorithm. For a given D we take different values of M and compare the results with that of the full-shift operator for which $M = 2^K - 1$. We do this since it is known that $B_{K,K}$ (extreme member of the Schack-Caves quantization of the baker's map which we mentioned in chapter 2) which is closely related to the shift operator is not hypersensitive [120]. In Fig (6.5) for $D = 16$ we have given the $g(\phi)$ distribution, information ($\Delta I(\phi)$), and entropy ($\Delta H(\phi)$) plots for $M = 11, 13$ and 15, whose orders are $10, 12$ and 4 respectively. From the $g(\phi)$ distribution we can see that the case with $M = 15$ has more pronounced peaks in comparison to

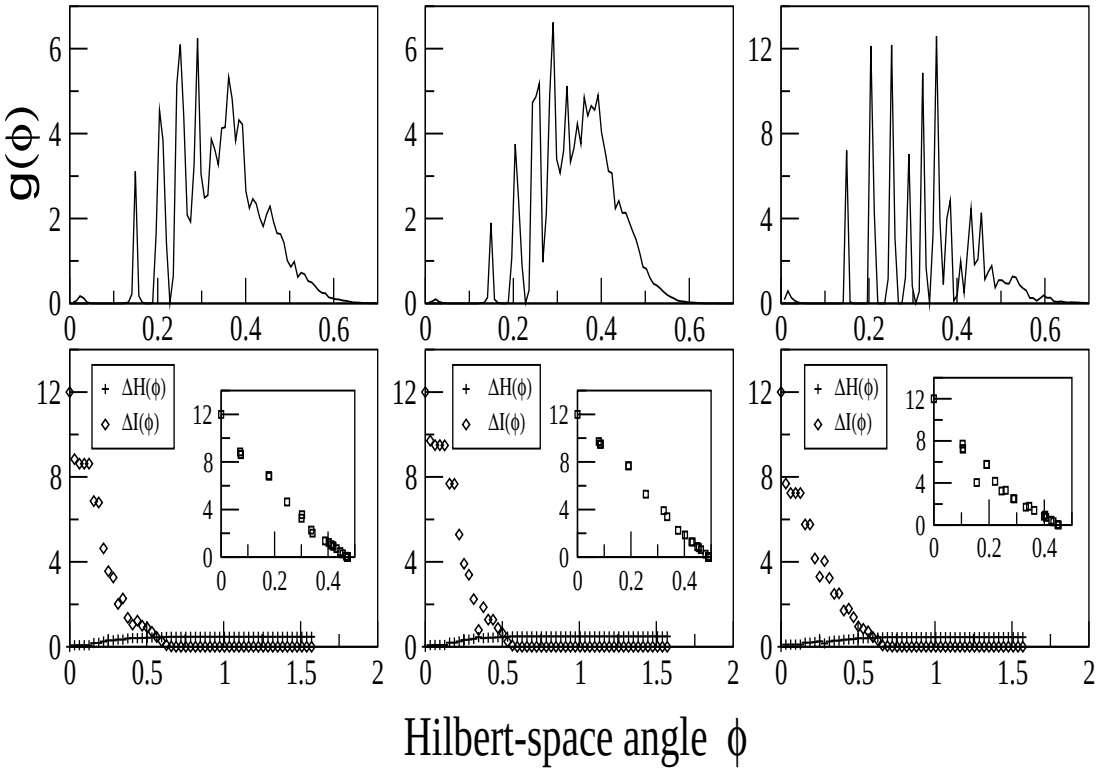

Figure 6.5: Plot of $g(\phi)$ vs.ϕ (first row), $\Delta I(\phi)$, $\Delta H(\phi)$ vs. ϕ (second row) for the shift operator (U_2) with an initial state $|\psi_0\rangle = |1\rangle$. $\Delta I(\phi)$ vs. $\Delta H(\phi)$ is plotted in the inset (second row). $\alpha = 0.005$, all 2^{12} vectors after 12 steps. $D = 16$ and $M = 11, 13$ and 15 from left to right.

other values of M. We could not see much difference from the $\Delta I(\phi)$ vs. $\Delta H(\phi)$ in terms of a steep slope near ΔH_S.

In Fig (6.6) for $D = 64$ we have given the $g(\phi)$ distribution, information ($\Delta I(\phi)$), and entropy ($\Delta H(\phi)$) plots for $M = 55, 59$ and 63, whose orders are $20, 58$ and 6 respectively. From the $g(\phi)$ distribution we can see that the case with $M = 63$ is broader in comparison to other values of M and we could see a smooth relationship from $\Delta I(\phi)$ vs. $\Delta H(\phi)$ for $M = 55$ and 59. In Fig (6.7) for $D = 256$ we have given similar plots for $M = 227, 239$ and 255, whose orders are $226, 119$ and 8 respectively. From $g(\phi)$ distribution we could not differentiate the hypersensitivity of U_2 with respect to the full-shift operator. However the $\Delta I(\phi)$ and $\Delta H(\phi)$ plot we could not see a steep slope near ΔH_S for $M = 255$ in comparison to other values of M. Thus we could differentiate the hypersensitivity of U_2 in comparison to the full-shift operator which has an order of value K. However we could not find much difference between U_2 with different orders.

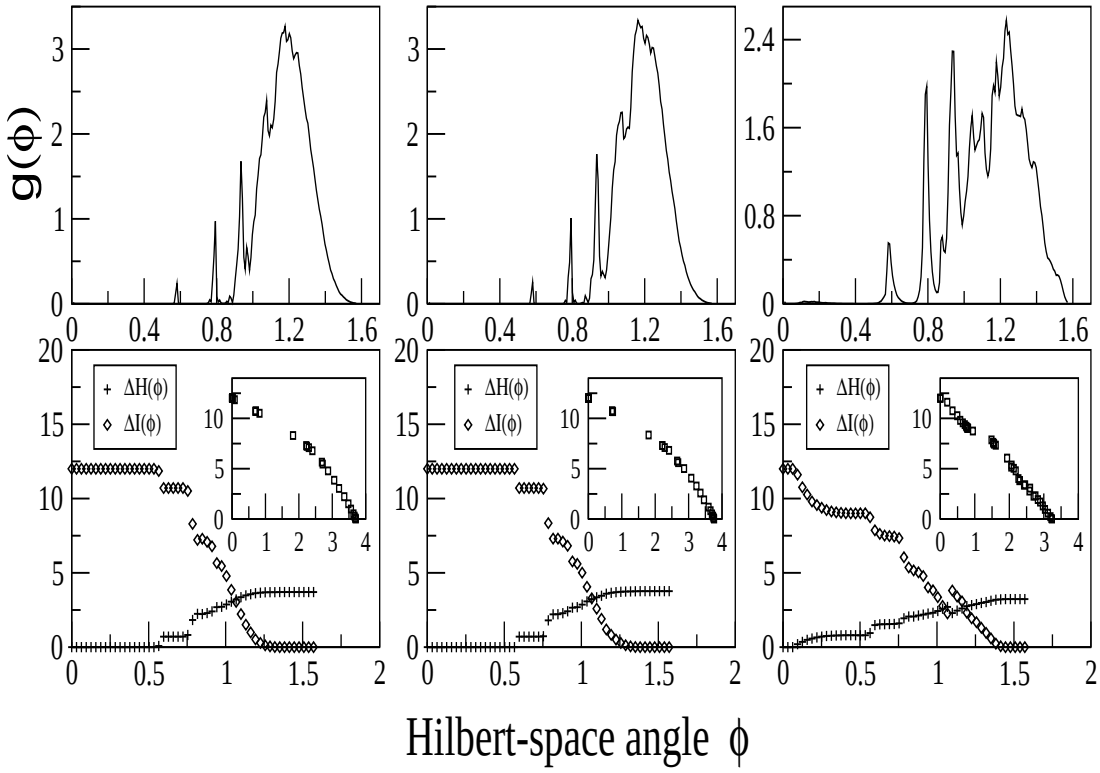

Figure 6.6: Same as Fig. (6.5), for $D = 64$ and $M = 55, 59$ and 63 from left to right.

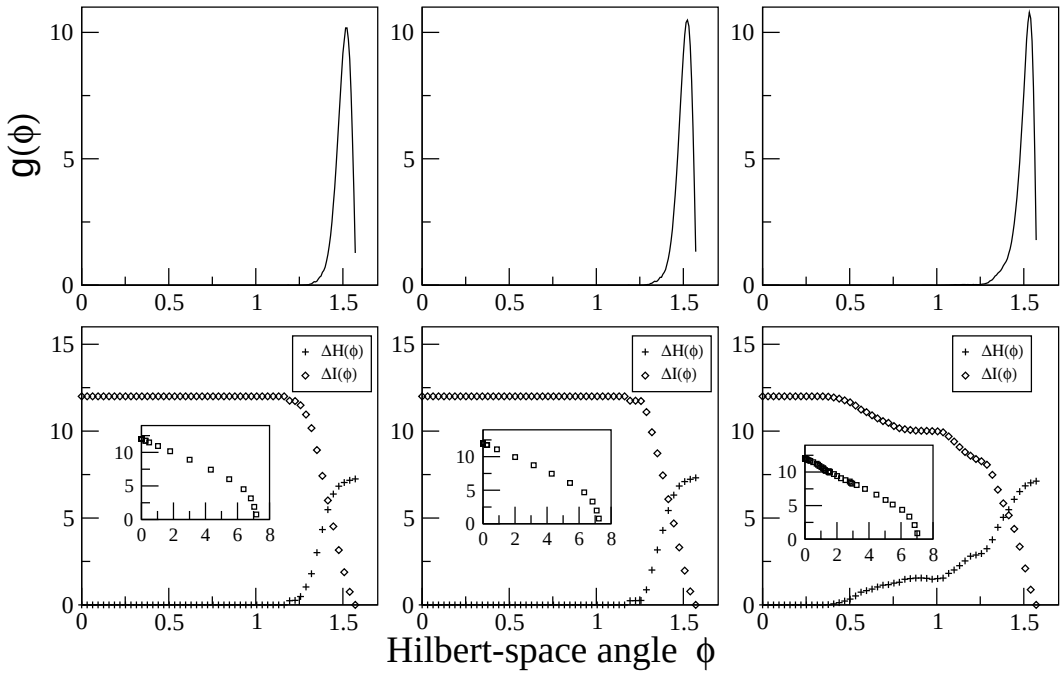

Figure 6.7: Same as Fig. (6.5), for $D = 256$ and $M = 227, 239$ and 255 from left to right.

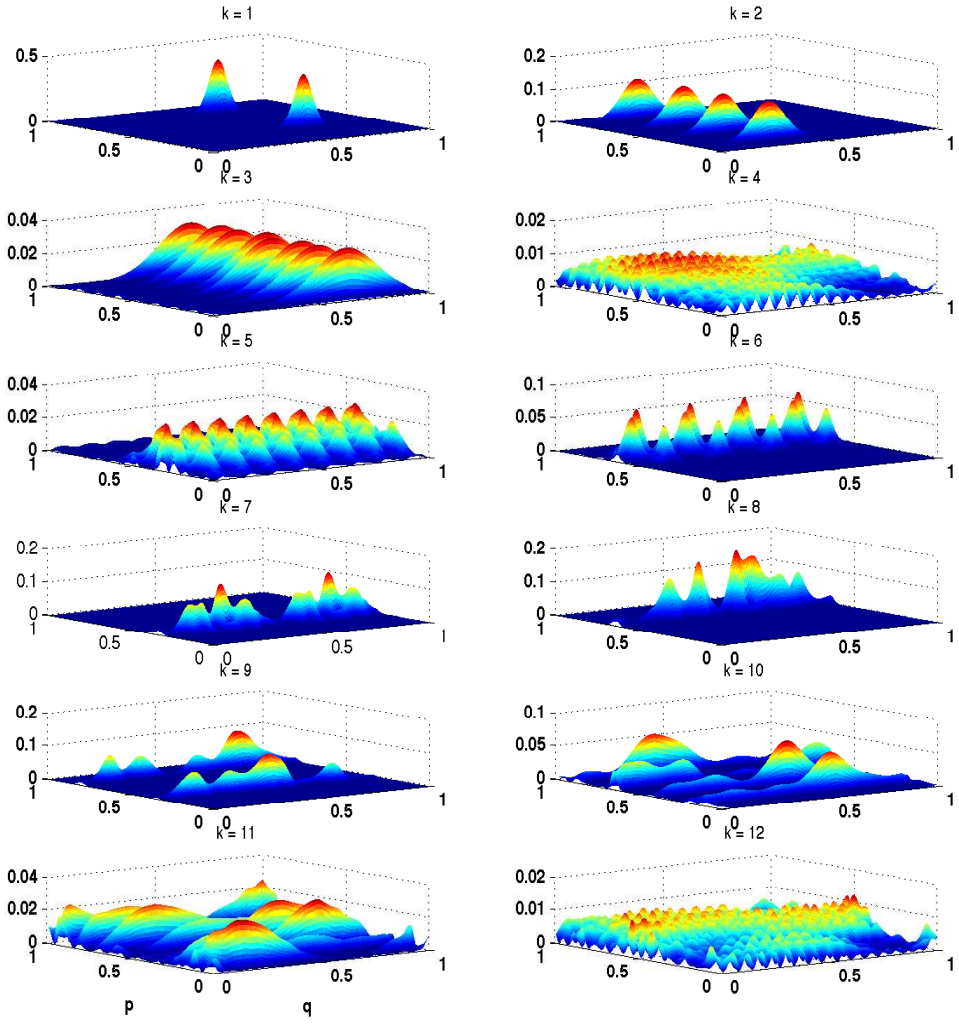

Figure 6.8: Time evolution of a coherent state placed at $|q_0, p_0\rangle = |1/3, 2/3\rangle$ for the shift operator, S with perturbation Π_G for the case of $N = 256$.

In Fig. (6.8) we have given the time evolution of a coherent state for the shift operator with the perturbation Π_G up to 12 times for $N = 256$. The sequence of the binary perturbations are chosen randomly namely Π_G or Π_G^{-1}. For the full shift operator without the perturbation the coherent state will recur after 8 time steps which is the order of the shift operator (see Fig. (2.2)) . When we compare the two cases we can see that up to 4 time steps the influence of the perturbation is small, however the differences between start to build up subsequently and there no recurrence to the initial coherent state after 8 time steps, for the case with the perturbation. Thus the full- shift operator shows sensitivity to perturbation for large time steps. In Fig. (6.9) and Fig. (6.10) we have given time evolution of a

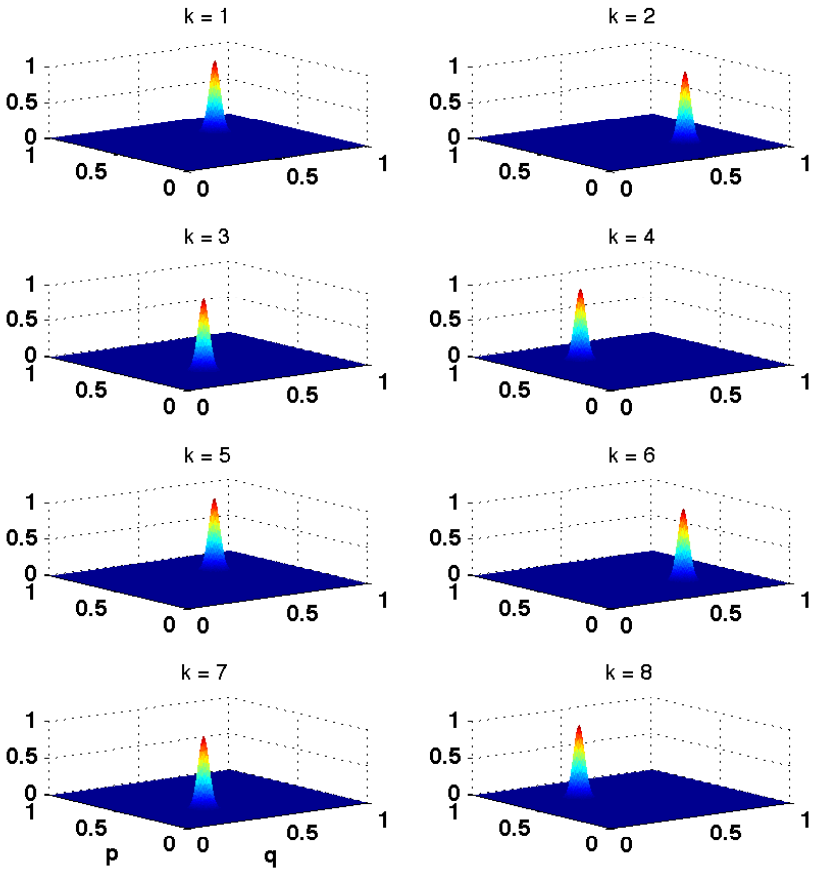

Figure 6.9: Time evolution of a coherent state placed at $|q_0, p_0\rangle = |1/3, 2/3\rangle$ for the Fourier transform, G_N with perturbation Π for the case of $N = 256$.

coherent state for the Fourier transform and Hadamard transform operator with the perturbation Π up to 8 times for $N = 256$. Here also we have chosen the case with a random sequence but with binary perturbations Π or Π^{-1}. We have used Π instead of Π_G since we used the perturbation Π for the hypersensitivity calculations for G_N and H_N. From the figure we can clearly see that the Fourier transform does not show any sensitivity to perturbation and it comes back to the initial coherent state after 4 times which is consistent with the property of the Fourier transform which qauntizes a 90° rotation. However for the Hadamard transform which has the property $H_N^2 = I$ does not show full revival except for all even times where they recur not exactly as a single wave packet but with extra copies of them which are also produced in the process of evolution. These figures are given to give a more concrete idea of the effect of the perturbations on the various operators.

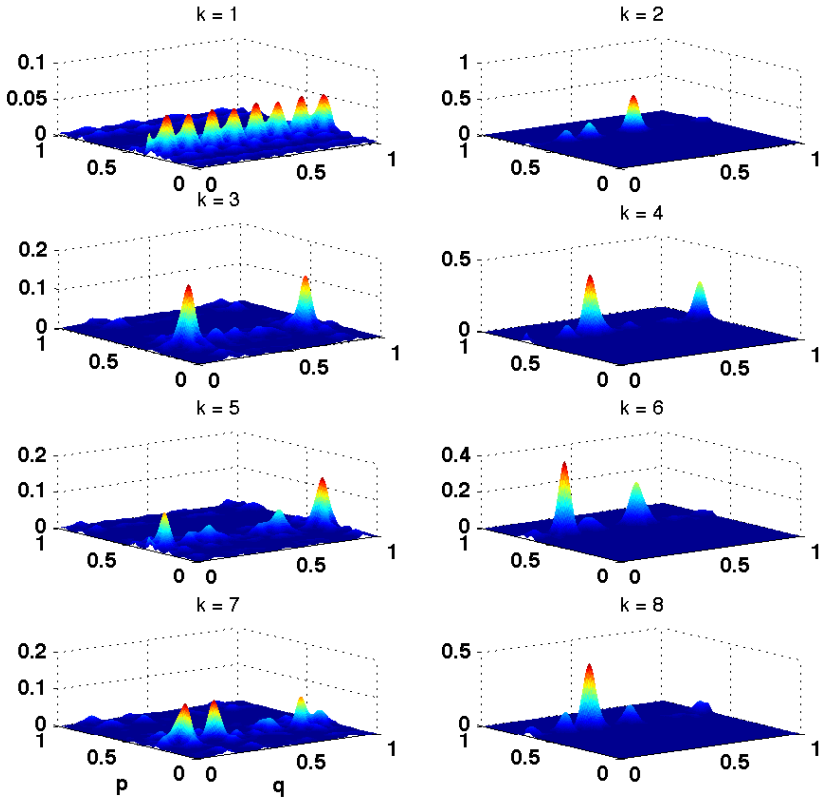

Figure 6.10: Same as Fig. (6.9) but for the Hadamard transform, H_N.

In conclusion in this chapter we have studied the hypersensitivity of various operators relevant to the usual quantum baker's map and Shor's factoring algorithm. The Fourier transform operator is not hypersensitive to perturbation. But Fourier transform of the Hadamard transform ($G_N H_N$) is hypersensitive to perturbation. The Hadamard transform and the full-shift operator shows intermediate level of sensitivity to perturbation. While the modular exponentiation operator U_2 seems to show hypersensitivity to perturbation.

CHAPTER 7

Conclusions

This thesis has primarily been on the quantum baker's map. The quantum baker's map has been extensively studied and used since its first appearance around 1989. As the arguably simplest model of quantum chaos it deserves to be better understood than what we currently do, especially in terms of an analytical understanding of its spectrum. The simple structure of the quantum baker's map in terms of finite or discrete Fourier transform makes it plausible that we maybe able to do so. The connection to the Fourier transform also makes possible an implementation using qubits and algorithms for the quantum Fourier transform. Indeed an experimental realization of the quantum baker has relied on this [44]. The qubit implementation naturally requires a Hilbert space that is a power of 2. For this case, we find that the eigenfunctions are almost exactly solvable and we have shown in this thesis that there are analytically explicit bases that almost diagonalize the quantum baker's map.

One of the significant results of this thesis maybe summarized by saying that the analytical structure of quantum chaotic eigenfunctions, of the baker's map, are made of *sequences*. Thus rather than any simple algorithmic procedure that constructs ordinary functions, these functions are built from sequences that have simple algorithmic generating rules, but which nevertheless produce rather random looking sequences. The sequence dominating the proceedings was the Thue-Morse sequence, first studied in the context of Languages by Thue [85] and later by Morse in the context of geodesic flows on surfaces of negative curvature [86]. A very large literature exists on the Thue-Morse sequence [87], which is known to be "automatic", but we believe that this thesis represents the first time it has appeared naturally in a physics related model. We showed that this sequence is an approximate eigenstate of the quantum baker's map.

This sequence and other related ones were uncovered in the work presented in this thesis for the first time with the use of the Hadamard transform. This transform that is used only second to the Fourier transform, especially in signal processing, works almost "magically" for the quantum baker's map. Taking states that are spread all over in the position space, it transforms them to very sharp peaks. We have quantified the simplification using the well-known measure of

participation ratio (PR) which measures how many states of a basis is used in the construction of a state. We found many states with a PR of around $N/2 = 2^{K-1}$ in the position basis have a PR of the order of K after the Hadamard transform. Thus in some sense the Hadamard transform compresses many states of the baker's map exponentially. The best example of this, and for every K, is a loner we called the "Thue-Morse" state as it was by far dominated by the Thue-Morse sequence.

The Fourier transform of the Thue-Morse sequence has been much studied and is a well-known example of a multifractal measure[92]. This thesis showed that due to the time-reversal invariance of the quantum baker's map, the Fourier transform was equally important, and hence we showed that the Thue-Morse state was practically reconstructable using only the Thue-Morse sequence and its Fourier transform. This state which looks quite complicated in the position (or momentum) representation was shown to have multifractal properties, however the exponents are quite different from those of the Fourier transform of the Thue-Morse sequence. In fact we went on and showed that apart from the Thue-Morse state there were other families that were similarly simplified and also that there are generalizations of the Thue-Morse sequences that are important.

The Fourier transform of the Hadamard transform turns out to be an important mathematical construct and we have studied for the first time in this thesis the multifractal measures that arise out of this and their relevance to the baker's map has been pointed out. It is worth noting that all of these eigenstates have very prominent scars, but primarily only due to period 2, period 4, the fixed point and their associated homoclinic orbits. It is very interesting that scarred states are constructed out of sequences such as the Thue-Morse and especially out of their Fourier transform. It is possible that some general feature of scarring may then be revealed in such simple mathematical objects.

A natural question that arose was *why* the Hadamard transform was special for the quantum baker's map. Significant work in this direction has been done by Ermann and Saraceno [26] who constructed operators such that their perturbations yield the quantum baker's map. We had taken a somewhat similar route and reasoned that the shift operator which is very close to the quantum baker's map ought to play an important role. The virtue of the shift operator is that it can be exactly analytically solved for all values of N. In fact we have presented in Chapter 2 the shift operator and used it to construct the quantum baker's map. The spectrum of the shift operator for N a power of 2 is however highly degenerate, and we used the two symmetries of the quantum baker's map to reduce the ambiguity in the choice of the eigenstates. These symmetries were the parity

and the time-reversal. Thus symmetry adapted eigenstates of the shift operator were used to construct a novel unitary transform, as detailed in Chapter 4. This we called as "basis-2" and showed that this does even *better* than the Hadamard transform in simplifying the eigenfunctions of the quantum baker's map. This also revealed why the Hadamard transform worked as the new transform is in fact a very interesting marriage between the standard Fourier and Hadamard transforms. We speculate that this new transform may have wider uses, including in signal processing.

Having studied the usual dyadic quantum baker's map we turned our attention to seeing how effective such methods are for other cases. The case of $N = 3^K$ was studied by us and a straightforward generalization of the binary Thue-Morse sequence to the triadic context was done and found to be somewhat successful. However we have not pursued this fully here and have not presented the results in this thesis. The results we do present continue to use the power of 2 theme, and the Hadamard and the new transform. Thus it was natural for us to skip the triadic and move on to the tetradic maps with 4 partitions. We found that these transforms continued to give "uniform satisfaction" and indeed did reduce the PR for most states considerably. We found states that are similar to the Thue-Morse state and other families as well, including other sequences. Somewhat surprisingly we found that even for a lazy baker map the transforms do remarkably well. This is surprising as the partitions of the lazy baker's map cut the phase space into unequal vertical and horizontal rectangles, are non-uniformly hyperbolic, does not possess parity symmetry, and instead of being a simple shift, is a subshift on *three* symbols[100]. Despite these the transforms do well, and we have uncovered actually two families of states that are akin to the Thue-Morse state. In a very different application we also studied an *open* baker's map, opening up the tetradic baker's map we have studied earlier. It shows that even the resonances of these maps are considerably simplified by the Hadamard transforms. All these are presented in Chapter 5, which as we have noted earlier is of an exploratory nature and we expect to use this for more in-depth studies of the systems mentioned.

In Chapter 6 we have taken up quite a different question. The thesis actually makes use of many operators that are somehow akin to the quantum baker' s map. These have been uncovered over a period of time, and the quantization family of Shack and Caves [60] has an important role to play in this, by way of introduction of partial Fourier transforms and partial shifts. In fact we believe that we have a *classical interpretation* of these varied quantizations in terms of a very peculiar symmetry of the classical baker's map. This is outlined in Chapter 2. In that

same chapter we had introduced the operator soup that we encounter in this thesis. Somewhat strangely perhaps it is the same set of operators that appear in Shor's famous factoring quantum algorithm. The close connections between Shor's operator and quantum chaos has indeed been studied [80, 62]. In Chapter 6 we have tried to test for hypersensitivity of these operators. Hypersensitivity which had been introduced by Schack and Caves [115] as an autonomous method of determining if a system has quantum chaos relies on information theoretic notions. In fact they had shown earlier that the quantum baker's map is hypersensitive. An earlier work had also shown that the Fourier transform was not hypersensitive and most likely Grover's search algorithm was not.[28]

Considering the close connections between the quantum baker's map and Shor's algorithm, it was natural to ask if the operators that go into this are hypersensitive. The crucial operators are the Hadamard transform, and the modular exponentiation operator. The latter operator is a generalization of the shift operator we have studied in this thesis, for example in Chapter 4. We note that perturbations may occur in may forms, as single qubit ones, or as multi-qubit ones and it is desirable that there is no special relation between the operator whose sensitivity we are testing and the perturbation itself. With this in mind we have chosen our perturbation schemes in Chapter 6. We find, consistent with earlier work that the Fourier transform is not hypersensitive. We find somewhat surprisingly that the Hadamard transform has "intermediate" level of sensitivity. This measure remains somewhat subjective and while we can say that the Hadamard is qualitatively different from the Fourier it is still not as sensitive as the baker's map. Thus it would seem desirable to replace Hadamard transforms by Fourier transforms, especially when there is a chance of the qubits having residual interactions. For instance in the case of Shor's factoring algorithm, while it is standard to use the Hadamard transform [84] it is possible to replace this with the Fourier. Even more interesting is the crucial modular exponentiation part which we study as the shift operator. If we have to order these we would place this between the Hadamard and the baker's map, more towards the bakers' map, and hence quite hypersensitive. All this indicates that Shor's algorithm may indeed have a very nontrivial level of hypersensitivity. Shor's algorithm has long been studied for effects of decoherence [121], and more recently for unitary perturbations [63]. We believe that our results add to the understanding of these studies.

Future directions include a more detailed understanding of the eigenstates. We believe that this thesis has opened a few possibilities especially for model systems that are based on the baker's map. As exceptional states, that violate

quantum ergodicity, they are primarily scarred by various classical orbits and are also multifractal. More detailed analytical work that perhaps classifies how families arise maybe possible. The application to open quantum systems, such as the open tetradic baker's map in understanding long-lived resonances is still mostly open. We have begun their study in this thesis, and merely skimmed the surface. There is a more broader and difficult question of whether we can find transforms that are as effective as the Hadamard was to maps other than the baker's map, such as for example the standard map. Finally it may of interest to see the properties of the new transform found in this thesis and explore possible applications.

REFERENCES

[1] M. C. Gutzwiller. *Chaos in Classical and Quantum Mechanics.* Springer-Verlag Berlin 1990.

[2] K. A. H. Van Leeuwen, G. V. Oppen, S. Renwick, J. B. Bowlin, P. M. Koch, R. V. Jensen, O. Rath, D. Richards and J. G. Leopold. *Microwave Ionization of Hydrogen Atoms: Experiment versus Classical Dynamics.* Phys. Rev. Lett. **55**, 2231 (1985).

[3] A. Holle, G. Wiebusch, J. Main, B. Hager, H. Rottke and K. H. Welge. *Diamagnetism of hydrogen atom in the quasi-Landau regime.* Phys. Rev. Lett. **56**, 2594 (1986).

[4] M. V. Berry. *Riemann's zeta function: a model for quantum chaos? in Quantum chaos and statistical nuclear physics, eds. T H Seligman and H Nishioka.* Springer Lecture Notes in Physics **263**, 1 (1986).

[5] L. Amico, R. Fazio, A. Osterloh and V. Vedral. *Entanglement in many-body systems* Rev. Mod. Phys. **80**, 517 (2008).

[6] A. Lakshminarayan. *Entangling power of quantized chaotic systems* Phys. Rev. E. **64**, 036207 (2001).

[7] G. Benenti. *Entanglement, randomness and chaos.* Riv. Nuovo Cimento **32**, 105 (2009).

[8] J. H. Hannay and A. M. Ozoria De Almeida. *Periodic Orbits and the correlation function for the density of states.* J. Phys. A. **17**, 3429 (1984).

[9] M. V. Berry. *Semiclassical theory of spectral rigidity.* Proc. R. Soc. A **400**, 229 (1985).

[10] O. Bohigas, M. J. Giannoni and C. Schmit. *Characterization of Chaotic Quantum Spectra and Universality of Level Fluctuation Laws.* Phys. Rev. Lett. **52**, 1 (1984).

[11] F. Haake. *Quantum Signatures of Chaos.* Springer Berlin 1991.

[12] R.L. Devaney. *An Introduction to Chaotic Dynamical Systems.* Addison-Wesley 1986.

[13] K.T. Alligood, T.D. Sauer and J.A. Yorke. *Chaos, an Introduction to Dynamical Systems* Springer New York 1996.

[14] A.J. Lichtenberg and M.A. Lieberman. *Regular and Chaotic Dynamics.* Springer New York 1992.

[15] J.H. Hannay and M.V. Berry. *Quantization of linear maps on a torus-fresnel diffraction by a periodic grating.* Physica D. **1**, 267 (1980).

[16] J.P. Keating. *The cat maps: quantum mechanics and classical motion.* Nonlinearity **4**, 309 (1991).

[17] B. Eckhardt. *Exact eigenfunctions for a quantised map.* J. Phys. A: Math. Gen. **19**, 1823 (1986).

[18] F. Faure, S. Nonnenmacher and S. De Bièvre. *Scarred eigenstates for quantum cats of minimal periods.* Commun. Math. Phys. **239**, 449 (2003).

[19] N.L. Balazs and A. Voros. *The quantized Baker's transformation.* Ann. Phys. (N.Y.) **190**, 1 (1989).

[20] M. Saraceno. *Classical structures in the quantized baker transformation.* Ann. Phys. (N.Y.) **199**, 37 (1990).

[21] E.J. Heller. *Bound-State Eigenfunctions of Classically Chaotic Hamiltonian Systems: Scars of Periodic Orbits.* Phys. Rev. Lett. **53**, 1515 (1984).

[22] S. R. Jain, B. Grémaud and A. Khare. *Quantum modes on chaotic motion: Analytically exact results* Phys. Rev. E **66**, 016216 (2002).

[23] M.R. Schroeder. *Number Theory in Science and Communication* Springer-Verlag Berlin 1986.

[24] J.-P. Allouche and J. Shallit. *Automatic Sequences: Theory, Applications and Generalizations* Cambridge University Press Cambridge 2003.

[25] A. Schnirelman. *Ergodic properties of the eigenfunctions.* Usp. Math. Nauk. **29**, 181 (1974).

[26] L. Ermann and M. Saraceno. *Generalized quantum baker maps as perturbations of a simple kernel.* Phys. Rev. E. **74**, 046205 (2006).

[27] S. Nonnenmacher and M. Zworski. *Fractal Weyl laws in discrete models of chaotic scattering.* J. Phys. A: Math. Gen. **38**,10683 (2005).

[28] D. Braun. *Quantum chaos and Quantum Algorithms.* Phys. Rev. A. **65**, 042317 (2002).

[29] M. Tabor. *Chaos and integrability in nonlinear dynamics: an introduction.* John Wiley 1989.

[30] L. E. Reichl. *The Transition to Chaos Conservative Classical Systems and Quantum Manifestations.* Springer 2004.

[31] C. Li and G. Chen. *Estimating the Lyapunov exponents of discrete systems.* Chaos **14**, 343 (2004).

[32] J. Banks, J. Brooks, G. Cairns, G. Davis and P. Stacey. *On Devaney's definition of chaos.* American Mathematics Monthly **99** 332 (1982).

[33] S. Tomsovic and A. Lakshminarayan. *Fluctuations of finite-time stability exponents in the standard map and the detection of small islands.* Phys. Rev. E **76** 036207 (2007).

[34] P. B. Wilkinson, T. M. Fromhold, L. Eaves, F. W. Sheard, N. Miura and T. Takamasu *Observation of 'scarred' wavefunctions in a quantum well with chaotic electron dynamics.* Nature **380**, 608 (1996)

[35] B. Georgeot and D. L. Shepelyansky. *Quantum chaos border for quantum computing* Phy. Rev. E **62**, 3504(2000).

[36] G. P. Berman, F. Borgonovi, F. M. Izrailev and V. I.Tsifrinovich. *Avoiding quantum chaos in quantum computation.* Phys. Rev. E **65** 015204 (2001).

[37] M. Srednicki. *Chaos and Quantum Thermalization.* Phys. Rev. E. **50** 888 (1994).

[38] W. H. Zurek. *Environment-Assisted Invariance, Entanglement, and Probabilities in Quantum Physics.* Phys. Rev. Lett. **90**, 120404 (2003).

[39] G. Casati, B. V. Chirikov, F. M. Izrailev and J. Ford. *Stochastic behavior of a quantum pendulum under a periodic perturbation.* Lecture Notes in Physics, Springer **93**, 334 (1979).

[40] M. V. Berry, N. L. Balazs, M. Tabor and A. Voros. *Quantum maps.* Ann.Phys N.Y. **122**, 26 (1979).

[41] S. W. McDonald and A. N. Kaufman. *Wave chaos in the stadium: Statistical properties of short-wave solutions of the Helmholtz equation.* Phys. Rev. A. **37**, 3067 (1988).

[42] J. Ford, G. Mantica and G. H. Ristow. *The Arnol'd cat: Failure of the correspondence principle.* Physica D. **50**, 493 (1991).

[43] C. F. Bharucha, J. C. Robinson, F. L. Moore, B. Sundaram, Q. Niu, and M. G. Raizen. *Dynamical localization of ultracold sodium atoms* Phys. Rev. E. **60**, 3881 (1999).

[44] Y. S. Weinstein and S. Lloyd and J. V. Emerson and D. G. Cory. *Experimental Implementation of the Quantum Baker's Map.* Phys. Rev. Lett. **89**, 157902 (2002).

[45] F. M. Izrailev. *Simple models of quantum chaos: Spectrum and eigenfunctions.* Phys. Rep. **196**, 299 (1990).

[46] R. Ketzmerick, K. Kruse and T. Geisel. *Efficient diagonalization of kicked quantum systems.* Physica D. **131**, 247 (1999).

[47] I. I. Satija. *Topological singularities and transport in kicked Harper model.* Phys. Rev. E. **71**, 056213 (2005).

[48] M. V. Berry. *Regular and irregular semiclassical wavefunctions.* J. Phys. A. **10**, 2083 (1977).

[49] A. Voros. *Stochastic Behavior in Classical and Quantum Hamiltonian Systems.* Ed. G. Casati and J. Ford, Lectures Notes in Physics. Springer, Berlin **93**, 326 1979.

[50] E. B. Bogomolny. *Smoothed wavefunctions of Chaotic Quantum Systems.* Physica D. **31**, 169 (1988).

[51] M. V. Berry. *Quantum scars of classical closed orbits in phase space.* Proc. R. Soc. A. **423**, 219 (1989).

[52] H. Rehfeld, C. Dembowski, H. -D. Graf, A. Heine, R. Hofferbert and A. Richter. *Quantum chaos and wavedynamical chaos in two- and three-dimensional microwave billiards.* Physica E. **9**, 518 (2001).

[53] I. C. Percival. *Regular and irregular spectra.* J. Phys. B: At. Mol. Phys. **6**, L229 (1973).

[54] L. Hufnagel, R. Ketzmerick, M.-F. Otto, and H. Schanz. *Eigenstates Ignoring Regular and Chaotic Phase-Space Structures.* Phys. Rev. Lett. **89**, 154101 (2002).

[55] M.C. Gutzwiller. *Classical Quantization of a Hamiltonian with Ergodic Behavior.* Phys. Rev. Lett. **45**, 150 (1980).

[56] A.M. Ozorio de Almeida and M. Saraceno. *Periodic orbit theory for the quantized baker's map.* Ann. Phys. (N.Y.) **210**, 1 (1991).

[57] M. Saraceno and A. Voros. *Towards a semiclassical theory of the quantum baker's map.* Physica D. **79** 206 (1994).

[58] H. A. Weidenmüller and G. E. Mitchell. *Random matrices and chaos in nuclear physics: Nuclear structure.* Rev. Mod. Phys. **81**, 539 (2009).

[59] F. J. Dyson. *Statistical Theory of the Energy Levels of Complex Systems - I.* J. Math. Phys. **3**, 140 (1962).

[60] R. Schack and C.M. Caves. *Shifts on a Finite Qubit String: A Class of Quantum Baker's Maps.* Appl. Algebra Engg, Comm. Comput. **10**, 305 (2000).

[61] O. Penrose. *Foundations of Statistical Mechanics.* Pergamon Press 1970.

[62] A. Lakshminarayan. *Modular multiplication operator and quantized baker's maps.* Phys. Rev. A **76**, 042330 (2007).

[63] I.Garcia-Mata, K.Frahm and D.L.Shepelyansky. *Shor's factorization algorithm with a single qubit and imperfections.* Phys. Rev. A **78**, 062323 (2008).

[64] P.W. O' Connor and S. Tomsovic. The unusual nature of the quantum Baker's transformation. Ann. Phys. **207**, 218 (1990).

[65] Newman. *Power laws, Pareto distribution and Zipf Law.* Contemp. Phys. **46**, 323 (2005).

[66] A. Lakshminarayan, S. Tomsovic, O. Bohigas and S. N. Majumdar. *Extreme statistics of complex random and quantum chaotic states.* Phys. Rev. Lett. **100**, 044103 (2008).

[67] J. Schwinger. *On the Unitary Operator bases.* Proc. Nat. Acad. Sci. **46**, 570 (1960).

[68] A. Lakshminarayan. *On the Quantum Baker's Map and Its Unusual Traces.* Ann. Phys. **239**, 272 (1995).

[69] J. J. Sakurai. *Modern Quantum Mechanics.* Addison-Wesley New York 1994.

[70] A. J. Scott and C. M. Caves. *Entangling power of the quantum baker's map.* J. Phys. A. **36**, 9553 (2003).

[71] M. M. Tracy and A. J. Scott. *The classical limit for a class of quantum baker's maps.* J. Phys. A: Math. Gen. **35** 8341 (2002).

[72] M. M. Tracy.*The classical limit of the quantum baker's map*, Ph. D Dissertation, Department of Physics and Astronomy, University of New Mexico, USA. December 2002.

[73] A. N. Soklakov and R. Schack. *Decoherence and linear entropy increase in the quantum baker's map.* Phys.Rev. E **66**, 036212 (2002).

[74] H. Naren. *Quantum bakers map*, M.Sc Dissertation, Department of Physics, IIT-Madras, Chennai, India. April 2004.

[75] E. W. Weisstein. *From Math World - A Wolfram Web Resource Riffle Shuffle.* http://mathworld.wolfram.com/RiffleShuffle.html (2009).

[76] A. Lakshminarayan and N. L. Balazs. *Relaxation and localization in interacting quantum maps* J. Stat. Phys. **77**, 311 (1994).

[77] A. Lakshminarayan. *Shuffling cards, factoring numbers, and the quantum baker's map.* J. Phys. A: Math. Gen. **38**, L597 (2005).

[78] P. Shor. *Proc. 35^{th} Annual Symposium on Foundations of Computer Science* (IEEE Press, USA) 1994.

[79] A. Lakshminarayan. *The modular multiplication operator and the quantized bakers maps* Phys. Rev. A. **76**, 042330 (2007).

[80] K. Maity and A. Lakshminarayan. *Quantum chaos in the spectrum of operators used in Shor's algorithm.* Phys. Rev. E. **74**, 035203(R) (2006).

[81] T. A. Brody, J. Flores, J. B. French, P. A. Mello, A. Pandey and S. S. M. Wong. *Random-matrix physics: spectrum and strength fluctuations* Rev. Mod. Phys.**53**, 385 (1981).

[82] M.D. Esposti and B. Winn. The quantum perturbed cat map and symmetry. J. Phys. A: Math. Gen. **38**, 5893 (2005).

[83] M. S. Santhanam, V. B. Sheorey, and A. Lakshminarayan. *Chaos and exponentially localized eigenstates in smooth Hamiltonian systems.* Phys. Rev. E. **57**, 345 (1998).

[84] M.A. Nielsen and I. L. Chung. *Quantum Computing and Quantum Information.* Cambridge University Press, Cambridge (2000).

[85] A. Thue. *Selected mathematical papers of Axel Thue.* T. Nagell ed. Universitetsforlaget, Oslo pp-139 1977.

[86] M. Morse. *Recurrent geodesics on a surface of negative curvature.* Trans. Amer. Math.Soc. **22**, 84 (1921).

[87] J.-P. Allouche and J. Shallit. *Sequences and their Applications.* Proc. SETA Conference. Niederreiter Springer Berlin 1999.

[88] P. Prusinkiewicz and A. Lindenmayer. *The Algorithmic Beauty of Plants* Springer-Verlag, 2004.

[89] A. Bovier and J.-M. Ghez. *Remarks on the spectral properties of tight-binding and Kronig-Penney models with substitution sequences.* J. Phys. A. **28**, 2313 (1995).

[90] M. Janssen. *Statistics and scaling in disordered mesoscopic electron systems.* Phys. Rep. **295**, 1 (1998).

[91] J.-P. Allouche, M. M. France. *Euler, Pisot, Prouhet ThueMorse, Wallis and the duplication of sines* math.NT. arXiv:math/0610525, (2006).

[92] C. Godreche and J.M. Luck. *Multifractal analysis in reciprocal space and the nature of the Fourier transform of self-similar structures* J. Phys. A **23**, 3769 (1990).

[93] T.C. Halsey, M.H. Jensen, L.P. Kadanoff, I. Procaccia and B.I. Shraiman. *Fractal measures and their singularities: The characterization of strange sets.* Phys. Rev. A. **33**, 1141 (1986).

[94] R.Yarlagadda and J.E.Hershey. *Spectral Properties of the Thue-Morse Sequence.* IEEE. **32** 974 (1984).

[95] N. J. A. Sloane, Ed. *Sequence number A104104. Online Encyclopedia of Interger Sequences.* http://www.research.att.com/ njas/sequences/

[96] P. Kurlberg and Z. Rudnick. *Hecke theory and equidistribution for the quantization of linear maps of the torus.* Duke Math. Jour. **103**, 47 (2000).

[97] G.H. Hardy and E.M. Wright. *An introduction to the theory of numbers.* Oxford Univ. Press 1979.

[98] F. Faure and S.Nonnenmacher. *On the Maximal Scarring for Quantum Cat Map Eigenstates.* Commun. Math. Phys. **201**, 245 (2004).

[99] N. Anantharaman and S. Nonnenmacher. *Entropy of semiclassical measures of the Walsh-quantized baker's map.* Annales Henri Poincaré **8** 37 (2007).

[100] A. Lakshminarayan and N. L . Balazs. *The Classical and Quantum Mechanics of Lazy Baker Maps.* Ann. Phys. **226**, 350 (1993).

[101] A. Lakshminarayan and N. L. Balazs. *On the noncommutativity of quantization and discrete time evolution.* Nuclear Physics A. **572**, 37 (1994).

[102] A. Lakshminarayan. *Studies in Quantum Maps.* Ph. D Dissertation, SUNY USA 1993.

[103] P. Gaspard and S. A. Rice. *Scattering from a classically chaotic repellor.* J. Chem. Phys. **90**, 2225 (1989).

[104] J. V. Jose and E. J. Saletan. *Classical Dynamics. A contemporary approach.* Cambridge Univ. Press 1998.

[105] M. Saraceno and R. O. Vallejos. *The quantum D-transformation.* Chaos **6**, 193 (1995).

[106] J. Sjöstrand. *Geometric bounds on the density of resonances for semiclassical problems.* Duke Math. J. **60**, 1 (1990).

[107] M. Zworski. *Quantum resonances and partial differential equations.* Not. Am. Math. Soc. **46**, 319 (1999).

[108] K. K. Lin. *Numerical Study of Quantum Resonances in Chaotic Scattering.* J. Comput. Phys. **176**, 295 (2002).

[109] K. K. Lin and M. Zworski. *Quantum resonances in chaotic scattering.* Chem. Phys. Lett. **355**, 201 (2002).

[110] J. P. Keating, M. Novaes, S. D. Prado, and M. Sieber. *Semiclassical Structure of Chaotic Resonance Eigenfunctions.* Phys. Rev. Lett. 97, 150406 (2006).

[111] J. M. Pedrosa, G. G. Carlo, D. A. Wisniacki and L. Ermann. *Distribution of resonances in the quantum open baker map.* Phys. Rev. E. **79**, 016215 (2009).

[112] L. Ermann, G. G. Carlo and M. Saraceno. *Localization of Resonance Eigenfunctions on Quantum Repellers.* Phys. Rev. Lett. **103**, 054102 (2009).

[113] J.P. Keating, S. Nonnenmacher, M. Novaes and M. Sieber. *On the resonance eigenstates of an open quantum baker map.* Nonlinearity **21**, 2591 (2008).

[114] J. Karthik, A. Sharma and A. Lakshminarayan. *Entanglement, avoided crossings, and quantum chaos in an Ising model with a tilted magnetic field.* Phys. Rev. A **75**, 022304 (2007).

[115] R. Schack and C.M. Caves. *Information-theoretic characterization of quantum chaos.* Phys. Rev. E. **53** 3257 (1996).

[116] H. S. Leff and A. F. Rex. *Maxwell's Demon: Entropy, Information, Computing.* Princeton University Press, Princeton, NJ 1990.

[117] L. Szilard. *Entropy and information for an automated Maxwell's demon.* Z. F. Physik **53** 840 (1929).

[118] C. H. Bennett. *Demons, Engines and the Second Law.* Scientific American **257**, 108 (1987).

[119] R. Landauer and J. A. Swanson. *Frequency Factors in the Thermally Activated Process.* Phys. Rev. **121**, 1668 (1961)

[120] A. J. Scott, T. A Brun, C. M. Caves and R. Schack. *Hypersensitivity and chaos signatures in the quantum baker's maps.* J. Phys. A: Math. Gen. **39**, 13405 (2006).

[121] I. L. Chuang, R. Laflamme, P. W. Shor and W. H. Zurek. *Quantum Computers, Factoring, and Decoherence.* Science. **270**, 1633 (1995).

LIST OF PAPERS BASED ON THESIS

1. Multifractal eigenstates of quantum chaos and the Thue-Morse sequence. **N Meenakshisundaram** and Arul Lakshminarayan. Phys. Rev. E **71**, 065303(R) (2005).

2. The Fourier transform of the Hadamard transform: Multifractals, Sequences and Quantum Chaos.
   N Meenakshisundaram and Arul Lakshminarayan. *Nonlinear Systems and Dynamics* Ed. M Lakshmanan and R Sahadevan Allied Publishers Chennai India. pp-69, 2006.

3. Using Hadamard and related transforms for simplifying the spectrum of the quantum baker's map. Arul Lakshminarayan and **N Meenakshisundaram**. J. Phys. A: Math. Gen. **39**, 11205 (2006).